SWS Instrument & Data Manual
Issue 1.0
SAI/98-095/Dc

K. Leech
ISO Science Operations, VILSPA
with contributions from
the SWS Instrument Dedicated Team (SIDT)
and
the SWS Instrument Support Team (SIST)

Contents

Chapter 1

Introduction

1.1 Purpose

This SWS Instrument & Data Manual is one in a series of five documents that explain the operations of the Infrared Space Observatory (ISO) and its four instruments, the data received from the instruments and the processing carried out on the data. Four of the five explain the individual instruments (CAM, LWS, PHOT or SWS), while the fifth explains the operations of ISO.

This document describes data processed with version 7 or later of the Off-Line Processing (OLP) system, available from the ISO Post-Mission Archive (PMA) at http://www.iso.vilspa.esa.es/.

1.2 How to use this manual

How to use this manual depends on whether this is the first time you've processed any SWS data. If it is, read Chapters 3 to 8 of this manual, describing SWS, its performance and what scientific processing happens to data between the time it is telemetered down from ISO and the time it is put in the archive. Then read "Getting started with SWS Data", section 2.

If you've received SWS data before just read "What's New", section 1.3, and anything that it points to.

1.3 What's new

This section describes major document changes between versions.

1.3.1 Issue 1

This was the first version, released after the end of ISO operations. It was produced using information from Version 3.1 of the SWS ISO Data Users Manual (SWS IDUM), Version 3.0 of the SWS ISO Observers Manual, and various documents produced during the operational phase of ISO. These are referenced in the text and a complete listing is given in section 1.5.

1.4 How to contact ESA or other institutes

There are two ways to contact or to get information from ESA.

1 Send a question to the helpdesk, 'helpdesk@iso.vilspa.esa.es'.

2 Look at the ISO WWW page, at "http://www.iso.vilspa.esa.es/". There is a SWS page linked to this, accessed via 'Instruments Specific Information'.

American observers can also obtain support from IPAC by:

1 Sending a question to the IPAC helpdesk, 'iso@ipac.caltech.edu'.

2 Looking at the IPAC ISO WWW page, at "http://www.ipac.caltech.edu/iso/iso.html".

The Short Wavelength Spectrometer team maintains two websites through which they may be contacted. Space Research Organization Netherlands (SRON) Groningen has an ISO page at http://www.sron.rug.nl/iso/ and the ISO Spectrometer Data Centre at the Max-Planck-Institut für extraterrestrische Physik (MPE), Garching, Germany has a web page at http://www.mpe-garching.mpg.de/iso/isosdc.html.

1.5 Relevant documents

The following documents were used in the writing of this manual and may be consulted.

- 1 ISO Data Products Document (IDPD), ISO-SSD-9111A

2 FITS, NASA Science Data Systems Standards Office (NSDSSO), see URL http://www.cv.nrao.edu/fits/

3 SWS Observers Manual. Version 2.0 was the pre-launch version, 3.0 was the post-launch version issued with the supplemental call.

4 SWS Instrument Data Users Manual (IDUM), SAI/95-221/Dc

5 ISO Satellite & Data Manual (ISDM), SAI/98-094/Dc

6 Possible Detector Memory Effects in SWS Grating range spectra (AOT S06) due to SWS Reference Scans, by K. Leech & P. Morris issued 27 May 1997 and accessible at URL xyz.

7 Effects seen in data induced by incorrect target coordinates or crowded fields, by K. Leech & A. Heras issued 12 June 1997 and accessible at URL xyz.

8 Grating instrumental profile and resolution, by M.E. van den Ancker, R. Voors & K. Leech issued 1 July 1997 and accessible at URL xyz

9 Single Detector Signal Jumps, by A. Heras issued 9 June 1997 and accessible at URL xyz

10 Wavelength Calibration, by Do Kester, Douwe Beintema & Edwin Valentijn issued 2 July 1998 and available at URL xyz.

11 Status of SWS Fabry-Pérot wavelength calibration and instrumental profile, by H. Feuchtgruber issued 5 May 1998, and available at URL xyz.

12 CROSS AOT COMPARISON, PART 1, issue 1.1 by A.M. Heras issued on 6 February 1997, and available at URL xyz

13 Cross AOT comparison-part 2, by A.M. Heras issued 21 April 1997 and available at URL xyz and also published in part in the 'First ISO Workshop on Analytical Spectroscopy', Eds A.M. Heras, K. Leech, N.R. Trams & M. Perry, ESA SP-419, p77.

14 Status of study on Gam-Dra fluxes and related pointing errors, by H. Feuchtgruber issued 10 June 1998 and available on the web at URL xyz.

15 Status of study of AOT02 line profiles and fluxes on NGC6543, by H. Feuchtgruber issued 2 June 1998 and available on the web at URL xyz.

16 The effects of the pointing jitter on SWS observations, by A. Heras, issued 6 August 1998 and available on the web at URL xyz.

17 SWS Beam Profiles and ISO Pointing, by A. Salama, issued 9 September 1998 and available at URL XYZ.

18 The Photometric Calibration of the ISO Short Wavelength Spectrometer, by S.G. Schaeidt *et al*, published in the A&A special issue (November 1996 Vol 315) devoted to ISO and available at URL xyz.

19 The Wavelength Calibration and Resolution of the Short Wavelength Spectrometer, by E. Valentijn *et al*, published in the A&A special issue (November 1996 Vol 315) devoted to ISO and available at URL xyz.

20 Observing with the ISO Short Wavelength Spectrometer, by de Graauw *et al*, published in the A&A special issue (November 1996 Vol 315) devoted to ISO and available at URL xyz.

Chapter 2

Processing SWS Data

2.1 Introduction

There are two software packages specifically written to further process SWS data beyond the standard pipeline products: the ISO Spectral Analysis Package for SWS and LWS Auto Analysis Results (ISAP); and (the soon to be released) OSIA. Users are encouraged to obtain both these packages from the ISO Web site http://www.iso.vilspa.esa.es/. Recipes are also available at this web site to guide you in the reduction of your data. Information of ISAP can also be found at http://www.mpe-garching.mpg.de/iso/observer/isap/isap.html

Users wishing to process SWS data with their favourite data analysis package are recommended to read the ISAP and OSIA recipes and the following sections in order to understand what has to be done to the data.

Whatever users choose, they will first have to obtain SWS data. Data downloaded from the Post-Mission Archive (PMA) will be in the correct format, but some users may have received data from the Post-Mission Archive on CD-ROM, or they may have CD-ROMs produced during operations containing their data. In both cases they will have to read the data off the CD first.

2.2 Reading the data from CD-ROM

Users should either read the relevant data (e.g. AAR or SPD files) from the CD-ROM to their diskspace and work on it from there, or read it from the CD-ROM straight into their data reduction software.

IDL

To read a the FITS files in using the IDL ASTRON library:

```
data = readfits( <file.fits>, header, exten_no = 1 )
```

reads in a data array. If <file.fits> was an AAR file then the array 'data' would have a size of 52 * length of SWAA file + header.

```
print, tbget( header, data, 1, 0)
```

for an AAR would print the first wavelength.

```
print, tbget( header, data, 1, 1)
```

for an AAR would print the second wavelength.

```
print, tbget( header, data, 2, 1012)
```

for an AAR would print the 1013th flux.

The header variable will tell you in what order variables appear in the data array. For AAR the order, given in section 9.4.1, is:

```
'SWAAWAVE'
'SWAAFLUX'
'SWAASTDV'
'SWAATINT'
'SWAADETN'
'SWAAITK '
'SWAAUTK '
'SWAARPID'
'SWAASPAR'
'SWAALINE'
'SWAASDIR'
'SWAASCNT'
'SWAASTAT'
'SWAAFLAG'
```

MIDAS

For MIDAS users the commands:

```
indisk/fits <file.fits> file
print/tab file file.dat
```

will output the fits file as plain ASCII which can then be imported into most packages (thanks to Paul Crowther of UCL).

2.3 Basic processing steps

Getting started with SWS data can be broken down into the following steps:

1 Selecting data

2 Using detector redundancy

3 Join AOT bands together

4 Smoothing and rebinning data

The easiest data to work with is the AAR data, as this contains fluxes against wavelength. The SPD and ERD can be worked with if required, but will require a more detailed knowledge of the instrument and software normally available only to the SOC or instrument team.

2.4 Having a quick-look at the data

You can now plot the data to get a quick look. Be aware that the AAR data covers all wavelengths seen by the instrument. There may be several wavelength regions containing flux data interspersed with regions without any data. Therefore it may be more useful to plot selected regions, or to extract subsets of the data to work with.

2.5 Selecting data

As explained in section 8.2.14, any flux data for which the Run flag (see table 9.7) is set and that can have an unique wavelength assigned to it is output in the AAR. Therefore some serendipitous data may be present in the AAR. This data may be useless (as in data from a detector array that was insufficiently illuminated).

Therefore all data should be examined, band by band, and any useless data thrown away.

Examples of data that can be considered bad includes data where the flag word SWSPFLAG or SWAAFLAG (see Table 9.8 for a discussion of it's contents) have:

1 bits 0 and/or 1 (corresponding to FLAG values 1, 2 or 3) set, indicating glitches. Be careful with fast AOT 1's though, as lines may be mistaken for glitches – see section 8.5, "Glitch removal effects on spectral lines in fast speed AOT1 observations".

2 bits 2 or 3 (corresponding to FLAG values 4 or 8) set, indicating partly or totally out of limit.

3 bit 4 (corresponding to FLAG value 16) set, indicating no data

4 bits 5, 6 and 7 (corresponding to FLAG value 224) set, indicating multiple order

5 no bits set, indicating no order.

Such data is in the SPD though, so users should AND SWSPFLAG/SWAAFLAG with the above values and mask out data so affected.

Data taken outside band regions should not be trusted. For example, band 1A data beyond $2.6\mu m$ should not be used. The AOT band associated with a particular line in the AAR file can be obtained from SWAADETN (ref Table 9.12) and masking the order bits in SWAAFLAG and aperture bits in SWAASTAT (ref Tables 9.8 and 9.7). If the wavelength in SWAAWAVE is outside an AOT band as defined by the detector number/order/aperture combination, the limits of which are given in Table 3.2, then the data should not be trusted. Alternatively, the band identification number for AOT 1's is kept in the SWAALINE field (ref section 9.4.2, "SWAALINE and SWAASCNT").

2.6 Using Detector Redundancy

No combining of up-down scans (see section 4.6.1) is carried out by the SPG pipeline. This is because the up part of the scan may have a different zero level from the down part, or a line may have a different shape in the two scans, both due to memory effects (see section 5.8). Also, one of the up-down scan pair may have been affected by a 'scan jump', ref section 5.7.

Users should check the two scans of their data to ensure features are present in both and that the scans are not behaving differently – SPD is probably the best dataset for this. If they do behave differently care should be taken analysing the data and in some cases it may be necessary to throw away any affected data.

Assuming up-down scans are present in your data and both scans are similar, you can either attempt to get the information you want (e.g linewidths) from each scan individually, or combine the scans then get the information.

2.7 Join AOT bands together

If you have AAR data spanning two or more AOT bands you can try to join the bands together. No attempt is made to do this in the SPG pipeline as the data in different bands may have a different zero level or may be affected differently by memory effects. Note that observations of extended sources through different apertures are not corrected for the different aperture sizes.

2.8 Smoothing and Rebinning data

If the AAR data is badly affected by noise or fringes, smoothing may be the best option. The AAR data have already had the fringes taken out by the best RSRF data available (which is present as the CAL25_x files). Do not attempt to remove any fringes out of AAR using the CAL25_x files. The CAL25_x files may be used to try and remove the fringes out of SPD.

Note the warning in section 6 concerning confusing the effects of fringes with spectral lines.

2.9 Current Caveats on SWS Data Products

Excellent results have been obtained from SWS, with very low noise measured, especially in band 1. The basic Off-Line Processing (OLP) products can be used in the analysis of your data, with special processing only needed for exceptional cases.

There are, however, some points to be aware of concerning the data products from OLP Version 7, primarily that the AOT testcases do not cover the entire parameter space of SWS observations and there are sets of input data for which the code gives non-optimal results. Many AOT testcases have been selected to test OLP V7, and all have been reduced and checked. However, these do not cover the entire range of possible SWS observations. Thus while there is no reason to believe the pipeline does not work correctly, it has not been proven correct for all input data.

Cases for which the pipeline is not optimised, and is therefore known to fail include:

1 Memory Effects

Memory effects are not accounted for in OLP V7 and so may affect the data. See section 5.8, "Memory Effects", for a discussion of this.

2 Low flux cases.

Cases where the continuum is weak can cause problems for dark current subtraction, especially when memory effects are included. When the amount of flux falling on the detector is small, there may be cases where (flux plus dark current plus noise) is less than the (dark current plus noise). Dark current subtraction then results in negative fluxes in the AAR product. The limiting flux for this can be quite high, e.g. of the order of a few Jy for band 2, and the actual level might be determined by the scan rate and/or number of scans at a required S/N. See section 5.4, "Detector Noise & Dark Current" for a discussion of dark currents and noise.

Such problems can also manifest themselves as distortions in the spectral energy distributions of low flux sources, especially noticeable in AOTs 1 & 6.

3 Fast SWS01 AOTs

There are two possible problems with fast AOT 1's.

- Datapoints near unresolved lines marked as glitched. This is because the grating is moving during one reset interval, which is not the case for the other AOTs. If the grating scans over an unresolved line the slope of the detector output for one reset interval will deviate from a straight line, leading the OLP software to incorrectly conclude a glitch is present. See section 8.5, "Glitch removal effects on spectral lines in fast speed AOT1 observations", for more information on this.
- The calculated flux for a line depending on actual wavelength of the peak of the line. This is because the observed fringe pattern is smeared version of the Relative Spectral Response Function (RSRF), due to the grating moving.

The result of both these effects is that the net line flux and the line profiles can be appreciably affected.

4 Flux/aperture points

SWS has three apertures (four if the virtual Fabry-Pérot aperture is counted) of different sizes and, for the grating, four detector bands each with detectors of different sizes. Observers of extended sources who switch between apertures/detector bands must be aware that their reported fluxes will jump as the apertures/detector bands change. This jump may be enhanced if incorrect target coordinates are used.

5 RSRF files

While the RSRF files have been greatly improved sections 6.5.1, "Present quality of RSRFs" and 6.6.1, "Spurious Spectral Features seen in Band 2C" should be read.

Chapter 3

Instrument overview

3.1 Introduction

The Short Wavelength Spectrometer (SWS) onboard ESA's InfraRed Space Observatory (ISO) provided medium and high spectral resolution in the wavelength region 2.38–45.2μm. Its two nearly independent grating spectrometers had a spectral resolution of $R \approx$ 1,000–2,000, corresponding to a velocity resolution of $\Delta v \approx$ 300-150 km s^{-1}. By inserting Fabry-Pérot (FP) filters, one for the range 15–26μm (with capability down to 11.4μm at reduced resolution) and the other for the region 26–35μm (with capability to 44.5μm at reduced sensitivity), the resolution could be increased to $R \approx 30,000$, $\Delta v \approx 10$ km s^{-1}.

The SWS wavelength range is of great scientific interest, not only because it is here that cool objects in the temperature range 1500–80 K radiate the bulk of their energy, but also because of its rich variety of atomic, ionic, molecular and solid-state spectral features. These provide unique and excellent tools for studies of the physical and chemical processes in the universe, especially of those regions optically hidden by interstellar dust. The SWS spectral resolution allows probing of kinematic processes in a variety of objects ranging from nuclei of galaxies to planetary atmospheres.

3.2 The Instrument

Fig. 3.1 gives an impression of the lay-out of the SWS, an optical block diagram is shown in Fig. 3.2, and an optical schematic is shown in Fig. 3.3.

Light from the telescope is reflected into the SWS by the ISO pyramidal mirror. The SWS had three entrance apertures, each with its own dichroic beamsplitter feeding the Short Wavelength section and the Long Wavelength section. The appropriate entrance aperture was selected by specific pointing of the ISO satellite. A four-position selection mechanism permitted opening of any one of these apertures or blocking of all three – see section 3.3.1 for further details.

Each grating had its own scanning mechanism, enabling the use of both parts of the spectrograph at the same time, albeit through the same aperture. Wavelength scanning was achieved by rotating a flat mirror close to each grating in discrete scan steps.

After reflection from the gratings, the light almost retraced its path and, by means of small-diameter re-imaging relay optics, the high resolution spectral image of each wavelength band was re-imaged onto the detector block. These relay optics have various functions:

– they relayed the high resolution image to a more easily-accessible location on the detector block,

– they changed the relative opening of the beam to a value that was optimised to the detector

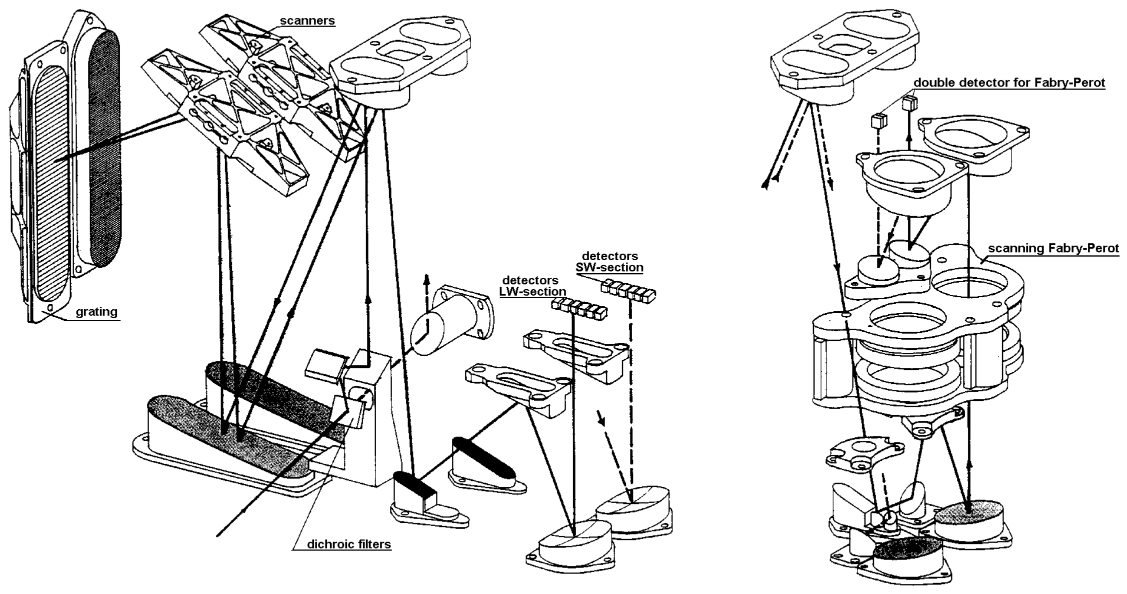

Figure 3.1: Lay-out of SWS

dimensions,
– they enabled efficient straylight rejection.

To use the F-P's, the radiation returning from the LW grating was collimated again, transmitted through a tunable F-P interference filter and imaged onto separate detectors in the detector block. This second light path is also shown in Figure 3.2. The two F-P's were mounted on a single pair of parallel plates. Their separation and parallelism could be varied by changing the currents in three pull coils.

The wavelength coverage of the SWS is broken down into 12 grating bands and 5 FP bands. For historical reasons they are named Astronomical Observation Templates (AOT) bands, and are listed in tables 3.1 and 3.2. The AOT bands are combinations of detector array, aperture and grating orders such that the relevant detector array sees an unique order. Other detector arrays may see only one order or may see a mixture of orders. The wavelengths of the SWS data products will not be on an equidistant wavelength grid and there may be gaps over certain wavelength ranges. There may also be flux jumps between spectra taken in adjacent AOT bands.

The SW and LW gratings are associated with 4 different detector arrays of 12 elements each. The 2 SWS Fabry-Pérots are associated with 2 double detectors. All $4 \times 12 + 2 \times 2 = 52$ detectors are operated simultaneously. The correspondence between detector number, bands and detector material is shown in table 3.1. At any given time, the astronomical source of interest to the observer was centered into one and only one of the three SWS apertures, feeding light on many, or all, of the 52 detector elements via two rotatable scanning mirrors, one for each grating system. While it was possible to find scanner settings such that all of the detector arrays will contain valid data, the instrument was normally operated such that only one or two of the detector arrays received *one* order of the grating spectrometer, the other four or five receiving a mixture of orders. The observer will, however, receive data from all 52 detectors.

Table 3.1: Detector definition for the SWS AOT bands

	band		order	aperture		area[5]	detector	detector	wavelength[8]
	name	number[15]			filter	(″×″)	type	number	(μm)
SW[1]	1A	1	4	1	t[3] Al_2O_3	14-20	InSb	1 - 12	2.38 - 2.60
SW	1B	2	3	1	t Al_2O_3	14-20	InSb	1 - 12	2.60 - 3.02
SW	1D	3	3	2	t LiF	14-20	InSb	1 - 12	3.02 - 3.52
SW	1E[13]	4	2	2	t LiF	14-20	InSb	1 - 12	3.52 - 4.08
SW	2A[13]	5	2	2	t LiF	14-20	Si:Ga	13 - 24	4.08 - 5.30
SW	2B	6	1	2	t LiF	14-20	Si:Ga	13 - 24	5.30 - 7.00
SW	2C[9]	7	1	3	t SrF_2	14-20	Si:Ga	13 - 24	7.00 - 12.0
LW[2]	3A	9	2	1	r[4] Al_2O_3	14-27	Si:As[14]	25 - 36	12.0 - 16.5
LW	3C	10	2	2	r LiF	14-27	Si:As[14]	25 - 36	16.5 - 19.5
LW	3D	11	1	2	r LiF	14-27	Si:As[14]	25 - 36	19.5 - 27.5
LW	3E	12	1	3	r SrF_2	20-27	Si:As[14]	25 - 36	27.5 - 29.0
LW	4	13	1	3	r SrF_2	20-33	Ge:Be	37 - 48	29.0 - 45.2
F-P1	5A	15	3	1	r Al_2O_3	10-39	Si:Sb	49 - 50[10]	11.4 - 12.2
F-P1	5B	16	2	1	r Al_2O_3	10-39	Si:Sb	49 - 50[10]	12.2 - 16.0
F-P1	5C	17	2	2	r LiF	10-39	Si:Sb	49 - 50[10]	16.0 - 19.0
F-P1	5D	18	1	2	r LiF	10-39	Si:Sb	49 - 50[10]	19.0 - 26.0
F-P2	6	19	1	3[12]	r SrF_2	17-40	Ge:Be	51 - 52[11]	26.0 - 44.5

Notes:

1. SW = short-wavelength grating region

2. LW = long-wavelength grating region

3. t = transmission

4. r = reflection

5. 'Aperture area' refers to the dimensions of the SWS entrance apertures projected on the sky – see section 3.3

8. AOTs SWS06 and SWS07 (SW grating) use finite (but small) band overlaps

9. Band 2C ends at 13.16 μm for AOT SWS07.

10. Detector 49 is used for FP observations in band 5.

11. Detector 51 is used for FP observations in band 6.

12. These observations are made through the virtual aperture 4 (see section 4.5) but are flagged in the data as being through aperture 3.

13. The band 1E/2A limit changed from 4.05 to 4.08 μm after the end of PV.

14. These are Back-illuminated Blocked impurity Band (BIBIB) detectors.

15. Band numbers are stored in the AAR and are explained in section 9.4.2, "SWAALINE and SWAASCNT".

Table 3.2: Wavelength range definition of the SWS AOT bands

	band name	band number[15]	detector number	wavelength[8] (μm)	resolution[6] ($R = \lambda/\Delta\lambda$)	L^7_{AOT}
SW[1]	1A	1	1 - 12	2.38 - 2.60	1870 - 2110	756
SW	1B	2	1 - 12	2.60 - 3.02	1470 - 1750	1043
SW	1D	3	1 - 12	3.02 - 3.52	1750 - 2150	1282
SW	1E[13]	4	1 - 12	3.52 - 4.08	1290 - 1540	867
SW	2A[13]	5	13 - 24	4.08 - 5.30	1540 - 2130	2115
SW	2B	6	13 - 24	5.30 - 7.00	930 - 1250	1377
SW	2C[9]	7	13 - 24	7.00 - 12.0	1250 - 2450	4276
LW[2]	3A	9	25 - 36	12.0 - 16.5	1250 - 1760	2047
LW	3C	10	25 - 36	16.5 - 19.5	1760 - 2380	1879
LW	3D	11	25 - 36	19.5 - 27.5	980 - 1270	2524
LW	3E	12	25 - 36	27.5 - 29.0	1300	500
LW	4	13	37 - 48	29.0 - 45.2	1020 - 1630	4324
F-P1	5A	15	49 - 50[10]	11.4 - 12.2	20600 - 24000	
F-P1	5B	16	49 - 50[10]	12.2 - 16.0	24000 - 32000	
F-P1	5C	17	49 - 50[10]	16.0 - 19.0	32000 - 34500	
F-P1	5D	18	49 - 50[10]	19.0 - 26.0	34500 - 35500	
F-P2	6	19	51 - 52[11]	26.0 - 44.5	29000 - 31000	

Notes:

1. SW = short-wavelength grating region

2. LW = long-wavelength grating region

6. The resolution given is that obtained when observing an extended source

7. L_{AOT} = total number of scan steps in AOT band

8. AOTs SWS06 and SWS07 (SW grating) use finite (but small) band overlaps

9. Band 2C ends at 13.16 μm for AOT SWS07.

10. Detector 49 is used for FP observations in band 5.

11. Detector 51 is used for FP observations in band 6.

13. The band 1E/2A limit changed from 4.05 to 4.08 μm after the end of PV.

15. Band numbers are stored in the AAR and are explained in section 9.4.2, "SWAALINE and SWAASCNT".

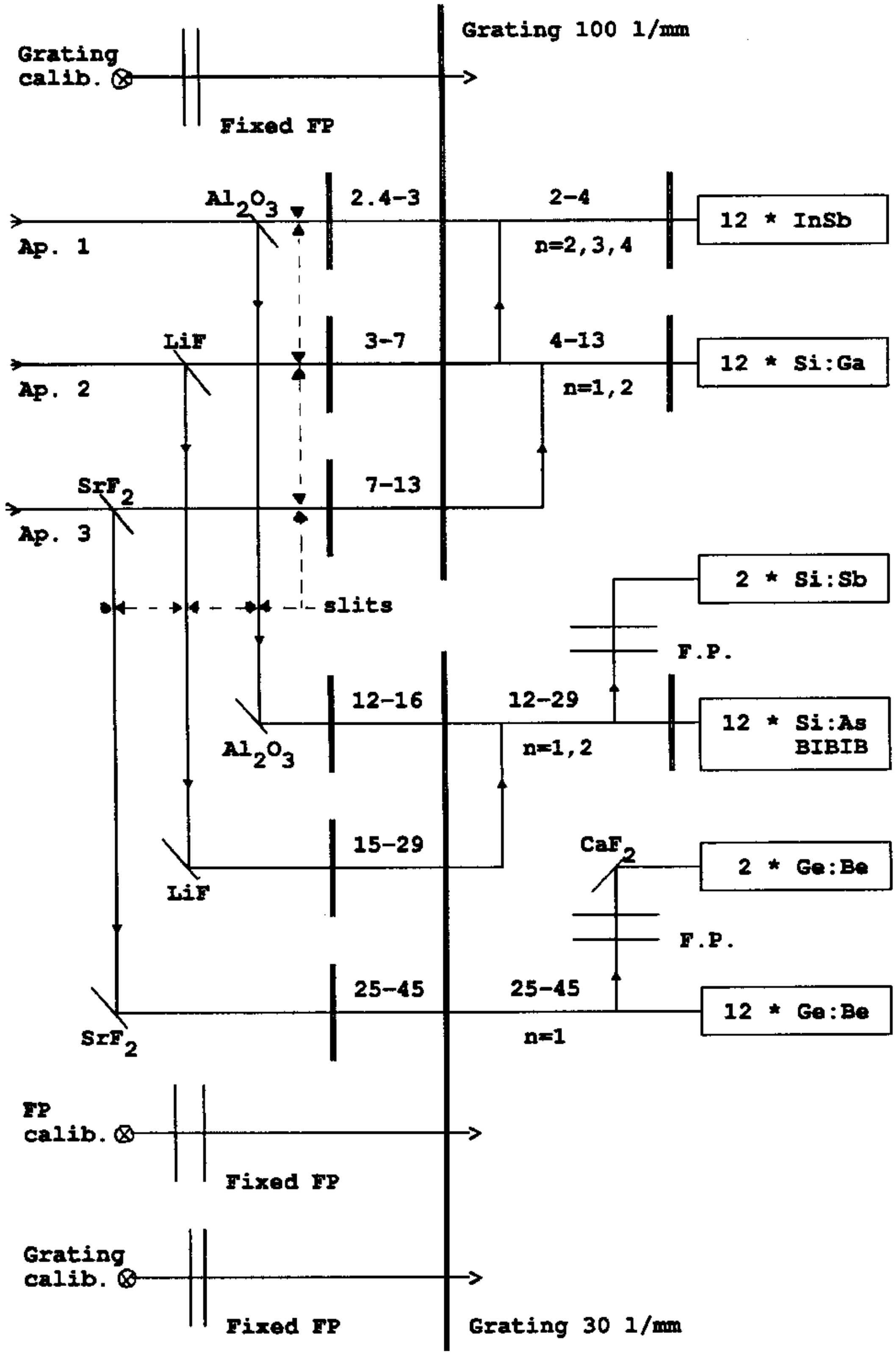

Figure 3.2: Block diagram of the SWS. The diagram shows the optical functions of the spectrometer, excluding its internal calibration sources, but including the shutter, the collimation and the imaging optics. It excludes band 3E.

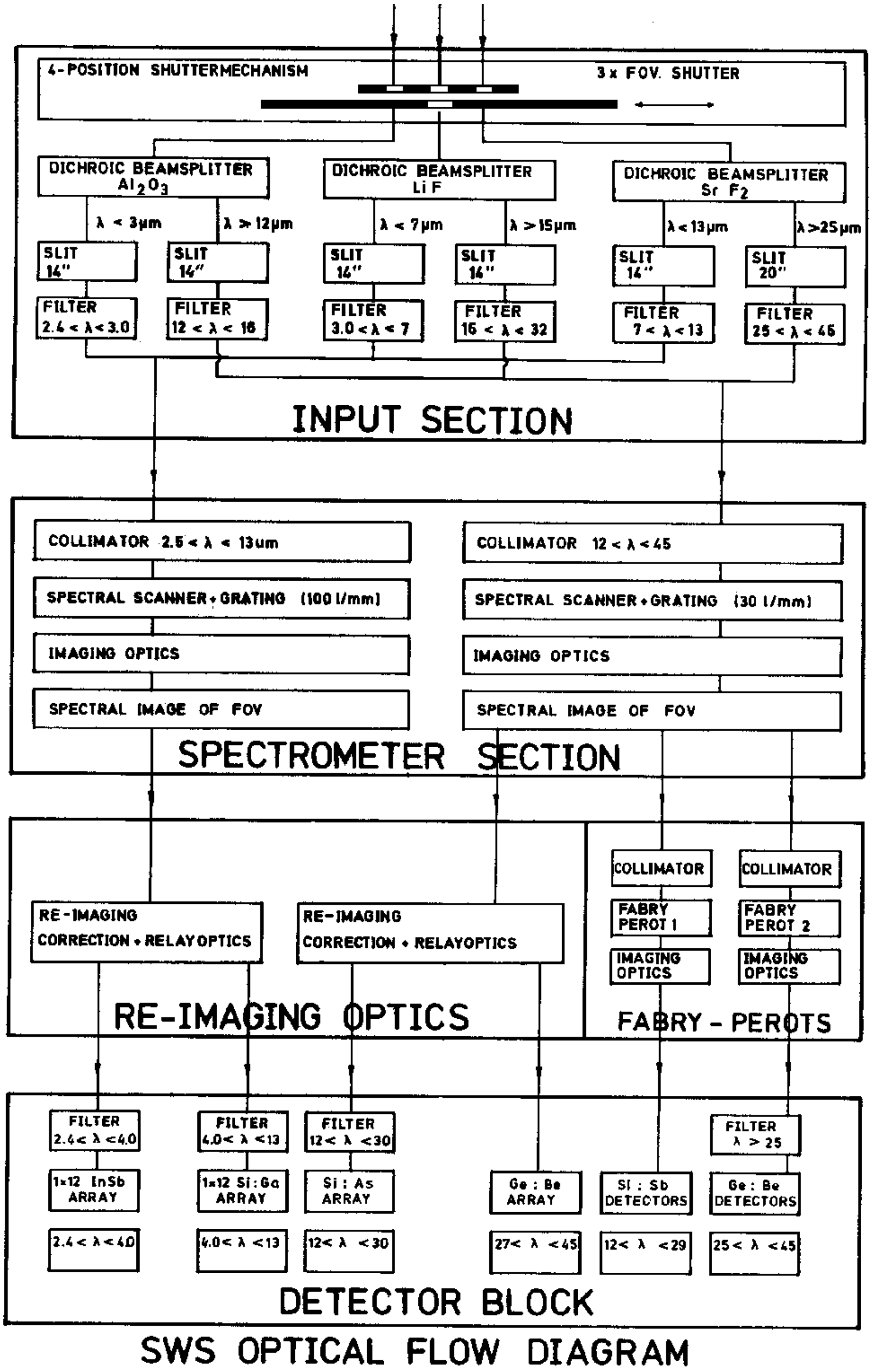

Figure 3.3: Optical schematic of the SWS. The diagram indicates the location of the six separate entrance slits behind the dichroics after the three apertures. It shows all the spectral order-separation filters and the internal wavelength calibrators. The shutters, collimation and imaging optics and band 3E have been left out

3.3 Entrance Apertures

3.3.1 Optics and detector fields of view

SWS has three different apertures (aperture 4, used by the LW FP, is a virtual aperture offset slightly from aperture 3 to increase the amount of light falling onto the FPs and hence improve efficiency, see section 4.5). A shutter system allows the selection of one aperture, while closing off the other two (the spacecraft pointing has to be adjusted so that the target is imaged onto the selected aperture).

Each aperture is used for two wavelength ranges, one for the short-wavelength (SW) section of the spectrometer and one for the long-wavelength (LW) section. Since those two sections are otherwise independent, two wavelength ranges can be observed simultaneously.

Beamsplitters, consisting of Reststrahlen crystal filters (Al_2O_3, LiF and SrF_2), are located behind the apertures. The beams transmitted by the first crystal enter the SW section; the reflected beams enter the LW section, after a second reflection against identical material. As is seen in the schematic (Fig. 3.3), the actual entrance slits are located behind the beam-splitting crystal. In this way, each of the 6 possible input beams has its own slit. All slits have been given the same width, except for the SrF_2 reflected input, which has a larger width, adapted to the larger diffraction image at these wavelengths (see Table 3.2). The slits are in the focus of the telescope, in the plane where the sky is imaged.

In the direction perpendicular to the dispersion, the slits are oversized. There the fields-of-view are determined by the dimensions of the detectors. The cross-dispersion dimensions are different for almost all detector bands. Since the imaging of the slits onto the detectors (or *vice versa*) is imperfect due to aberrations and diffraction, the short sides of the fields of view (detector edges) are more fuzzy than the long sides (the slit jaws).

Small offsets of the fields of view perpendicular to the dispersion can be caused by alignment errors. The internal alignment specification adhered to amounts to 10% of the detector size alias spectrum width.

The monochromatic images of the grating detectors fill about 55% of the slit widths. This means that the spectral resolution for point sources is significantly higher than for extended sources, in a ratio that is affected, of course, by diffraction.

For the Fabry-Pérot section the situation is more complex. There the monochromatic detector images just fill the slit width. With the spectral channeling by the FPs, a subtle interplay arises between spectral and spatial properties. Effectively, the spatial resolution may increase due to the narrowness of the F resonance. Point sources have less leakage in unwanted FP orders than extended sources. Spatial extent does not influence the spectral resolution of the FP's.

3.3.2 Entrance apertures and spacecraft axis

The edges of the apertures are oriented along the spacecraft y- and z-axis.

y-axis (sometimes called m), parallel to the spacecraft y-axis, is the non-dispersion, or cross-dispersion, direction.

z-axis (sometimes called n), parallel to the spacecraft z-axis, is the dispersion direction.

Along the y-axis, the effective size of the aperture is determined by the projection of the detector array on the sky. This amounts to 20, 27 or 33 arcsec for bands 1A to 4, and from 39 to 40 arcsec for the FP bands 5A to 6.

Along the z-axis, the aperture size is determined by entrance slit width (14 or 20 arcsec) for bands 1A to 4. For the FP bands 5A to 6, the aperture is effectively as wide as a detector image on the sky, i.e. either 10 or 17 arcsec.

To derive the position angle of an aperture information on the spacecrafts position on the sky must be used. This can be found in the header keywords INSTRA, INSTDEC, INSTROLL found, for example, in the AAR. Specifically, INSTROLL is the angle, measured anticlockwise, between north and the spacecraft z-axis (ref. the ISDM for a description of these keywords). See also section 5.10.

Information on how the spacecraft pointing can affect observations of extended objects can be read in the document 'Status of study of AOT02 line profiles and fluxes on NGC6543', by H. Feuchtgruber issued 2 June 1998. In this case the observed line fluxes varied by 10% over the course of several months. This was attributed to the spatial extent of NGC 6543, the SWS slit size projected on the sky and the change in roll angle between the observations. This is also discussed in section 5.10.

3.3.3 Beam Profile

Beam profiles for all bands were derived during flight by raster observations of point sources (stars). An example of a band 1 beam profile is shown in figure 3.4. More information on the beam profiles can be found in the document 'SWS Beam Profiles and ISO Pointing', by A. Salama, 9/9/98, which should be consulted by observers needing further information on the beam profile of the various bands.

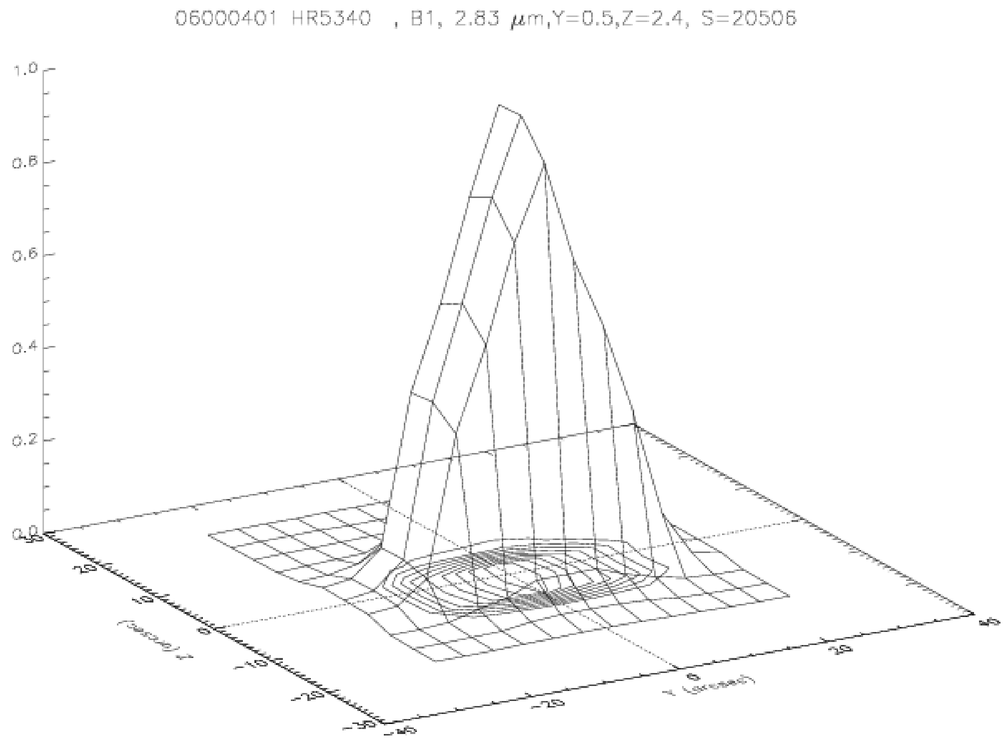

Figure 3.4: Example beam profile for band 1

3.4 SWS Detectors and operation

The detector material is shown for all bands in table 3.2. The InSb, the Si:As (BIBIB) and the Si:Ga detectors are operated at a temperature of 4-5 K; the Si:Sb detectors for the FP are heated to 10 K (FP); and the Ge:Be detectors are cooled by a thermal conductor to the 2 K cryostat heat sink. The detectors are used with integrating pre-amplifiers with non-destructive read-out, employing heated JFET's.

As photons fall onto the detectors the current generated charges up a capacitor (one per detector). The voltage across this capacitor is read-out non-destructively 24 times a second and digitised into a bit value between 0 and 4095. After a set interval the capacitor is discharged with a destructive readout (basically short-circuited). The time interval between two detector resets is automatically determined from the user's input data (flux and SNR, or execution speed) and is either 1, 2 or 4 seconds. This destructive readout affects the readout electronics, which then take some time to return to normal.

Figures 5.7 and 5.9 give examples of data in which the individual datapoints from the non-destructive readouts and reset pulses can be seen.

To observe faint sources, integrations over several reset intervals are used. Raw data is saved in an Edited Raw Data (ERD) file, with an ERD file for one second consisting of an array of 52 ramps of 24 read-out's each. The Standard Processed Data (SPD) and Auto-Analysis Results (AAR) files contain for each detector a single flux estimate for each reset interval. As mentioned previously, normally only a subset of the array will contain clearly interpretable data.

Examples of ERD, SPD and AAR for each AOT are shown in sections 4.2 to 4.5 with the processing chain that generates SPD & AAR from ERD discussed in chapter 8.

Chapter 4

AOT overview

4.1 AOT Introduction

Astronomical observations with ISO are carried out via observing modes known as AOTs, Astronomical Observation Templates. These are modes in which the basic operating parameters for the instruments are predefined (e.g. which sub-instrument to use at what wavelength resolution), leaving the user to select wavelengths to scan between, enter flux levels etc.

There are two main observing modes with the SWS.

1. **Grating-Only Observations (Medium spectral resolution)**. The spectral region of interest is directed to an array of 12 detectors. The spectral range instantaneously covered by the array is about 8 grating resolution elements, with gaps between the individual detectors (except for Band 3). For an observation, the grating is scanned in small steps to fully sample the desired wavelength range and provide a certain redundancy in case of detector failures or detector memory effects. Different scan schemes are used to obtain high fidelity line profiles, scans of wavelength ranges, and quick low-resolution full scans of the SWS wavelength range.

2. **Fabry-Pérot / Grating Combination Observations (High spectral resolution)**. The wavelength is selected by setting the Fabry-Pérot unit to a gap where one of the transmitting orders matches the correct wavelength. The F-P unit is then scanned in steps of about 1/4 F-P resolution element. The grating is used as an order sorter, with the maximum of the grating transmission tuned to the desired wavelength so that unwanted F-P orders are suppressed. Because the two detectors of a F-P detector pair look at slightly different grating resolution elements, this tuning can normally be done only for one detector. The other detector will not simultaneously deliver a useful signal as use of this redundant detector would require commanding of a slightly different grating position.

Figure 4.1 gives an overview of the wavelength ranges that could be simultaneously covered by the SW and LW or FP detector systems.

During an AOT observation, SWS scans the source spectrum by rotating the scanning mirror of the grating or varying the gap of the Fabry-Pérot. Each AOT may perform one or more exposures with an internal calibrator for a photometric check and a number of dark current measurements with the aperture closed. Hence, the data produced by any single AOT is generally of several different types.

Four AOT's, listed below, are defined for SWS. Operating modes have changed since the start of PV, and any such changes are noted in this document.

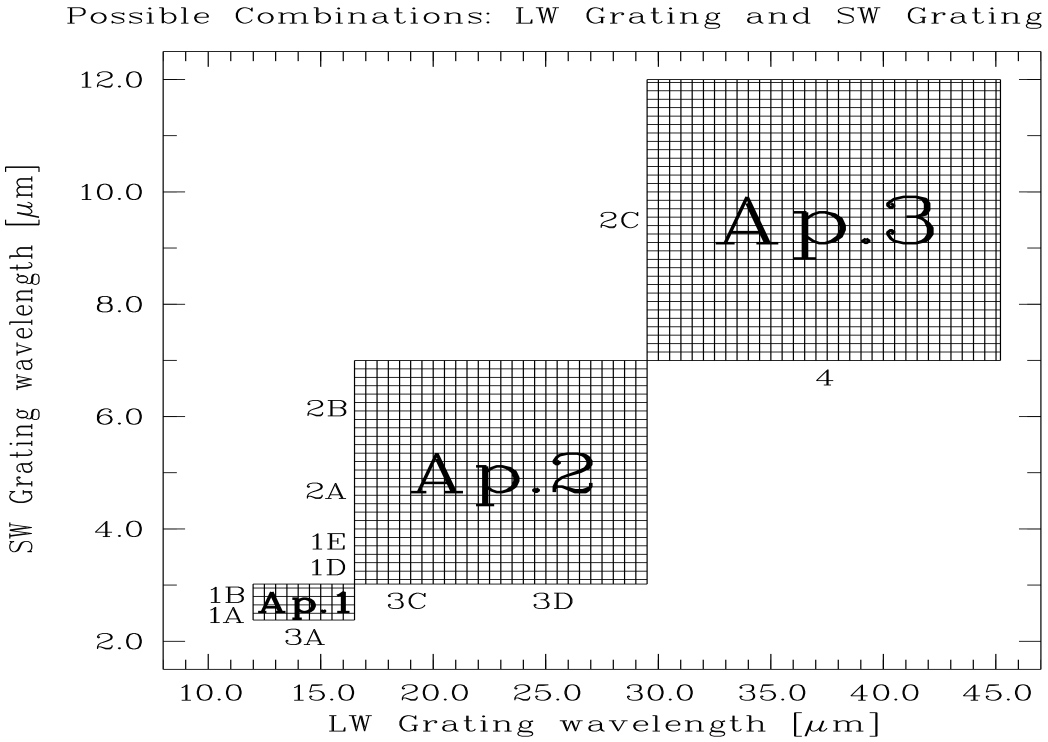

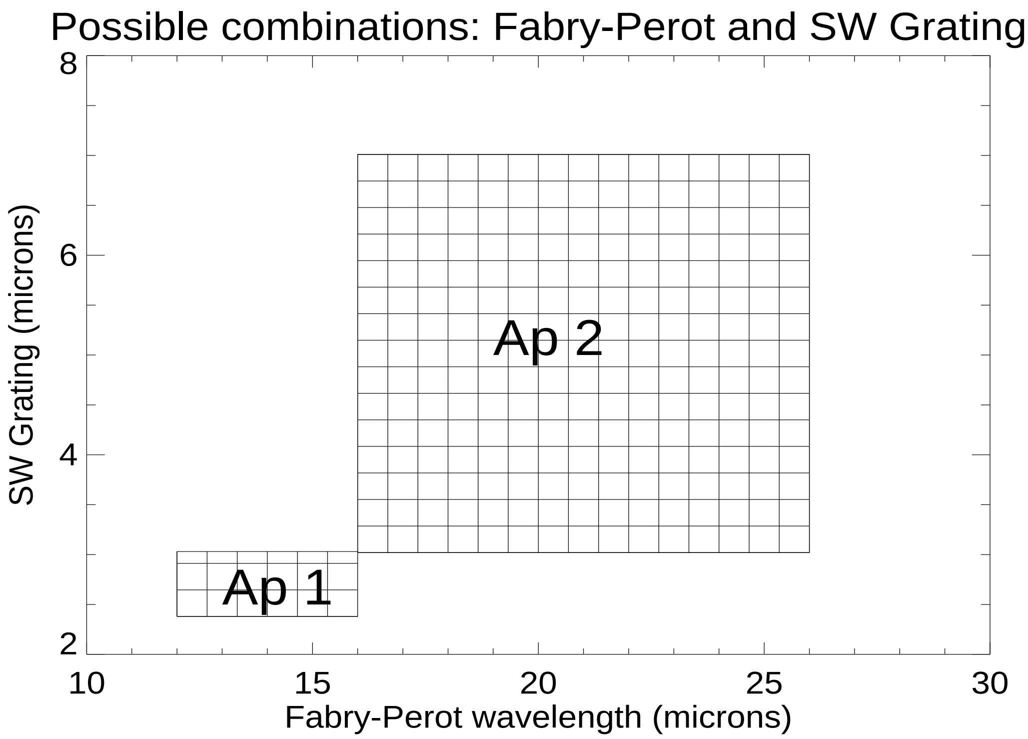

Figure 4.1: Overview of possibilities for simultaneous use of LW grating and SW grating (top) and FP and SW grating (bottom). Only combinations within the hatched area were allowed, and simultaneous observations through aperture 3 when observing with the FP were not allowed. The corresponding AOT band designations and aperture numbers are indicated.

- **AOT 1**: a single up-down scan for each aperture. It has four possible scan speeds and is primarily intended to quickly scan the entire SWS wavelength range at degraded resolution.
- **AOT 2**: slow short up-down scans, designed to measure line profiles.
- **AOT 6**: medium length grating scans with various options. Programmed as long up-down scan, possibly with reference scan. Used to observe long wavelength regions
- **AOT 7**: LW section devoted to FP observations. The SW section does almost the same as in AOT 6. In this AOT priority is given to the FP.

Tables 4.1 and 4.2 summarise their properties. In all of these AOT's the measurements of photometric check, dark current and science data are interleaved in the ERD and SPD, while the AAR only contains science detector data for which an unique wavelength could be assigned to the light falling on that detector.

Table 4.1: Various SWS AOT options

AOT #		scan direction	reference scan
1		up-down	no
2		up-down	no
6		up-down	possible
7	LW/FP	up	no
	SW/grating	up-down	possible

Example output from all AOTs are given in sections 4.2 to 4.5.

Table 4.2: Possible combinations of reset interval t_r, step size L_s in scanner steps, and number of scans n_{scan} for each of the SWS AOT's

AOT	Band									notes
SWS01	all	t_r	1	2	2	2				
		L_s	32	32	16	8				a
		n_{scan}	2	2	2	2				1 up, 1 down
		n_{int}	24	24	24	24				b
		resolution	$R/8$	$R/8$	$R/4$	$R/2$				c
		duration	1172	1944	3846	6570				seconds
SWS02	1	t_r	1	2	4	4			..	
		L_s	1	1	1	1			..	
		n_{scan}	2	2	2	4			..	up, down, etc.
		n_{int}	110	110	110	110			..	b
		duration	1.3	2.7	5.4	10.8			..	minutes
SWS02	2	t_r	1	2	2				..	
	3	L_s	1	1	1				..	
		n_{scan}	2	2	4				..	up, down, etc.
		n_{int}	110	110	110				..	b
		duration	1.3	2.7	5.4				..	minutes
SWS02	4	t_r	1	2	2				..	
		L_s	2	2	2				..	
		n_{scan}	2	2	4				..	up, down, etc.
		n_{int}	90	90	90				..	
		duration	1.3	2.7	5.4				..	minutes
SWS07 F-P	5-6	t_r	1	2					..	
		L_s								1/4 $\Delta\lambda$
		n_{scan}	2	2					..	unidirectional
										3 times or more
SWS06	1	t_r	1	2	2	4	4	4	..	
+		L_s	4	4	2	2	1	1	..	
SWS07		n_{scan}	2	2	2	2	2	4	..	up, down, etc
SW section		n_{int}	27	27	55	55	110	220	..	
SWS06	2-3	t_r	1	2	2	2	2	..		
+		L_s	4	4	2	1	1	..		
SWS07		n_{scan}	2	2	2	2	4	..		up, down, etc
SW section		n_{int}	27	27	55	110	220	..		
SWS06	4	t_r	1	2	2	2	2	2	..	
		L_s	6	6	3	2	1	1	..	
		n_{scan}	2	2	2	2	2	4	..	up, down, etc
		n_{int}	30	30	60	90	180	360	..	

Notes:

a. Effectively. Actually 8 steps per sec.

b. n_{int}, the number of integrations per resolution element. This is the product of n_{scan}, the number of detectors in an array (12), and the ratio between resolution and stepsize.

c. Approximate effective spectral resolution cf AOT 2 – see section 4.2.4.

4.1.1 ICS

In all cases AOTs were actually commanded as sets of ICSs, Instantiated Command Sequences. These are more basic instrument commands to open the shutter, start the grating moving etc. The eight ICSs defined for SWS are listed in table 4.3. The use of these ICSs is described in the following sections.

Table 4.3: ICSs

ICS	Use
SS0001	Diffuse cal (not used)
SS0002	Grating cal (dark - on low - wait)
SS0004	SW grating scan for AOT 7
SS0005	SW/LW grating scan for AOTs 1, 2 & 6
SS0006	Dark and Wait for AOTs 1 & 2
SS0007	Reset ICS
SS0008	Reset ICS
SS0009	FP LW

4.2 AOT 1

4.2.1 Introduction

AOT 1 scans the entire SWS wavelength range at a reduced spectral resolution. The scans are effectively continuous, using small and frequent steps, and on a timescale much shorter than the selected reset interval of the detector pre-amplifiers. The integration in time translates into a smoothing of the spectrum, which prevents aliasing problems due to insufficient sampling.

Table 4.4 shows the reset intervals, dwell times, stepsize and number of up-down scans for AOT 1. The reset interval is the time between detector resets, the dwell time is the time between the grating moving and the stepsize, in LVDT, is the amount by which the grating moves every dwell time. An LVDT is an internal unit of measurement of the grating position. A movement of 1 LVDT corresponds to approximately 1/8 of a resolution element. The pipeline resolution degradation is discussed in section 4.2.4.

Table 4.4: AOT 1 parameters

Speed	Duration sec	Reset interval sec	Dwell time sec	Stepsize LVDT	Number of up-down scans	Pipeline Resolution degradation
1	1172	1	1/8	4	1	7
2	1944	2	1/8	2	1	7
3	3846	2	1/8	1	1	4
4	6570	2	1/4	1	1	2

For an AOT 1 measurement, where the grating moves during a reset interval, the grating position in the SWSPGPOS field of the SPD is set to the start position of the grating during the reset interval. This contrasts with the wavelength in the SWSPWAVE field of the SPD which is the effective wavelength, i.e. calculated from the middle valid sample. For example, for a one second reset interval, the grating position is that of the first sample. As samples are thrown away due to the reset pulse (see section 5.6, operation described in section 8.2.2), the wavelength is that from sample (24 - Cal-G file 3) / 2 (assuming no data contains glitches, is all within limits etc).

4.2.2 AOT SWS01 sample time-line

The timeline an AOT 1 follows is as follows:

1. Acquisition - point aperture 1 to target
2. Dark current measurement (20 sec)
3. Single scan up, bands 1A, 1B, 3A (70 sec)
4. Single scan down, bands 1A, 1B, 3A (70 sec)
5. Dark current (20 sec)
6. Internal photometric calibration (40 sec)
7. Switch to aperture 2 (10 sec)
8. Dark current measurement (20 sec)
9. Single scan up, bands 1D, 1E, 2A, 2B, 3C, 3D (170 sec)
10. Single scan down, bands 1D, 1E, 2A, 2B, 3C, 3D (170 sec)
11. Dark current measurement (20 sec)
12. Switch to aperture 3 (10 sec)

13. Dark current (20 sec)
14. Single scan up, bands 2C, 3E, 4 (150 sec)
15. Single scan down, bands 2C, 3E, 4 (150 sec)
16. Dark current (20 sec)
17. Internal photometric calibration (40 sec)

After resetting the instrument, the AOT is composed of three SS0005 ICSs, one for each aperture. The sequence is aperture 1, 2 then 3. Each ICS 5 stars with a dark, then makes the measurement. An ICS 6 (dark) is used to make another dark current measurement after each ICS 5. A photometric check is made between the aperture 1 ICS 6 and aperture 2 ICS 5. From May 1996 an extra photometric check was added at the end of the AOT.

4.2.3 Example AOT 1 data

Figures 4.2 and 4.3 show ERD data for detectors 1, 13, 25 and 37 (bands 1, 2, 3 & 4) during an example AOT 1 observation. The signal is shown in bit values against time (ITK) and only four samples are shown out of the 24 per second for clarity. The periods when apertures 1, 2 & 3 are used, times of dark current measurements and photometric checks are indicated.

Figures 4.4 and 4.5 show the wavelengths seen by the middle detector of each band during the AOT 1 observation along with the scanner position (LVDT). The nature of up-down scans can be seen in the plots, ref section 4.6.1.

Figure 4.6 shows SPD data, in $\mu V/sec$, for detector 1 of each band against time. Figure 4.7 shows the AAR for the same observation, now as flux (Jy) against wavelength. The spread of flux between different detectors in the same band can be seen in the band 4 data. Figure 4.8 shows what can be achieved after further processing of such data in either ISAP or IA.

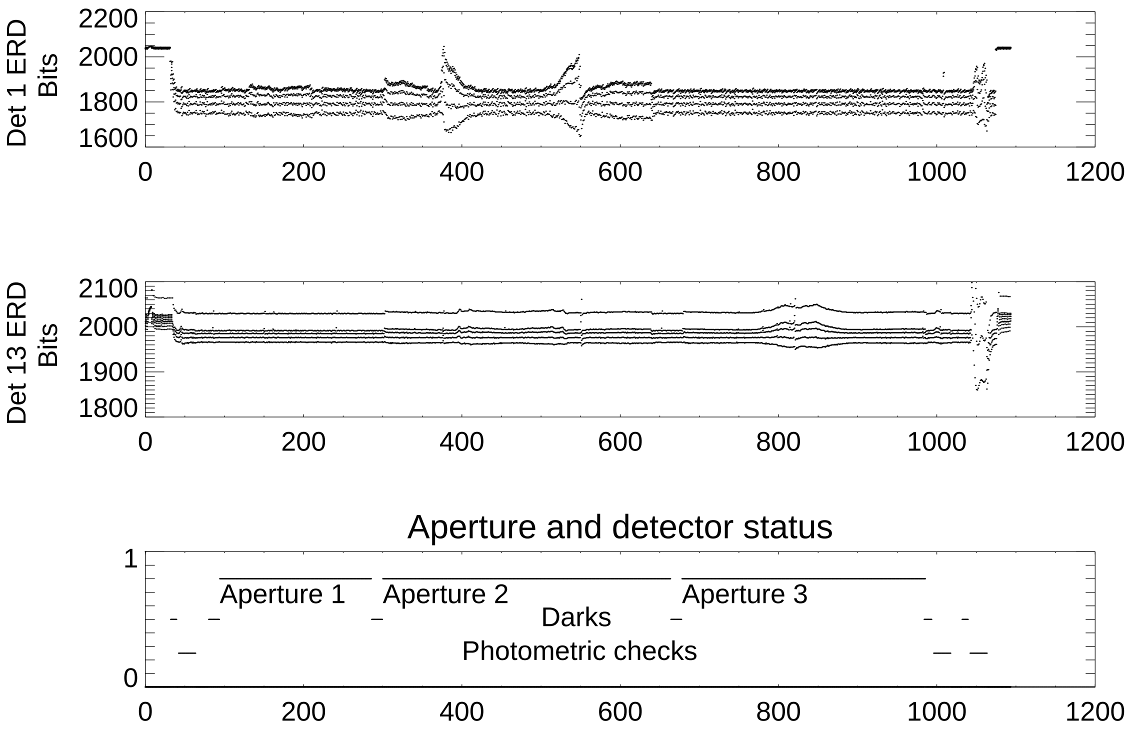

Figure 4.2: ERD band 1 & 2 data for AOT 1

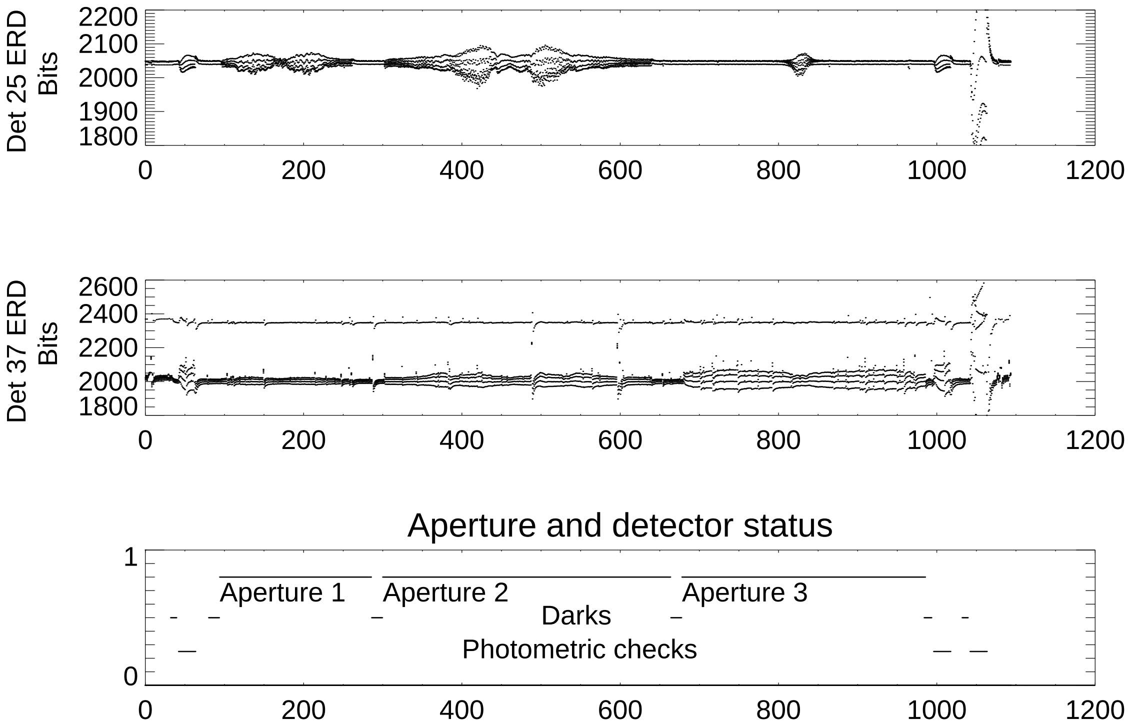

Figure 4.3: ERD band 3 & 4 data for AOT 1

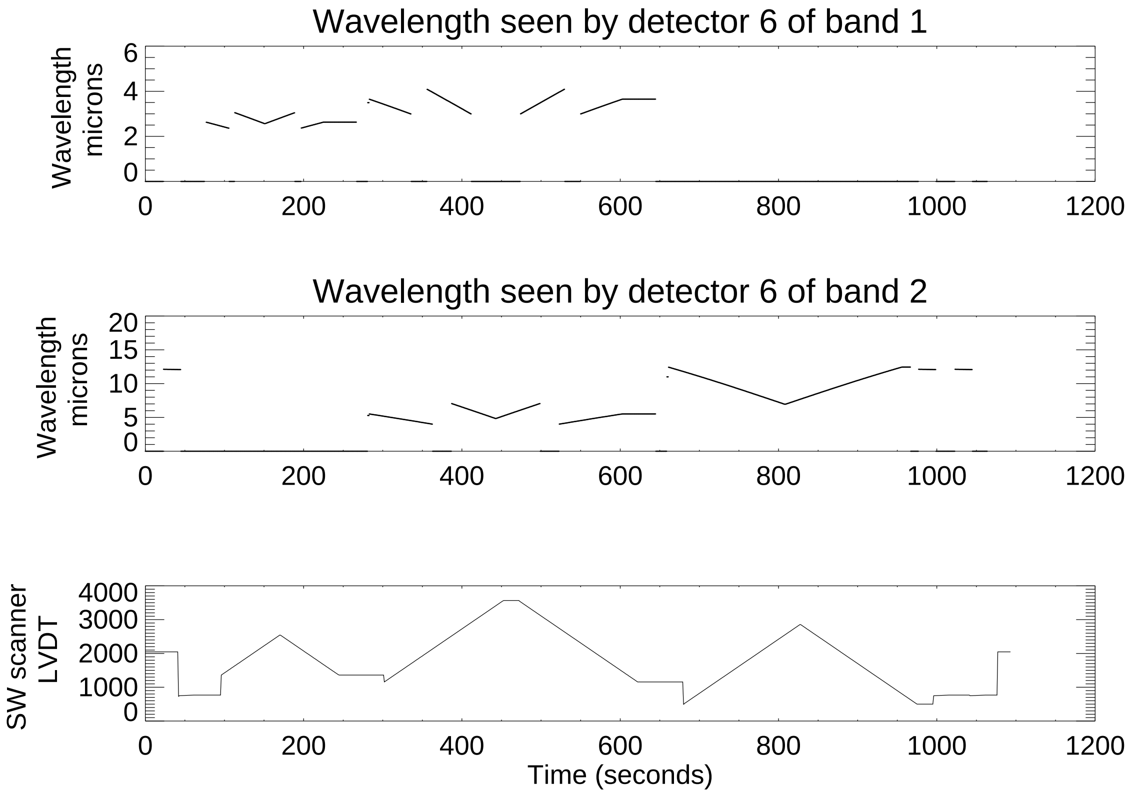

Figure 4.4: Wavelengths seen by bands 1 & 2 during an AOT 1

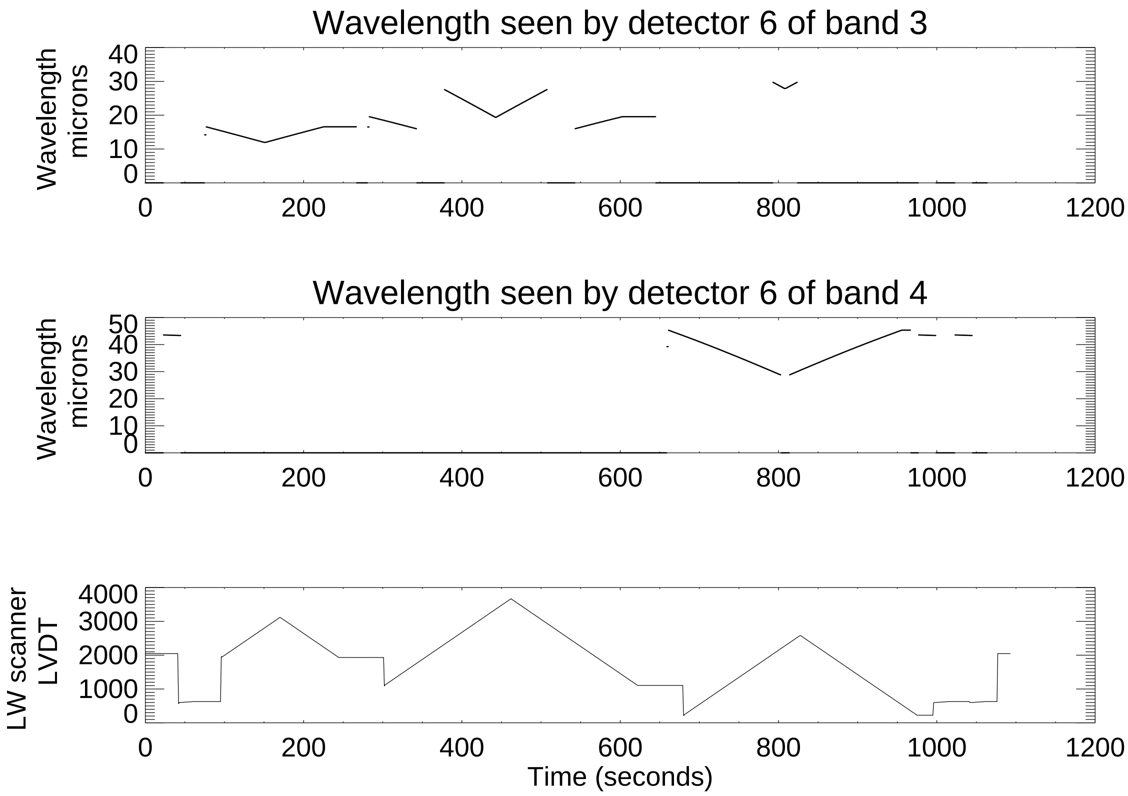

Figure 4.5: Wavelengths seen by bands 3 & 4 during an AOT 1

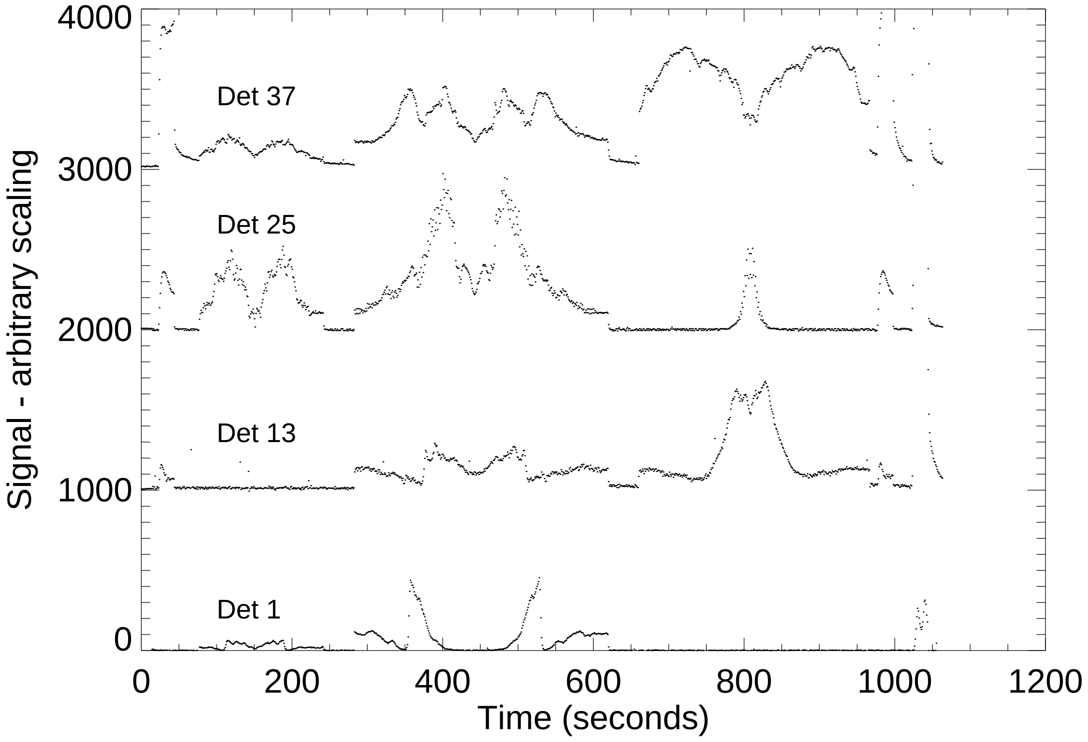

Figure 4.6: SPD data from the first detector of each band during an AOT 1. The signals have been arbitrarily scaled.

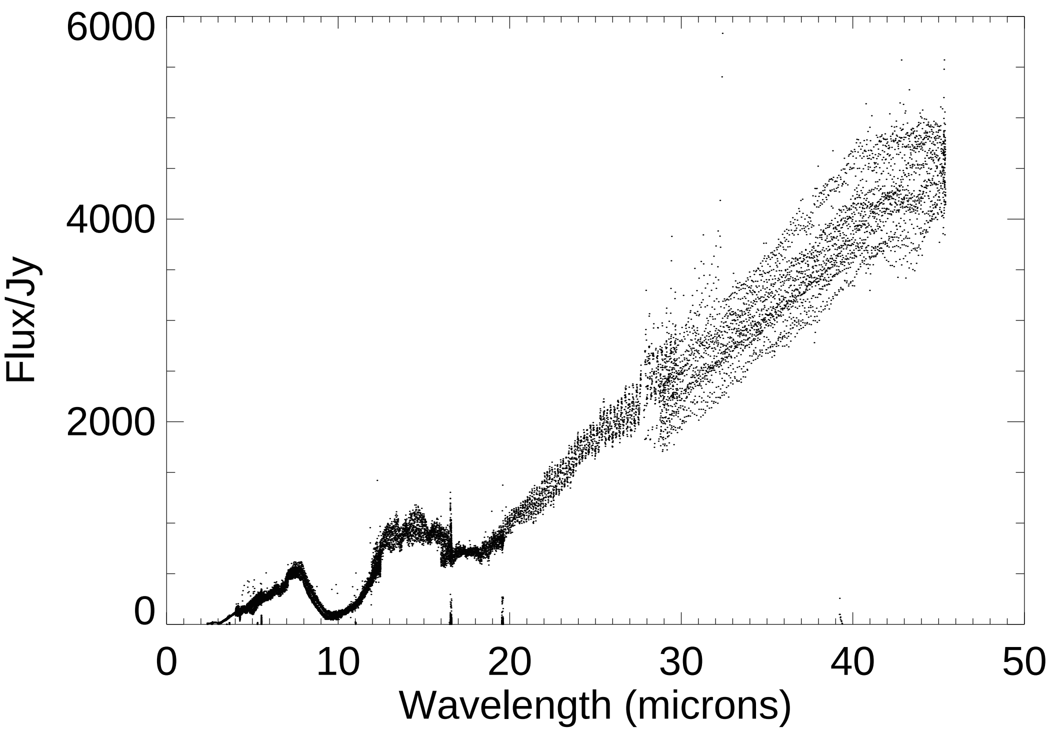

Figure 4.7: AAR data from all detectors against wavelength

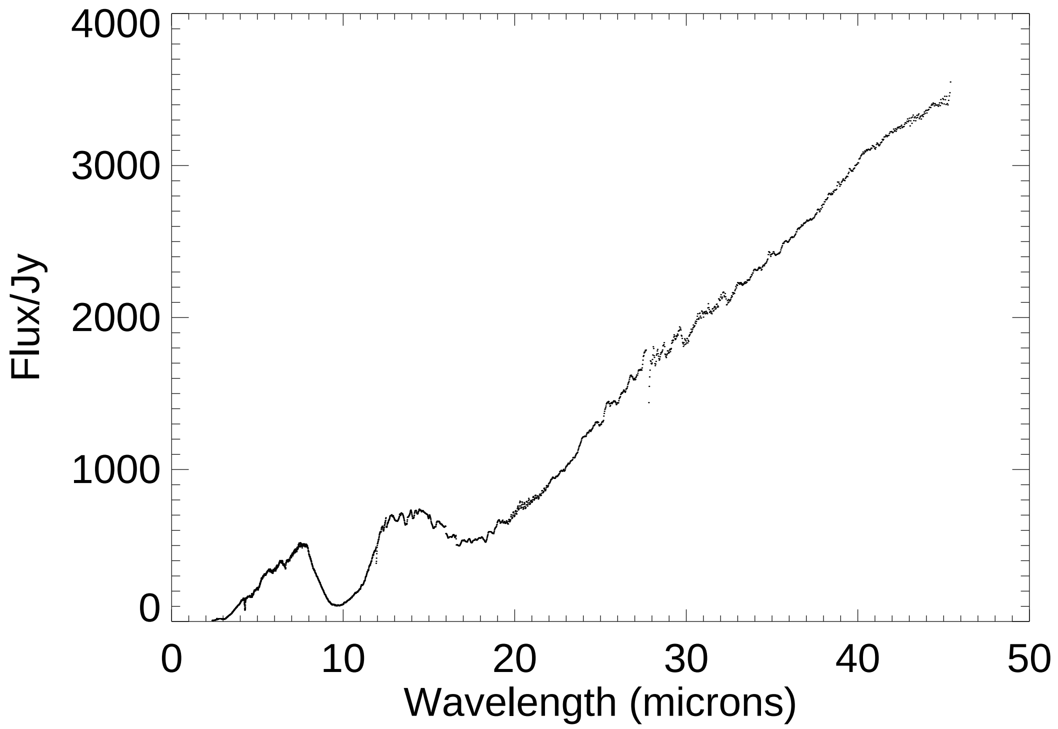

Figure 4.8: An example of what can be achieved by the further processing of OLP data

4.2.4 AOT 1 Spectral Resolution

The pipeline resolution degradation, given in table 4.4 is the amount by which the resolution of the spectrometer is degraded after the data has been processed by the pipeline. The pipeline processes data for blocks of length of the reset interval (1 or 2 seconds), during which the grating will have moved several times. The pipeline effectively smears out the resolution. Both theory and observations can be used to characterise the amount of degradation.

Theory

The degradation is given by the equation:

$$Resolution\ degradation = \frac{reset\ time}{dwell\ time} \times \frac{stepsize}{steps\ per\ res.\ element}$$

For a source filling the slit, the number of steps per resolution element is about 4.5, except for bands 3E and 4, where it is about 7.0.

Hence the effective resolution of AOT 1 data processed by the pipeline is between a factor of 2 and 7 worse than that expected from an AOT 2 pipeline product.

Observations

Preliminary measurements of the resolution of AOT 01 scans at all four speeds were carried out on observation of the PNe NGC 6543 and a speed 4 observations was carried out on the PNe NGC 7027. The assumption was made that the lines from these objects would not be resolved by the SWS01 scans. NGC 7027 contained by far the most lines of the two objects.

Table 4.5: NGC 7027 speed 4 AOT 1 resolution

Wavelength μm	Resolution $\lambda/FWHM$	Wavelength μm	Resolution $\lambda/FWHM$
2.407	1388	7.902	1123
2.626	1216	9.666	1550
3.092	1458	10.51	1697
3.741	1143	12.81	1149
4.052	1236	13.10	1186
4.487	1366	13.52	1176
4.530	1347	14.32	1357
4.654	1422	15.55	1411
5.610	818	18.71	1663
6.986	1144	24.32	1004
7.319	1149	25.89	1049
7.460	1031	34.81	1619
7.653	1227	36.02	1459

The measurements on NGC 7027 give more reliable results than those on NGC 6543. No systematic difference between the speed 4 resolutions of the two objects could be found.

Table 4.6: NGC 6543 all speeds AOT 1 resolution

Wavelength μm	Speed 4 Resolution $\lambda/FWHM$	Speed 3 Resolution $\lambda/FWHM$	Speed 2 Resolution $\lambda/FWHM$	Speed 1 Resolution $\lambda/FWHM$
7.46	983	0	0	0
8.99	1332	771	388	393
10.51	1670	0	463	538
15.55	1344	834	0	526
18.71	1718	1060	529	585
33.48	1323	677	0	560
36.00	1426	886	0	603

AOT 1 spectral resolution conclusions

The speed 4 resolutions vary between approximately 800 and 1700, increasing with wavelength per order. This is approximately half of the AOT 2 resolution, matching expectations. The FWHM remains nearly constant.

We can compare the resolutions of the different speeds using the NGC 6543 observations. The results, which match expectations, are:

R(3) / R(4) = 0.6

R(2) / R(4) = 0.3

R(1) / R(4) $\approx$ 0.3 - 0.4

4.3 AOT 2

AOT 2 is used to observe up to 64 individual lines in an objects spectrum using the SWS grating mode. The wavelength interval covered when observing a line is approximately 10 resolution elements, i.e., 3,000-1,500 km/s.

Table 4.4 shows the reset intervals, dwell times, stepsize and number of up-down scans for AOT 2. The dwell time may be higher for some merged scans.

Table 4.7: AOT 2 parameters

Detector Band	reset interval sec	dwell time sec	stepsize LVDT	Number of up-down scans
1	1, 2, 4	= reset	1	n
2,3	1, 2	= reset	1	n
4	1, 2	= reset	2	n

The band start wavelengths for AOT 2 are given in table 4.8.

Table 4.8: AOT 2 wavelength ranges

Detector Array	Detector material	Aperture	Grating order	Band start μm
1	InSb	1	4	2.38
1	InSb	1	3	2.60
1	InSb	2	3	3.02
1	InSb	2	2	3.52
2	Si:Ga	2	2	4.08[1]
2	Si:Ga	2	1	5.30
2	Si:Ga	3	1	7.00
3	Si:As	1	2	12.0
3	Si:As	2	2	16.5
3	Si:As	2	1	19.5
3	Si:As	3	1	27.5
4	Ge:Be	3	1	29.0

Note:

1. The band 2A start wavelength was changed from 4.05 to 4.08 μm in May 1996, and hence the band 1A end wavelength was moved accordingly.

4.3.1 Example AOT 2 timeline

AOT 2 is executed the following way:

- The telescope is pointed to the target position.

- A range of 10 resolution elements around each wavelength specified in the AOT is observed. Each range is scanned back and forth to provide redundancy. The minimal scan time is 100 seconds.
- Dark current measurements are only performed before and after the spectral scan.
- A photometric check is performed, using the internal stimulators.

As an example, to observe lines at 10, 12, 35 & 40 μm AOT 2 would carry out the following sequence:

1. Acquisition - point aperture 1 to target
2. Dark current measurement (20 sec)
3. Scan line at 12 μm, up (50 sec)
4. Scan line at 12 μm, down (50 sec)
5. Dark current measurement (20 sec)
6. Switch to aperture 3 (10 sec)
7. Dark current measurement (20 sec)
8. Simultaneously scan lines at 10 and 40 μm, up (100 sec)
9. Simultaneously scan lines at 10 and 40 μm, down (100 sec)
10. Dark current measurement (20 sec)
11. Simultaneously scan lines at 10 and 35 μm, up (100 sec)
12. Simultaneously scan lines at 10 and 35 μm, down (100 sec)
13. Dark current measurement (20 sec)
14. Internal photometric calibration (40 sec)

This timeline is carried out using chains of ICS 5. Each ICS 5 starts with a dark, then observes a line. ICS 6 is used to make a dark measurement when: the gain changes; the reset interval changes; or the aperture changes. Every approximately 3600 s there is a photometric check. If the entire observation takes less than 3600 s a photometric check is done at the end.

The length of the up and down scans in an AOT 2 may occasionally differ by small amounts. This is due to the runflag going down too early, signifying an early end to the observation.

4.3.2 Example AOT 2 data

Figure 4.9 shows the ERD and SPD from detector 25 as SWS scans across one particular line with an AOT 2. Figure 4.10 shows LW scanner positions, aperture information and wavelength seen by detector 25 during the same period, while 4.11 shows the SPD and AAR data from detector 25 during the same period.

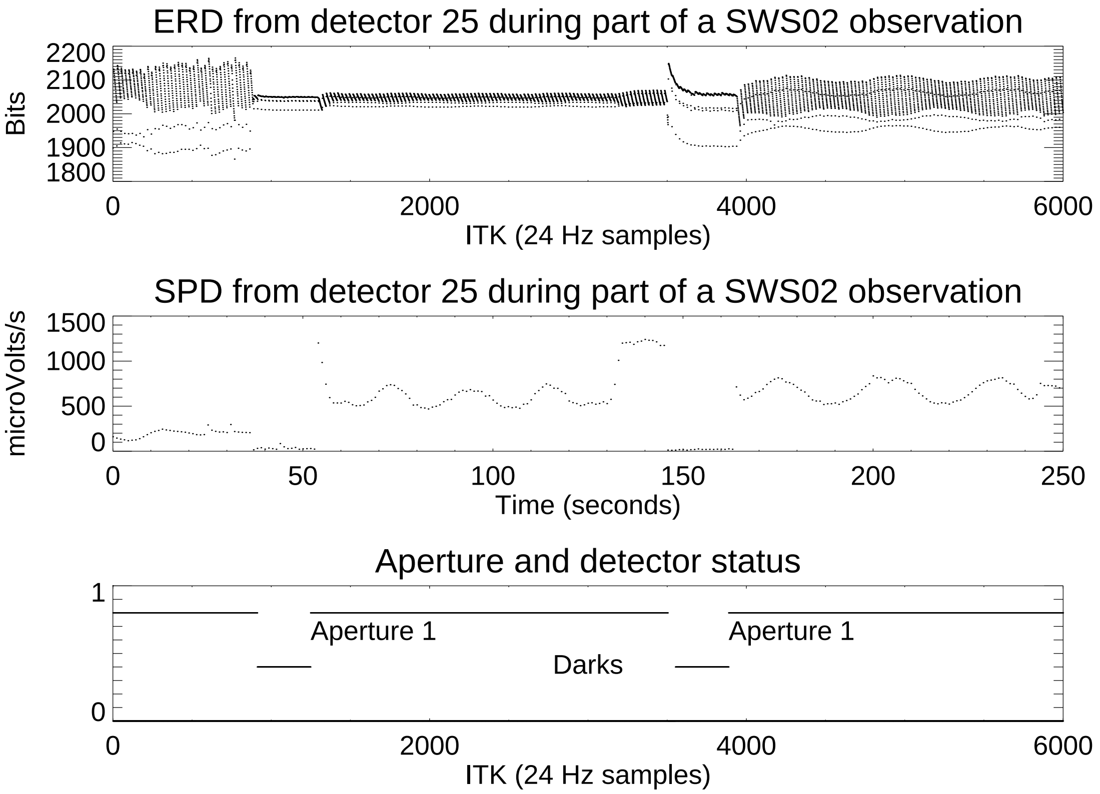

Figure 4.9: ERD and SPD data for part of an AOT 2

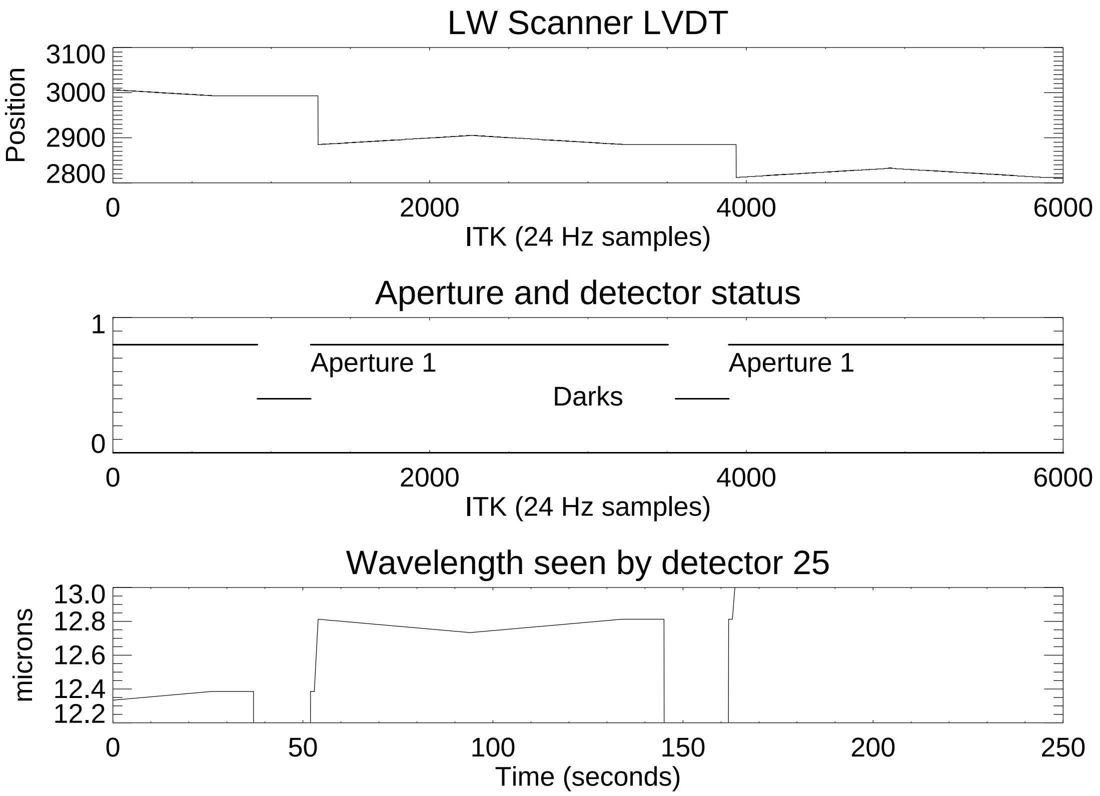

Figure 4.10: Scanner position, apertures and wavelength seen by detector 25 during an AOT 2

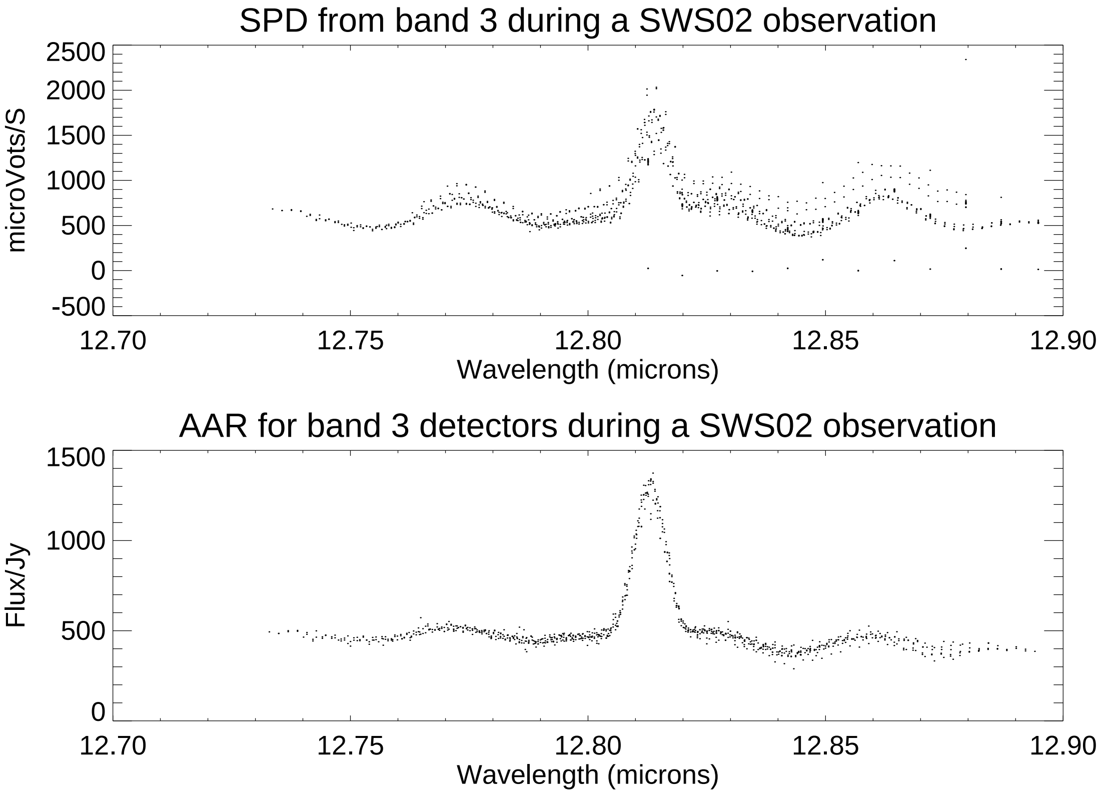

Figure 4.11: SPD and AAR data from band 3 for AOT 2

4.4 AOT 6

AOT 6 was used to make observations over wavelength ranges, as opposed to observing individual lines. Up to 64 wavelength ranges could be chosen anywhere in the SWS grating range, i.e., between 2.38 and 45.2μm, under the restriction that each range falls within one of the AOT bands (see Table 3.2).

Table 4.9 shows the reset interval, dwell times, stepsize and number of up-down scans for AOT 6. The dwell time stops at 4 secs, and for higher sensitivity the scans repeat. This was not always the case. Earlier versions of the logic (prior to May 1996) had the dwell time increasing. After May 1996 the scanning strategy used to reach the desired S/N ratios was:

1 use 1 sec reset with the max step size.

2 if the S/N ratio is insufficient use a reset interval 2 sec.

3 while the S/N ratio is insufficient and the stepsize is greater than 2 halve the stepsize.

4 if the S/N ratio is still insufficient and it is band 1 then use a reset interval 4 sec.

5 if the S/N ratio is still insufficient then increase the number of scans.

Table 4.9: AOT 6 parameters

Detector band	reset interval sec	dwell time sec	stepsize LVDT	Number of up-down scans
1	1, 2, 4	$\geq$ reset	1, 2, 4	n
2, 3	1, 2	$\geq$ reset	1, 2, 4	n
4	1, 2	$\geq$ reset	1, 2, 3, 6	n

The wavelength coverage of AOT 6 is given in table 4.10. Note that there is a slight overlap between bands. Band 3E was introduced after PV because band 3D suffered from a light leak at the long wavelength end, rendering observations around 28–29μm problematical.

4.4.1 Example AOT 6 timeline

AOT SWS06 was executed by pointing the telescope to the target position, and then for each wavelength range (or pair of merged ranges):

- A dark-current measurement is done.
- A measurement on the reference wavelength is performed, if the spectral scan is long enough to need it.
- The wavelength range specified in the AOT is observed. Each range is scanned back and forth to provide redundancy.
- The reference measurement (if any) is repeated.
- A dark current measurements is done.

Table 4.10: AOT 6 wavelength ranges

Detector Array	Detector material	Aperture	Grating order	Band	Band start μm	Band End μm
1	InSb	1	4	1A	2.38	2.61
1	InSb	1	3	1B	2.60	3.03
1	InSb	2	3	1D	3.02	3.53
1	InSb	2	2	1E	3.52	4.08[1]
2	Si:Ga	2	2	2A	4.05	5.31
2	Si:Ga	2	1	2B	5.30	7.01
2	Si:Ga	3	1	2C	7.00	12.1
3	Si:As	1	2	3A	12.0	16.6
3	Si:As	2	2	3C	16.5	19.6
3	Si:As	2	1	3D	19.5	27.6
3	Si:As	3	1	3E	27.5	29.0
4	Ge:Be	3	1	4	28.9	45.2

Note:

1. The band 1E end wavelength was changed to 4.08 μm from 4.05 μm from May 1996 onwards.

- Very long observations are interrupted by wavelength switching to the reference wavelength, as an additional photometric check.
- If a single up and down scan does not provide enough sensitivity, the measurement sequence is repeated as often as necessary
- Photometric checks using the internal calibrator are done at regular intervals, at least once per AOT.

As an example, an AOT 6 observation around 10, 12, 33 & 40 μm would have the following timeline:

1. Acquisition - point aperture 1 to target
2. Dark current measurement (16 sec)
3. Scan up around 12 μm (24 sec, fast)
4. Scan down around 12 μm (24 sec, fast)
5. Dark current measurement (16 sec)
6. Switch to aperture 3 (10 sec)
7. Dark current measurement (16 sec)
8. Reference scans near 10 and 33 μm (16 sec)
9. Scans around 10 and 33 μm , up (360 sec)
10. Reference scans near 10 and 33 μm (16 sec)
12. Scans around 10 and 33 μm, up, continued (360 sec)
10. Reference scans near 10 and 33 μm (16 sec)
14. Scans around 10 and 33 μm, down (360 sec)
10. Reference scans near 10 and 33 μm (16 sec)
16. Scans around 10 and 33 μm, down, continued (360 sec)
10. Reference scans near 10 and 33 μm (16 sec)
18. Dark current measurement (16 sec)

19. Dark current measurement (16 sec)
20. Reference scans near 10 and 40μm (16 sec)
21. Scans around 10 and 40μm, up (96 sec)
22. Scans around 10 and 40μm, down (96 sec)
20. Reference scans near 10 and 40μm (16 sec)
24. Dark current measurement (16 sec)
25. Internal photometric calibration (40 sec)

Only ICS 5's are used (after the instrument has been set up). The ICS starts with a dark current measurement (at the reference wavelength), then makes a reference scan. Then the grating(s) is commanded up to observe a wavelength region. Another reference scan occurs before the down scan of the up-down pair. A final reference scan and dark current measurement are then made. This operation is repeated until all wavelength regions have been scanned.

For short scans the reference scans are dropped, as they take too much time. Every approximately 3600 s there was a photometric check. If the entire observation takes less than 3600 s a photometric check was done at the end.

4.4.2 Example AOT 6 data

Figures 4.12 and 4.13 show ERD data from all bands taken during an AOT 6. Data for detectors 1, 13, 25 and 37 (bands 1, 2, 3 & 4) is shown in bit values against time (ITK). Only five samples are shown out of the 24 per second for clarity. The periods when apertures 1, 2 & 3 are used, times of dark current measurements and photometric checks are indicated.

Figures 4.14 and 4.15 show the wavelength as seen by the middle detector of each band, along with the SW and LW scanner position (LVDT) for the same period. Figures 4.16 and 4.17 show the SPD, in $\mu V/sec$ against time, and AAR, flux (in Jy) against wavelength, for the same observation. Figure 4.18 shows what can be achieved after further processing of such data in either ISAP or IA.

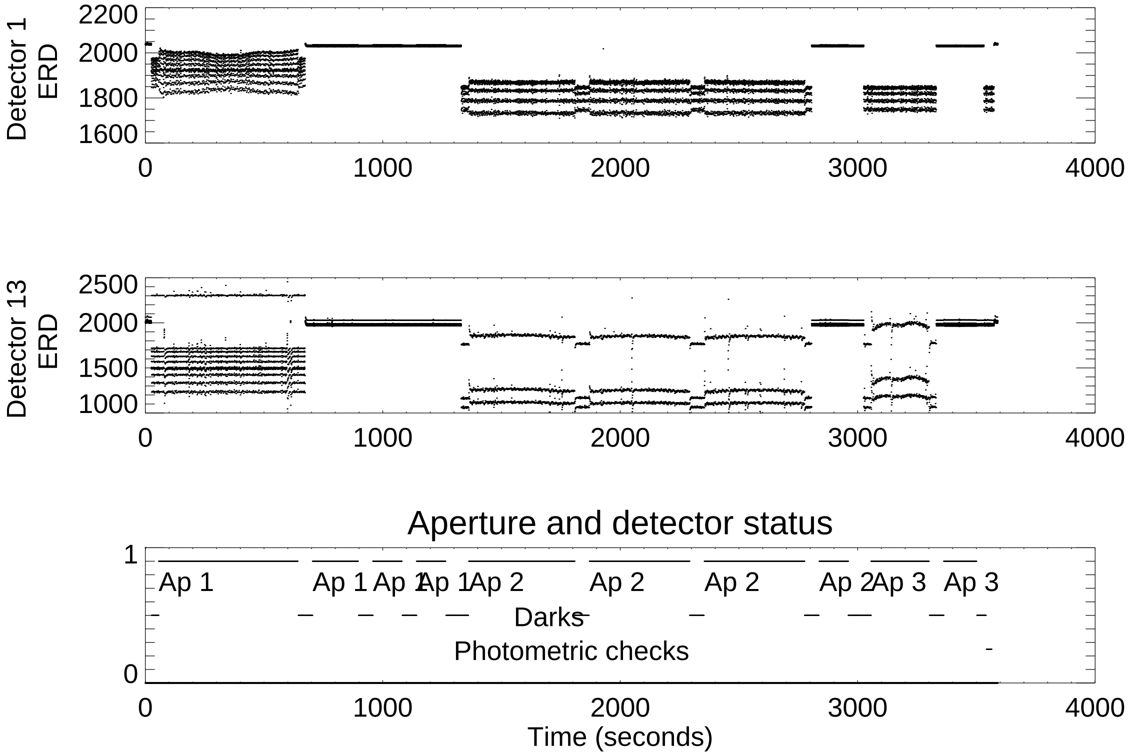

Figure 4.12: ERD data for detectors 1 and 13 during an AOT 6

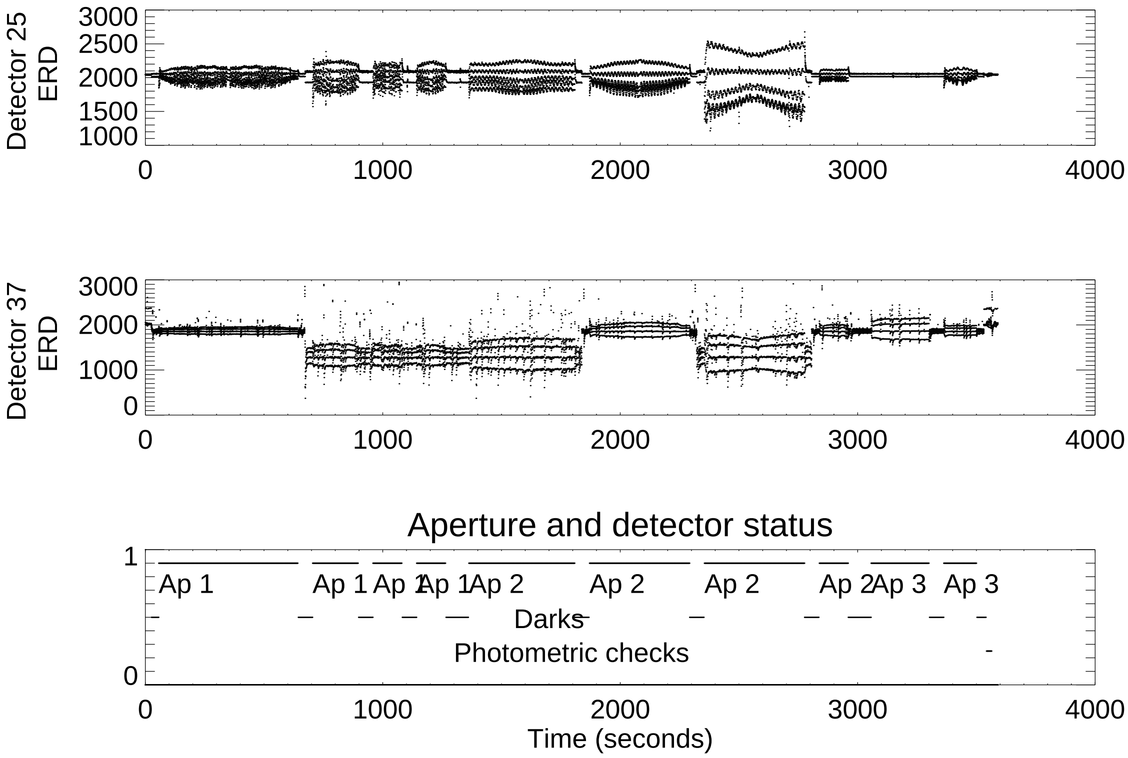

Figure 4.13: ERD data for detectors 25 and 37 during an AOT 6

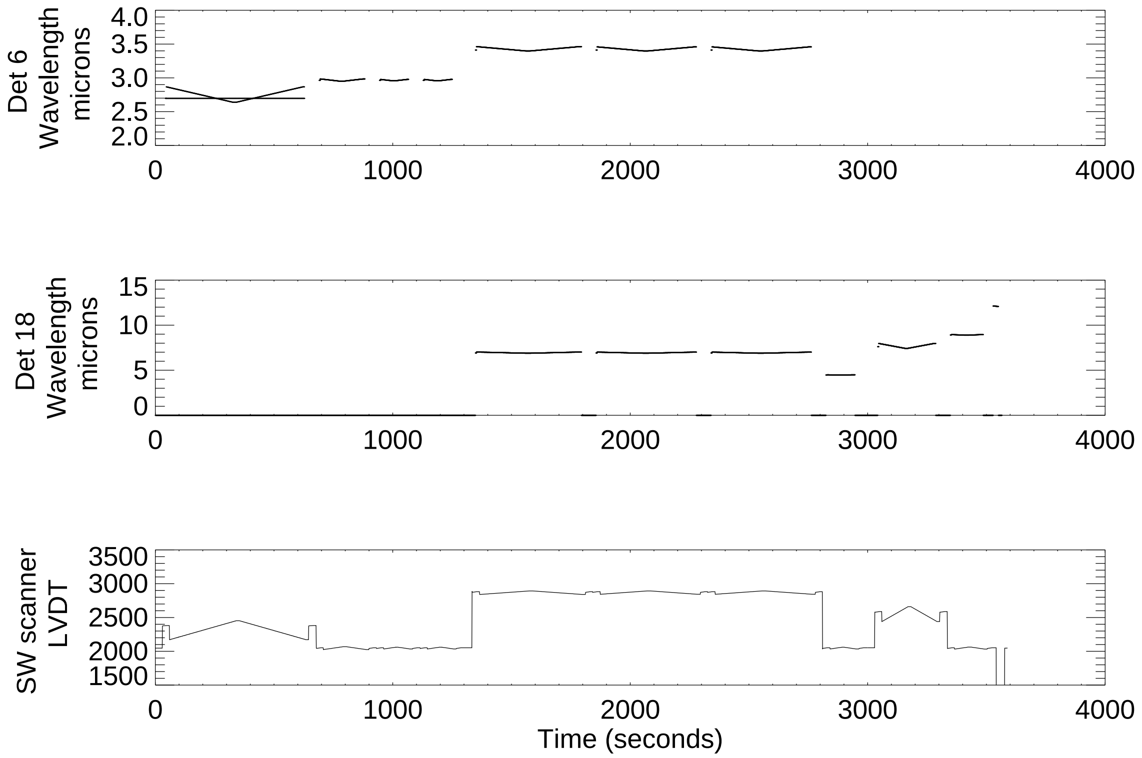

Figure 4.14: Scanner position and wavelength seen by detector 6 for bands 1 & 2 during an AOT 6

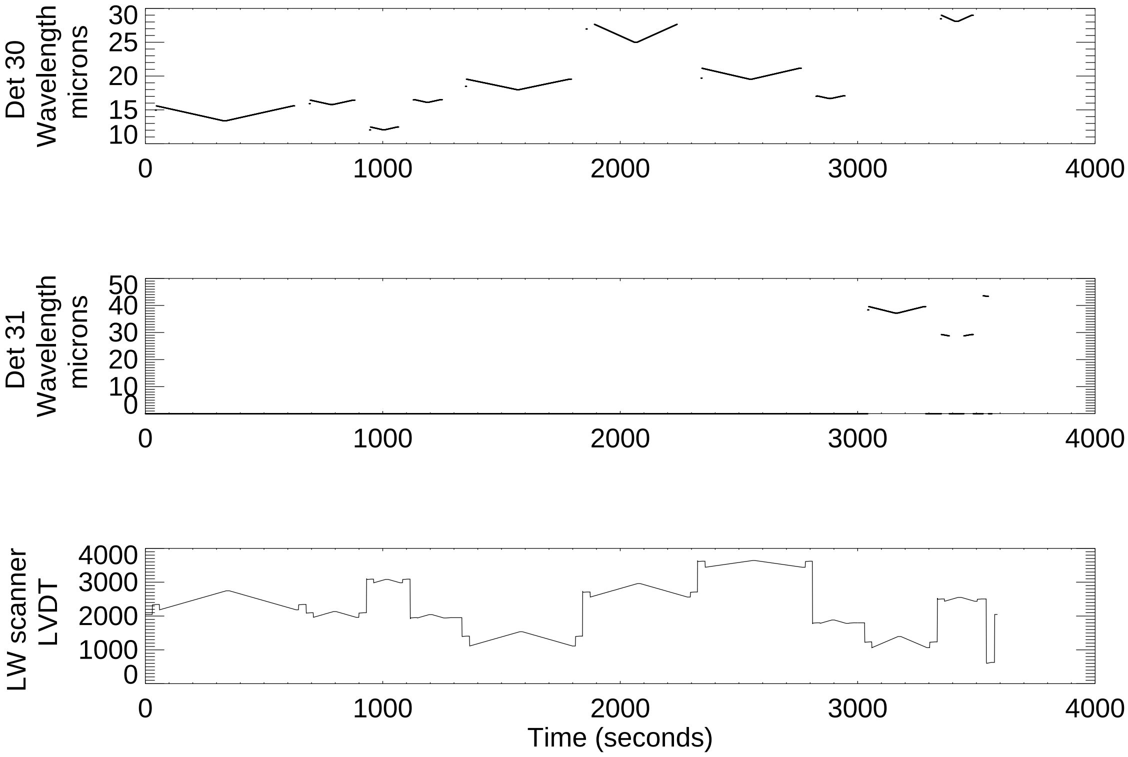

Figure 4.15: Scanner position and wavelength seen by detector 6 for bands 3 & 4 during an AOT 6

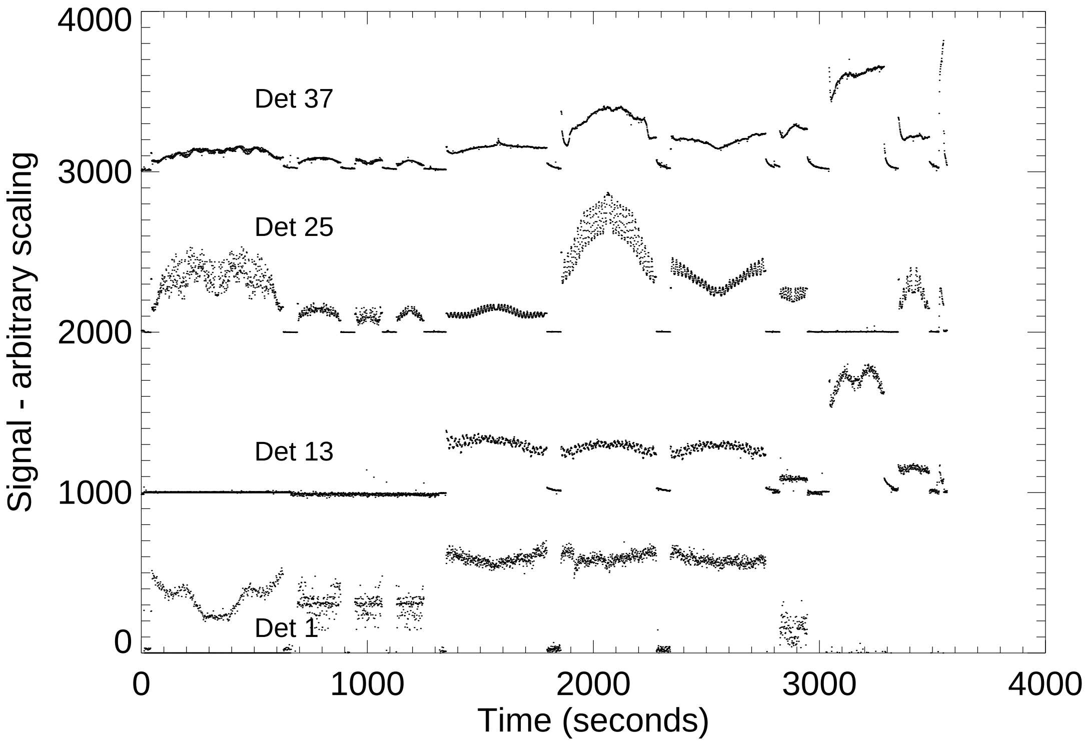

Figure 4.16: SPD data, in $\mu V/sec$, for the first detector of each band during an AOT 6

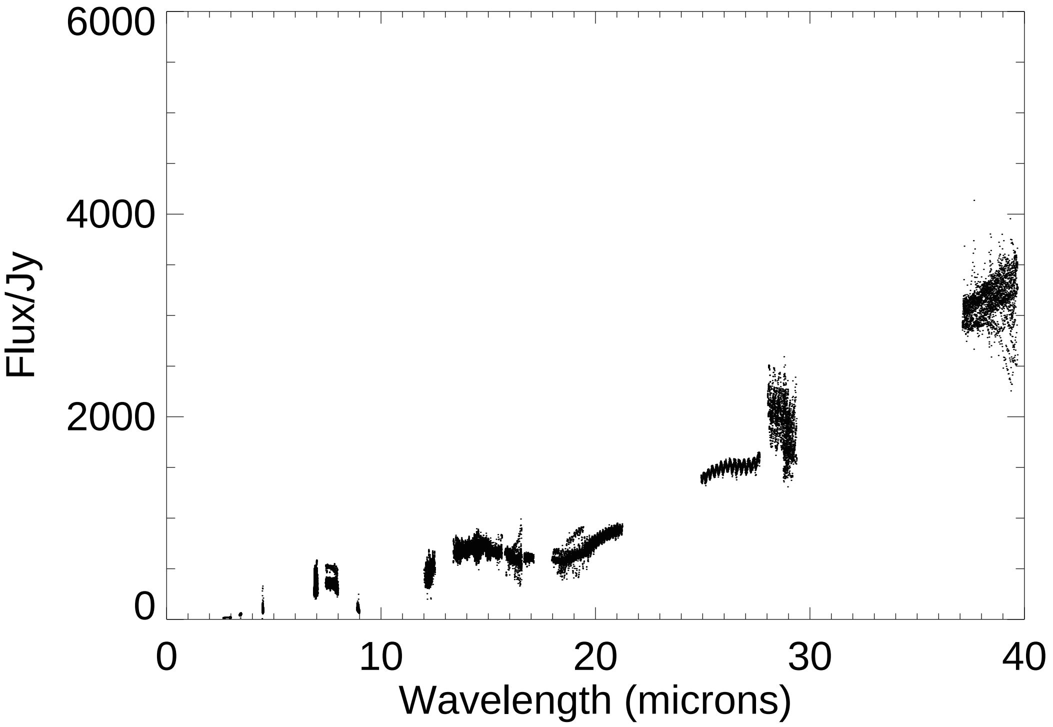

Figure 4.17: AAR data from all detectors for an AOT 6

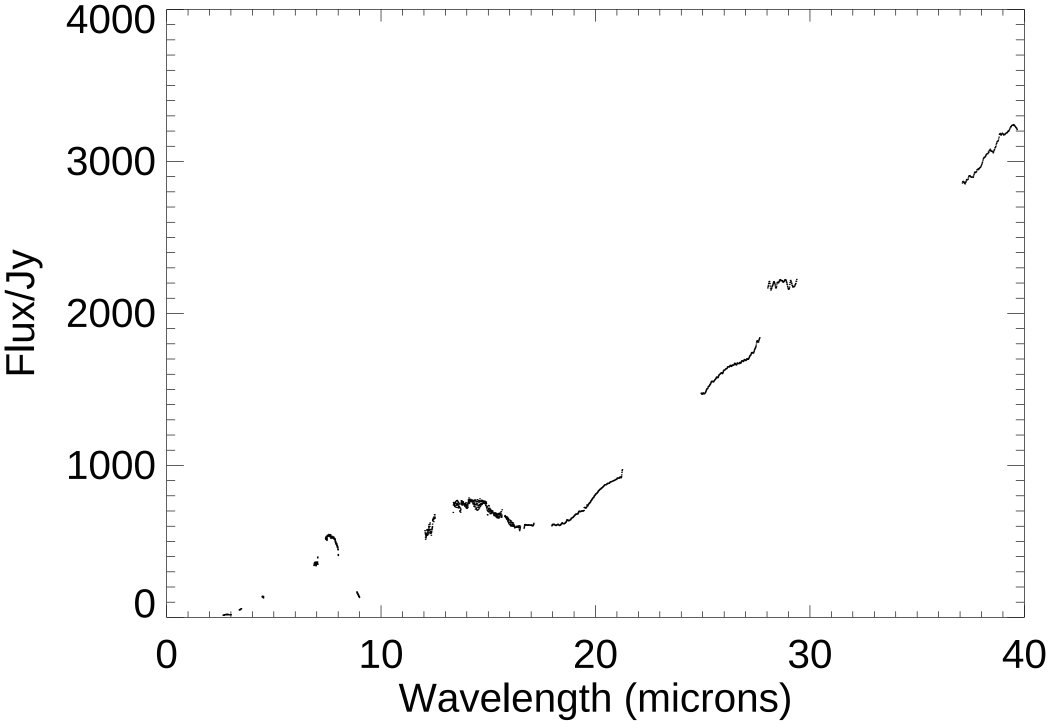

Figure 4.18: An example of what can be achieved by processing AOT 6 data further in either IA or ISAP

4.5 AOT 7

The purpose of AOT 7 was to make Fabry-Pérot observations. If requested, Short Wave grating observations were made in parallel.

For the FP the stepsize is always two FP units, about 1/4 of an FP wavelength resolution. Reset intervals are 1 or 2 seconds, with the dwell time equal to the reset interval. The number of scans is greater than, or equal to, three, and only "up" grating scans are commanded.

Any requested SW grating observations were carried out in an identical manner to those of an SWS06 measurement. Users should read section 4.4 for a description of that.

Due to a slight internal misalignment of the Long Wave FP there are problems merging FP observations with grating observations when observing through aperture 3. The 'effective' aperture of the FP was displaced from the center of the grating aperture by approximately 10 arcseconds, causing an approximately 40% drop in throughput of the FP when pointing is determined by the grating. The solution decided on was to define a fourth 'effective' aperture, centered on the FP aperture, and carry out all observations through this. This meant the SW grating lost approximately 40% of its throughput. Therefore LW FP observations ($26 - 44\,\mu m$) and SW grating observations ($7.0 - 13.16\,\mu m$) through aperture 3 could not be merged. Any requested aperture 3 grating observations were performed after the FP observations. This change was considered acceptable as the main purpose of AOT 7 was FP observations. Merging was still performed on observations using apertures 1 or 2.

However, some early AOT 7 observations were carried out before this change was implemented. Observers may therefore receive FP data merged with SW grating observations in the range 7 to $13.16\,\mu m$.

Note that band 2C ends at $13.16\,\mu m$ for AOT SWS07 - see table 3.2.

4.5.1 Example AOT 7 timeline

The AOT SWS07 was executed the following way:

- The telescope is pointed to the target position.
- The F-P lines and grating wavelength ranges specified in the AOT are observed. Each FP line is scanned at least three times and each SW wavelength range is scanned at least twice to provide redundancy.
- Dark current checks are performed at regular intervals, at least before and after a set of FP scans on the same line and at least once before the reference wavelength of each SW range.
- F-P scans may have to be broken into segments because the end of the mechanical F-P range is reached and the scan has to be continued in a different F-P order.
- With all F-P scans the LW grating is scanned slowly in coordination with the F-P scan to keep the pre-dispersion tuned to the actual wavelength.
- The phasing of the measurements is essentially independent for the two spectrometer sections, at the cost of increased overheads but giving flexibility in combination.
- If the line list contains wavelengths corresponding to different SWS apertures, the aperture is switched accordingly and the satellite re-pointed to bring the source to the center of the new aperture.

- At regular intervals, between observations, photometric checks are performed, at least once per AOT.

AOT 7 is achieved by using combinations of ICS's 9 and 4. After the instrument has been set up ICS 9 is used to make a dark-current measurement. Another ICS 9 is then used to start the FP. While the FP is operating ICS 4 is used to make SW grating scans, if any are requested. More than one of these may be uplinked while the FP scan is continuing. To observe more lines with the FP more ICS 9's are uplinked. Again ICS 4's could be uplinked to observe with the SW grating section. After all observations have concluded a final ICS 9 is used to make a dark measurement.

4.5.2 Example AOT 7 data

Figure 4.19 shows ERD, SPD and aperture data for part of an AOT 7. The ERD is shown as signal in bit values against time (ITK), and the SPD as signal (in $\mu V/sec$) against time (seconds). While the line is hard to see in the ERD, it can easily be seen in the SPD.

Figure 4.20 shows the LW grating position, the FP position and the resulting wavelength of light falling on detector during the part of an AOT 7.

Figure 4.21 shows SPD signal (in $\mu V/sec$) and AAR flux (in Jy), both against wavelength, for the same period of the example AOT 7. Note the wavelength shift in the location of the peak between the SPD and AAR. This is because the SPD wavelength scale is 'ISOcentric', whereas the AAR is corrected to be heliocentric.

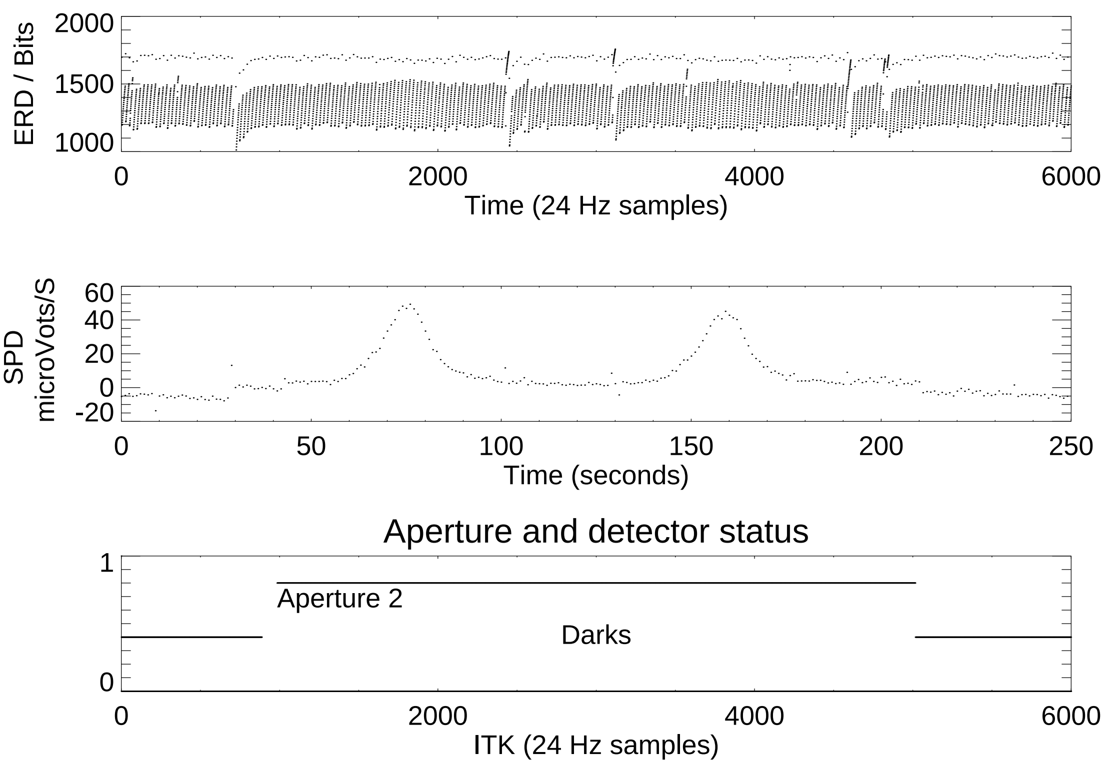

Figure 4.19: ERD, SPD and aperture data for part of an AOT 7

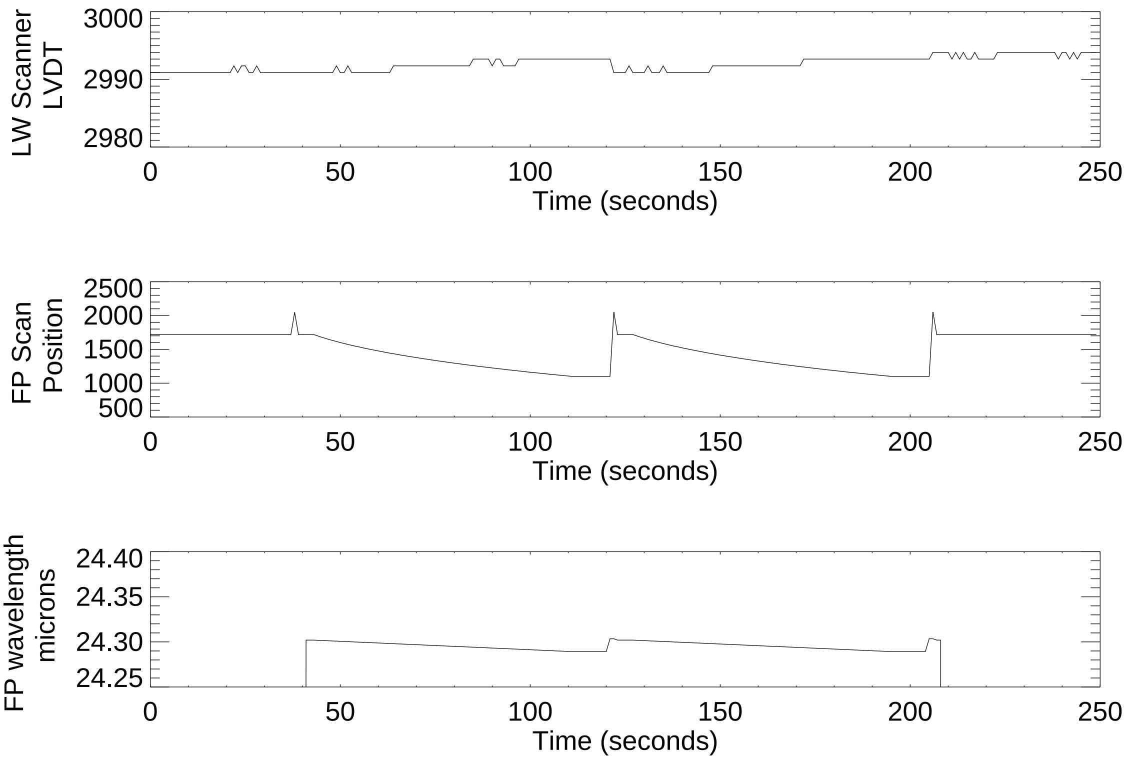

Figure 4.20: LW grating position, FP position and resulting wavelength for part of an AOT 7

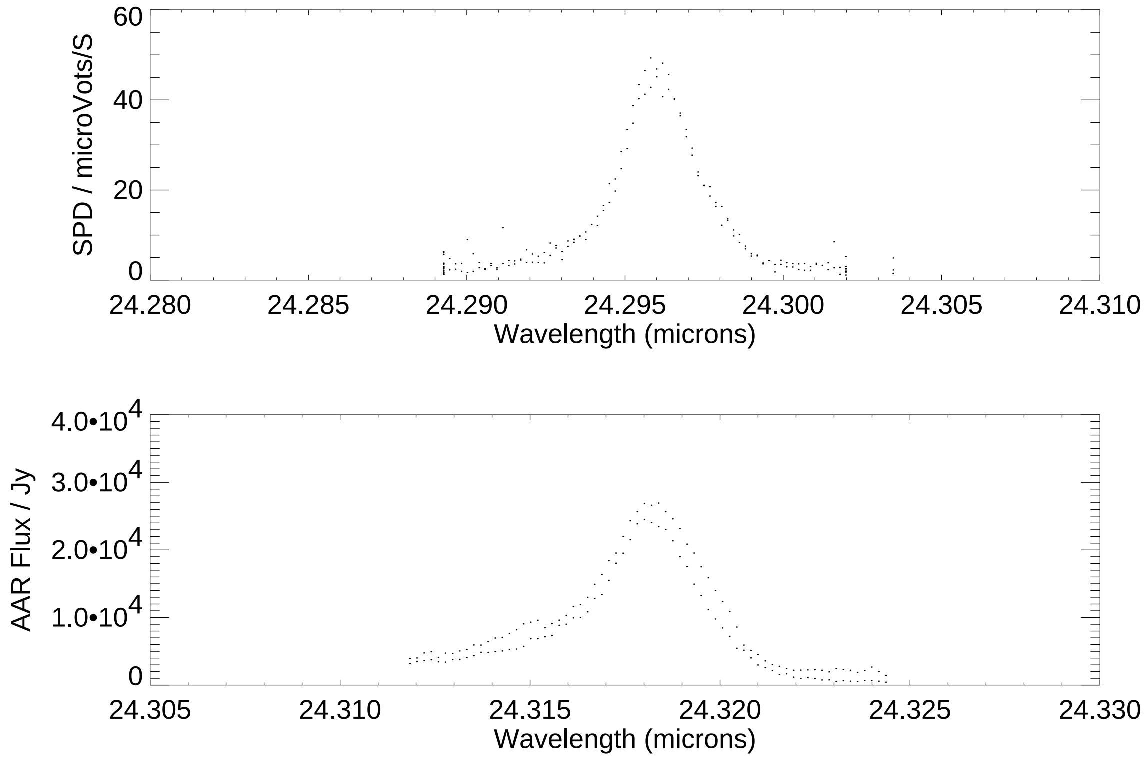

Figure 4.21: SPD and AAR data for AOT 7

4.6 AOT behaviour

4.6.1 up-down scans

Up-down scans initially scan a wavelength range in one direction, then reverse direction to cover the same wavelength region again. e.g. the scanner may start at $35\,\mu m$, scan down to $30\,\mu m$ and then go back up to $35\,\mu m$. Having two scans, in different directions, enables a discrimination to be made between real spectral structure and detector memory effects, as the latter can mimic the former. They are called up-down scans, rather than down-up scans, as it is the LVDT number that increases then decreases, and wavelength is inversely correlated with LVDT. Table 4.1, "Various SWS AOT options", indicates if a particular AOT uses up-down scans.

The SWAASDIR field indicates whether an AAR datapoint is from an up or a down-scan. 1 means the datapoint is part of an up scan, -1 a down scan, and 0 is undefined. Note that 'up-down scans' only refer to what the grating is doing. For FP observations the grating always increased.

An example of an up-down scan is shown in figure 4.22, taken from an SWS01 observation. Plotted are the wavelengths seen by the first detectors in bands 1 and 2 and the SW scanner position. The relationship between the scanner position and wavelength can be seen along with cases of up-down scans where the wavelength seen by a detector decreases then increases. The periods when apertures 1, 2 & 3 are used, times of dark current measurements and photometric checks are indicated.

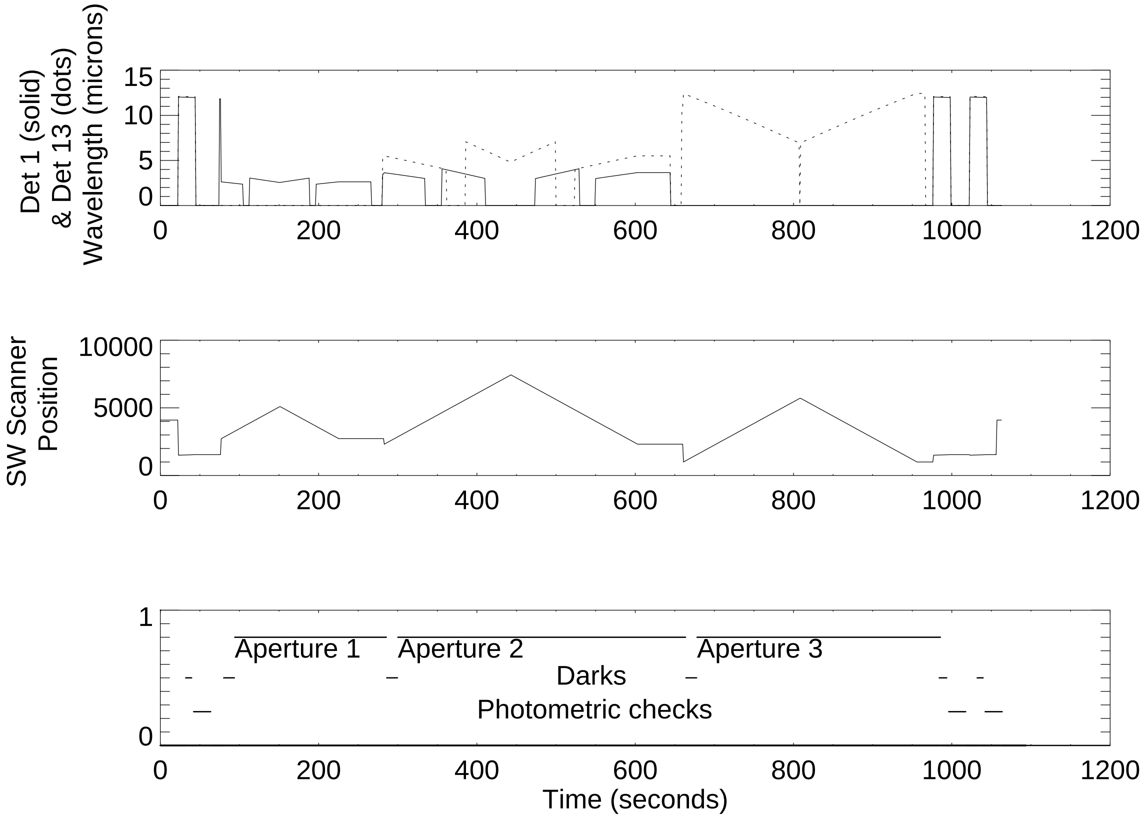

Figure 4.22: Example of up-down scans

Note that for bright sources (> 1000 Jy) the flux seen in the up-scan can differ by 20% compared to the that seen in the down-scan due to memory effects – see sections 5.8, "Memory Effects" and 7.4, "Flux Calibration Accuracy".

4.6.2 Reference scans

AOT 6 and 7 observations planned before July 10 1997 employed what was known as reference scan calibrations. These were supposed to guard against detector drifts caused by memory effects. The method used was for the grating to occasionally switch back to a set grating position, and hence wavelength. Any changes in the detector response at this wavelength over the timescale of the observation were due to detector memory effects, which could be calibrated out. These reference scans were only present in long AOTs. For example, the interval between reference measurements with detector band 3 was 1000 seconds - band 3 is extremely sensitive to detector drifts because of the strong fringing in the detector spectral response function.

However, because of a problem in the pipeline module handling reference scan data any such data was unused from OLP V6 onwards. Furthermore, it was found that including such reference scans actually harmed observations – this is described in section 5.9 – and the reference scans were therefore deleted from observations planned from July 10 1997.

More information on this can be found in the document "Possible Detector Memory Effects in SWS Grating range spectra (AOT S06) due to SWS Reference Scans", by K. Leech & P. Morris.

For users who's observations were planned before this date, scans at the reference wavelengths can be recognized through the "R" flag in the SWAASTAT or SWSPSTAT fields in the AAR or SPD. It is also present in TDATA. TDATA, or Transparent Data (so called because its contents are not seen by the uplink/downlink system), not only flags the reference scans, but also indicates to which measurements the reference scans (and the normal scans) belong. TDATA is kept in the EOHIMSG1 field in the EOHI, Executed Observation History Per ICS, file. This file is described in the ISO Satellite & Data Manual.

4.6.3 Recognising the start of an AOT

If you look at ERD data you will want to know when the AOT actually starts. This can be determined by looking at the runflags (byte 13 of frame 8) in the GEHK file, which indicates when ICS's start. The GEHK UTK timekey where changes occur can be correlated with the ERD ITK. Refer to the ISO Satellite & Data Manual for a discussion of the GEHK file.

All ICSs, Instantiated Command Sequences, except the reset ICSs SS0007 and SS0008 start with a pre-amble to set up the instrument, then initiate the real action by setting one or more run flags (bits) described in Table 4.11.

Table 4.11: Run flags in frame 8

ICS	Meaning	Bits set
SS0001	(diffuse calibrator)	4
SS0002	(grating calibrator)	4, 5 and 6
SS0004	(SW scan in AOT7)	5
SS0005	(grating scan)	5 and/or 6
SS0009	(FP)	5, 6 and 7

In all these cases the indicated run flags simultaneously change from 0 to 1. In the AOTs, setting run flags 4-7 does not occur anywhere else. From a practical point of view, the execution of an ICS starts when these flags are set. The only detector data of interest with these flags not set are dark-current measurements at the start of ICSs SS0001 or SS0002 (all AOTs) and SS0005 (AOTs 1 and 2).

Setting run flags 4-7 happens always a few seconds after the start of the ICS execution. At that moment the TDATA for the running ICS is valid. After the run flag goes up, the ICS always lasts at least another 8 seconds (the run flag itself remains set at least 4 secs), to which may be added the uplink time for the next ICS, so that the TDATA for the next ICS is not valid yet.

Interpret a change from 0 to 1 of any of the run flags 4, 5, 6, or 7 as the start of an ICS, and expect the latest arrived TDATA to be applicable. Run flags 0 to 3 must be ignored for this purpose.

4.6.4 Cross AOT Flux Comparisons

Several comparisons have been made between the spectra obtained from different AOTs. Information on these comparisons can be found in the documents 'CROSS AOT COMPARISON, PART 1', issue 1.1 6 February 1997 by A.M. Heras, and 'Cross AOT comparison-part 2', 21 April 1997 by A.M. Heras also published in part in the 'First ISO Workshop on Analytical Spectroscopy', Eds A.M. Heras, K. Leech, N.R. Trams & M. Perry, ESA SP-419, p77. In general AOT 1 was compared with AOT 6 and AOT 2 with AOT 7.

The cross AOT comparisons reported in these publications have proved to be a good tool to understand how the different factors that are part of data processing (dark currents, photometric checks, memory effects, pipeline software) influence the final AAR product. The results can be summarised as follows:

1 The discrepancies found in line fluxes between AOT 1 and AOT 6 observations of the same source are below 30%, except for some cases corresponding to band 3E or associated with very low signals.

2 The most consistent AOT 1 to AOT 6 results are found for detector band 1.

3 Memory effects in band 2 are relevant to the discrepancies found between AOT 1 different speeds and AOT 6 observations. In particular:

   a Dark current measurements for band 2B are carried out differently in an AOT 1 compared to an AOT 6. Due to the flux history, the interpolated dark current in the AOT 1 is usually lower than in the AOT 6, leading to a higher flux in the AOT 1.

   b If the flux is high and the observation is long enough, the photometric check value increases with time. As a consequence, the choice of photometric check in an observation may have an important effect on the fluxes and on the result of the comparison. In the objects studied, this is relevant to bands 2A and 2C, but not to band 2B.

   c In case of very high fluxes, the impact of memory effects on dark currents prior to the photometric check is important, to the extent that the dark subtracted photometric check fluxes have anomalous levels and profiles. This is particularly relevant to AOT 6 observations of moderate duration, in which the photometric check is done at the end of the observation.

   d Memory effects cause some points in the AAR obtained when the grating is not scanning (SWRUN flag not set) to introduce non-negligible errors in the final product.

   e The up- and down-scans in AOT 6 observations of high flux sources are remarkably different, with the downscan profiles in better agreement with the AOT 1 profiles.

4 Pointing errors have been identified as the cause for the discrepancies in band 3 of Gamma Dra observations. See 5.10 for a discussion of pointing problems.

5 The only important AOT 1 to AOT 6 discrepancies found for band 4 are due to the low signal to noise ratio for most of the objects in that spectral region.

6 The only comparison of an AOT 1 versus an AOT 2 observation (Eta-Car) shows a very good agreement.

7 AOT 2 and AOT 7 line fluxes agree to within 40% in the analyzed observations, except for in cases in which the S/N is low and/or the continuum level is difficult to determine.

8 Line fluxes of NGC 7027 show a good agreement in an AOT 1 (speed 3), AOT 2 and AOT 6 comparison except for AOT 1 speed 3 in band 2C, where memory effects seem to cause problems, and for AOT 6 in band 3, which was affected by pointing errors.

Chapter 5

Instrumental Characteristics

5.1 Introduction

This section discusses the behaviour of the instrument, detectors etc as determined from in-orbit measurements.

5.2 Grating Performance Overview

The SWS instrumental signal-level unit is μVs^{-1}, the average rise of the voltage of the ramp during one second of time (see section 3.4 for an explanation of this). It is found that the signal response of the instrument is a linear function of the illumination over a very large range of input signals (0.5 – 100,000 Jy), when hysteresis effects are ignored. Therefore this unit is fully qualified for simple linear calculations backwards and forwards relating source flux density, instrument signal level, instrument noise level and noise equivalent flux density (*NEFD*, *i.e.*, the input flux density which gives an output signal with a signal-to-noise ratio $SNR = 1$). The SWS grating sections produce a ~1.3-3 μVs^{-1} signal on a single detector element for a source flux density of 1 Jy.

Both the response and the noise of the detectors have been characterized as function of signal strength. Table 5.1 summarizes the overall properties of the detectors.

For sensitivity calculations, the noise per reset interval may be summarized as

$$N[\mu V/s] = \frac{\sqrt{N_R^2 + (N_D^2 + N_S^2 S)t_r}}{t_r} \tag{5.1}$$

with S the signal in μV/s and t_r dimensionless (happens to be equal to the reset interval in seconds). The empirically determined noise parameters N_R (read noise, in μV/s) N_D (dark current noise, in μV/s), and N_S (signal shot noise, μV$^{0.5}$/s$^{0.5}$) have been obtained by forcing a fit through this function, and are summarized in Table 5.2. For the SW grating and the FP detectors the function works well up to a $t_r \approx 8$ sec (although 8 second resets were only used for a short period at the start of the mission). For the LW grating detectors the function does not work well in describing the t_r dependency, and the resulting values are not necessarily directly to be associated with read noise and dark noise. Parameter values are chosen in such a way that they give the best description for the short reset intervals.

For Band 4, test measurements show consistently a very poor increase of SNR for $t_r > 2$ sec. The parameters listed apply to $t_r = 1$ sec and $t_r = 2$ sec. For longer t_r no improvement in noise should be expected, but the $\sqrt{t}$ function still applies.

Table 5.1: Summary of SWS detector properties for a reset interval $t_r = 2$ sec

detector	T	bias	minimum system noise[3]		int.[4]	average response
	(K)	(V)	(μV/s) gain=16	(electrons)	(μV/s)	(μV/s/Jy)[5]
Gr–InSb	3	-	0.7	35	0.32	3.0
Gr–Si:Ga	3	12	1.5	75	0.32	1.6
Gr–Si:As	4.5	3.0	3.0	150	0.40[2]	1.5
Gr–Ge:Be	2	0.6	2.0	100	1.00	1.3
F-P–Si:Sb	10	1.1	1.1[1]	70	0.40	0.007
F-P–Ge:Be	2	0.6	3.0	200	0.40	0.0037

Notes:

1. values listed for element 2; noise = 0.7 μV/s for element 1
2. excess photon noise at *Signal* > 1000μV/s
3. measured at a signal power at which photon noise is negligible; except FP-Ge:Be where still some photon-noise is suspected; estimated photon-noise free $NEP_2 = 1.05 \times 10^{-16}$ W/$\sqrt{Hz}$
4. int. is intercept: photon noise at signal = 10 μV/s
5. 1 Jy = 10^{-26} WHz$^{-1}m^{-2}$, ISO telescope area taken as 0.28 m^2

Table 5.2: Grating noise parameters

Band	1	2	3	4
detector	InSb	Si:Ga	Si:As	Ge:Be
range (μm)	2.38-4.05	4.05-12.0	12.0-29.5	29.5-45.2
N_R	0.75	0.75	1.00	1.56
N_D	0.70	1.50	3.00	2.00
N_S	0.10	0.13	0.14	0.32

5.3 Fabry-Pérot Overview

The SWS Fabry-Pérot section may be used at wavelengths between 11.4 and 44.5μm. Instrument levels tests showed that performance in the extended wavelength range outside the nominal design wavelength range of 15–35μm was good enough to make the extended range available. A few remaining peculiarities of the extended range are discussed together with the following performance description. Results throughout this section refer to use of the Fabry-Pérot AOT bands of Table 3.2 that have been selected to give the best tradeoff between the various design goals (high sensitivity, low leakage etc.).

5.3.1 Spectral Resolution

The Fabry-Pérot spectral resolution was measured at a few discrete wavelengths using solid state laser sources. Fig. 5.1 shows the spectral resolution as a function of wavelength, interpolated between these measurements. The spectral resolution decreases towards the short wavelength ends of the wavelength ranges covered by the two Fabry-Pérots, where the wavelengths corresponding to the resonances of the reflective meshes are approached.

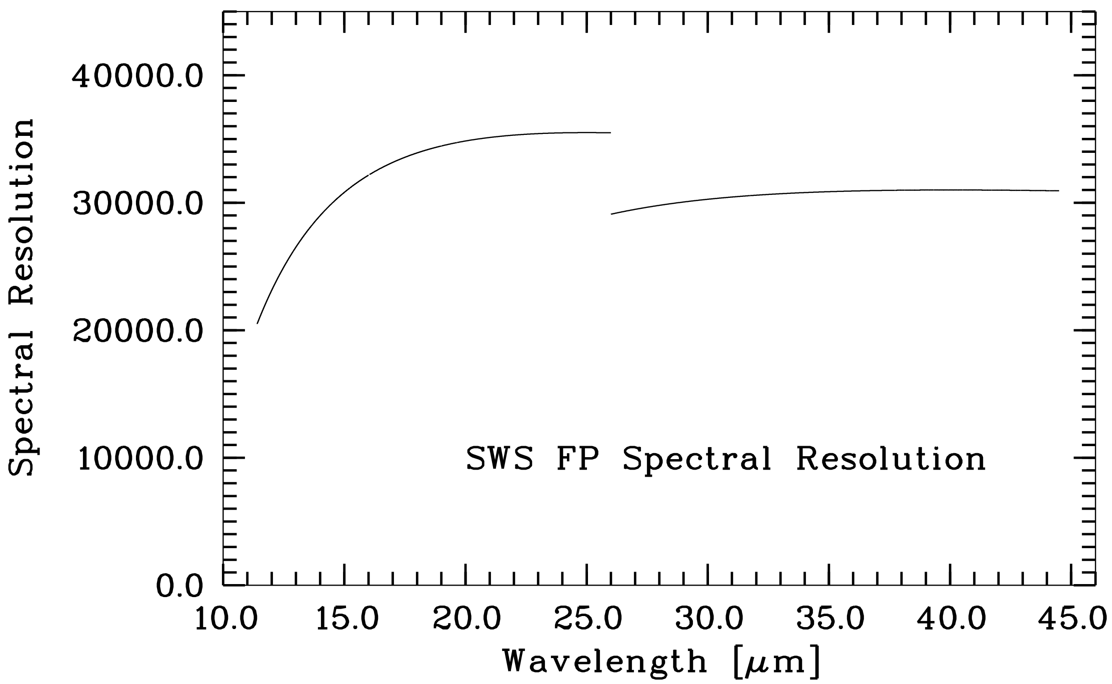

Figure 5.1: SWS Fabry-Pérot spectral resolution as a function of wavelength, computed from measured mesh properties and confirmed by checks at selected wavelengths

The Fabry-Pérot spectral resolution depends on precise parallelity of the F-P plates. An in-orbit spectral resolution very close to Figure 5.1 was obtained after execution of the in-orbit parallelisation procedure of the SWS F-P.

5.3.2 Sensitivity

The F-P sensitivity was characterized in instrument levels tests by doing measurements on a calibrated blackbody source within the test cryostat. Fig. 5.2 shows the SWS Fabry-Pérot spectral response. The conversion between units applicable to astronomical sources (Flux density of a point source in Jy) and the resulting instrumental signal (μV/s) is given as a function of wavelength. Diffraction losses caused by the fact that the aperture is comparable in size to the ISO diffraction disk have been taken into account; the flux used to derive Fig. 5.2 is the true point source flux. The effect of these diffraction losses is however not large (Fig. 5.3).

The spectral response curve has structure on various wavelength scales. Large scale trends are determined by the counteracting effects of detector spectral response increasing with wavelength until close to the detector cut-off wavelength, and decreasing transmission of the Fabry-Pérot interferometer. Structures on scales of microns or tenths of microns can be traced to the detector spectral response curves and filter transmission curves. A rapid low-amplitude modulation in the 11.4–16μm range (not resolved in Fig. 5.2) is caused by reflections between the surfaces of the transmission filter used behind slit 1 in the long-wavelength section of SWS. This 'parasitic Fabry-Pérot' effect is also observed for grating data using the same slit. The stronger modulation detected at $\lambda \geq 40\mu m$ in the long-wavelength extended range is again caused by a parasitic Fabry-Pérot effect, this time in a reflecting CaF_2 filter. The nearby reststrahlen resonance of CaF_2 causes strong variations with wavelength of the indices of refraction and absorption,

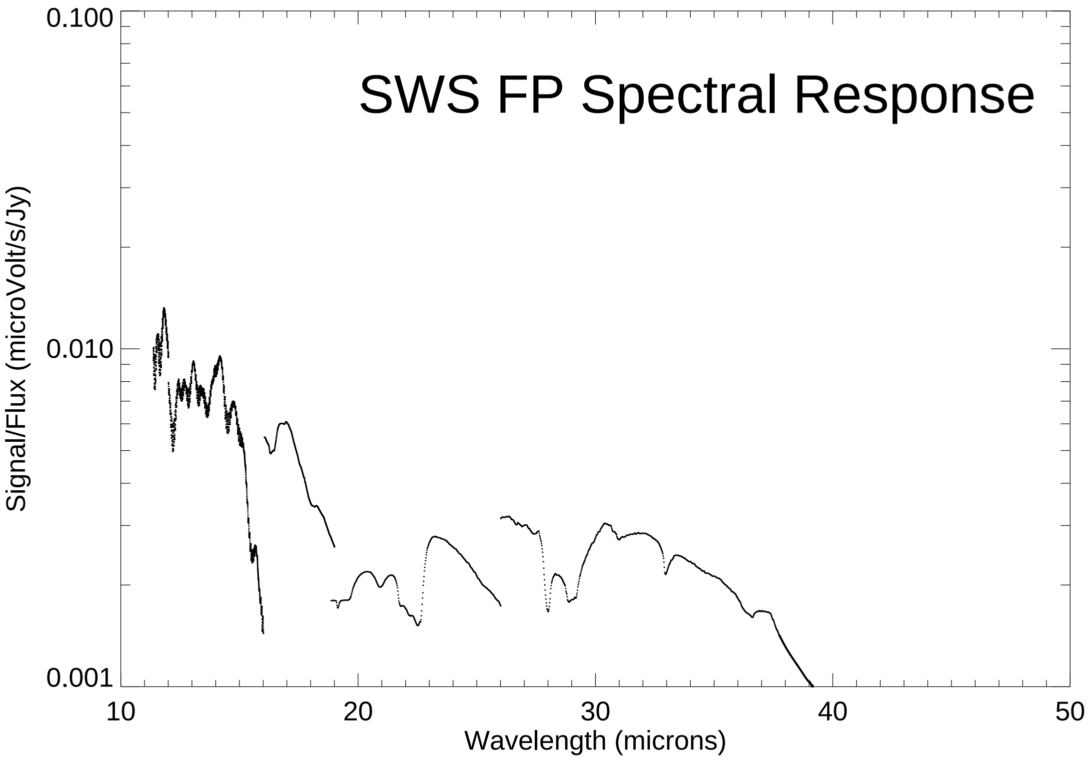

Figure 5.2: SWS Fabry-Pérot spectral response. The flux scale corresponds to a point source, diffraction losses at the aperture have been taken into account

leading to the observed modulation pattern. The modulations were characterized with sufficient accuracy to allow good flux calibration in the extended wavelength ranges.

5.3.3 Noise

Measurements of noise for various reset intervals and signal levels during the SWS instrument level tests resulted in the following characterization of the noise behaviour of the F-P detector and integrating preamplifier system:

- Noise at low signal levels is independent of signal. Here, noise as a function of reset interval can be approximately modelled as the quadratic sum of a constant read noise term and a dark current noise term increasing with time. Deviations from this model exist but may be ignored for simple sensitivity estimates
- At higher signal, *SNR* improves only with the root of the signal, indicating dominance of shot noise.

For sensitivity calculations, this may be summarized as

$$N[\mu V/s] = \frac{\sqrt{N_R^2 + (N_D^2 + N_S^2 S)t_r}}{t_r}$$

with S the signal in μV/s and t_r dimensionless (happens to be equal to the reset interval in seconds). The empirically determined noise parameters N_R (read noise, in μV/s) N_D (dark

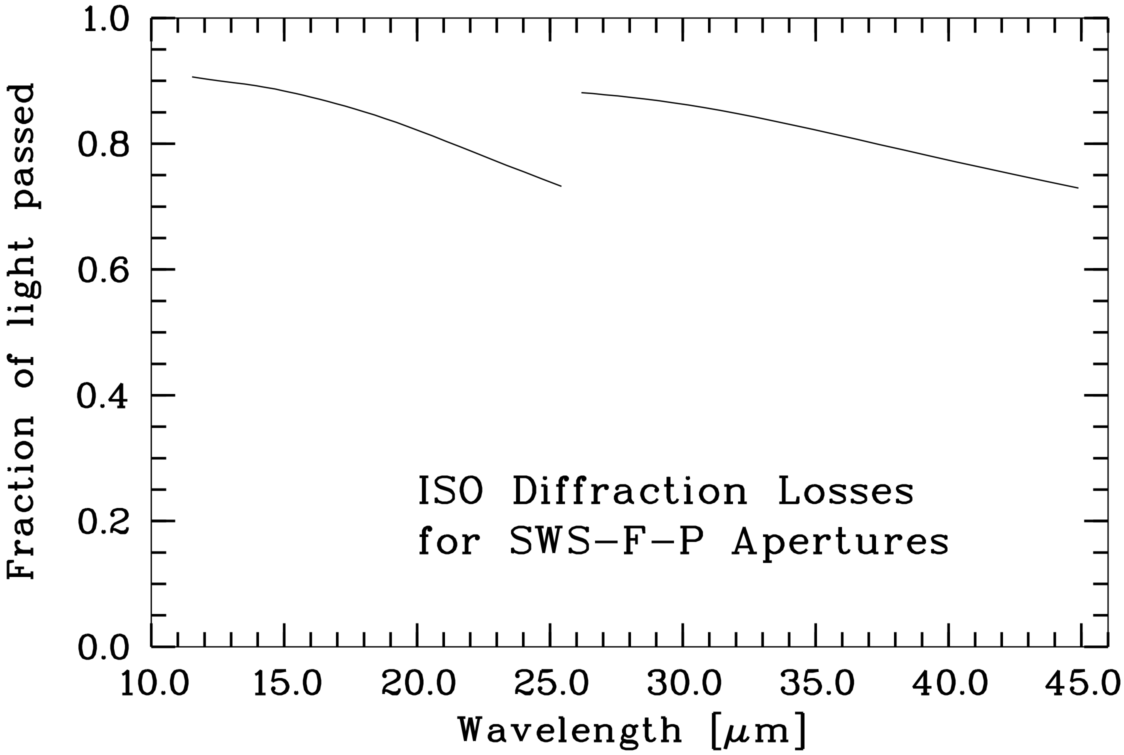

Figure 5.3: Computed ISO diffraction losses for the SWS F-P channels. The fraction of the ISO diffraction disk accepted by the effective SWS F-P aperture is shown as a function of wavelength

current noise, in μV/s), and N_S (signal shot noise, $\mu V^{0.5}/s^{0.5}$) for the two F-P detector materials are summarized in Table 5.3.

Table 5.3: Fabry-Pérot noise parameters

Band	5	6
detector	FP-Si:Sb	FP-Ge:Be
range (μm)	11.4-26	26-44.5
N_R	0.63	0.89
N_D	1.00	3.00
N_S	0.18	0.13

5.3.4 Saturation

No saturation problems are expected for the SWS Fabry-Pérot detectors. The saturation limit is given by the fact that the integration ramp for 1s detector reset interval does not hit the saturation level of the warm electronics for signals less than about 20,000 μV/s. Although not foreseen in the current design of the offline data processing, it is in principle possible to obtain data for signals about seven times stronger by analysis of partial integration ramps. It is assumed here that the expected strong flux has been correctly specified in the AOT input, since only then the gain and reset time are set properly. Taking typical values from Fig. 5.1 and Fig. 5.2, the 20,000 μV/s limit corresponds to a saturating flux density of about 2×10^6 Jy, or a saturating flux in an unresolved line of about 10^{-11} Wm^{-2}.

5.3.5 Leakage

The Fabry-Pérot section uses the grating as an order sorter that suppresses unwanted F-P orders. This suppression is not complete for part of the SWS wavelength range. Neighbouring F-P orders 'leak' through the wings of the grating instrumental profile, contributing significantly to the total measured signal (See Figure 5.4). For observations of a single line superposed on a smooth continuum, the only drawback of leakage is a more complicated flux calibration, since leakage will increase the observed continuum but not the line. More serious effects occur in crowded spectra, where strong lines seen in the 'wrong' F-P order may significantly distort the observed spectrum, requiring observations of wider wavelength ranges in order to determine the severity of this effect and 'clean' the spectrum (See Fig. 5.6).

Leakage has been quantified by analysis of the grating instrumental profile as seen by the F-P detectors in scans of solid state laser lines. Figure 5.5 shows the leakage as a function of wavelength. It must be considered preliminary, since it is based on extrapolating the grating instrumental profile from measurements only at a few wavelengths of laser lines.

The spectral response data in section 5.2.2 have not been corrected for the effects of leakage, i.e. they refer to the total signal.

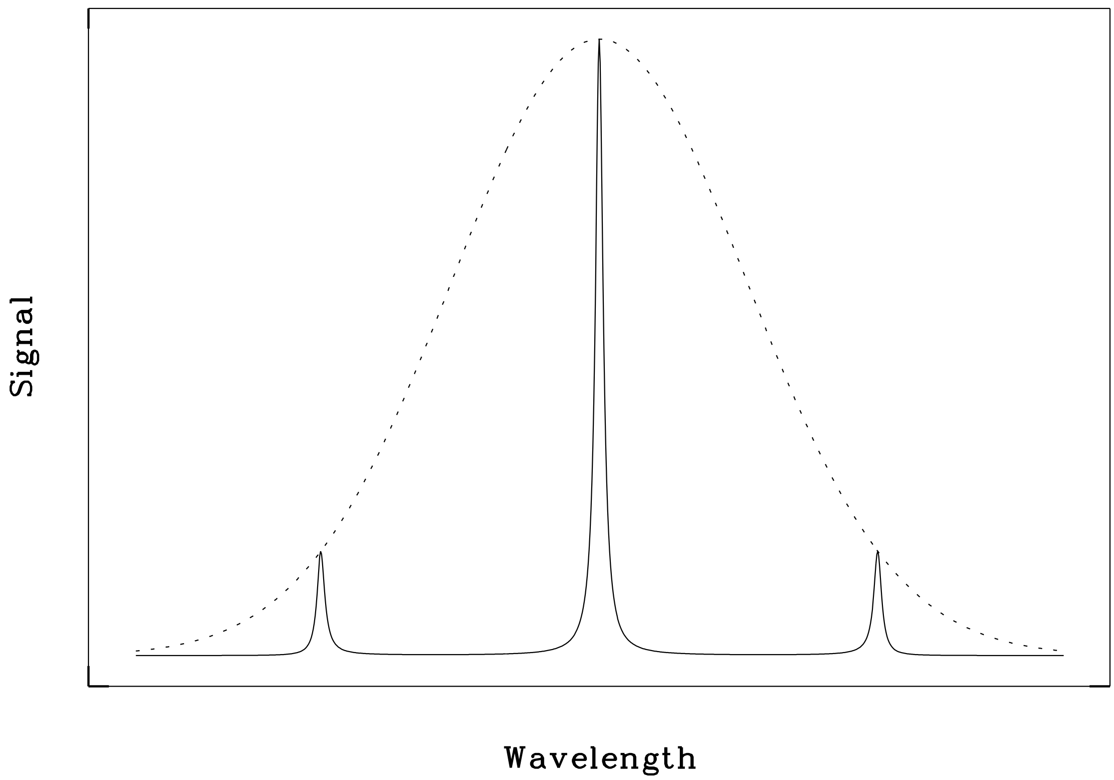

Figure 5.4: Basics of leakage in F-P spectra. The instrumental profile of the combination of F-P and grating is given by the solid line. Residual transmission from neighbouring F-P orders occurs if the instrumental profile of the grating alone (dashed line) is too wide

5.3.6 Tracking Noise

The coordination between Fabry-Pérot scans and the movement of the grating that tracks the F-P scan is a source of signature (or, loosely, 'noise') that ultimately limits the quality of F-P spectra on bright sources. For all but very short F-P scans, the wavelength sampled by the F-P would soon be no longer tuned to the transmission peak of the grating if there were no tracking. The discrete steps of the grating's tracking movement result in the final F-P scan of a pure continuum source looking like a repetition of a small section of the grating instrumental profile.

The amplitude of this 'noise' depends on various factors like quality of grating wavelength calibration, ratio between grating stepsize and line profile FWHM, pointing stability. It is hence difficult to predict for an observation at a certain wavelength. Instrument level tests with optimized grating wavelength calibration showed 'signal-to-noise' around 200. In the case of an observation of a single line on a smooth continuum, part of the 'noise' could be calibrated out by observing a larger region of continuum around the line, provided the non-systematic contribution of pointing jitter is not too large.

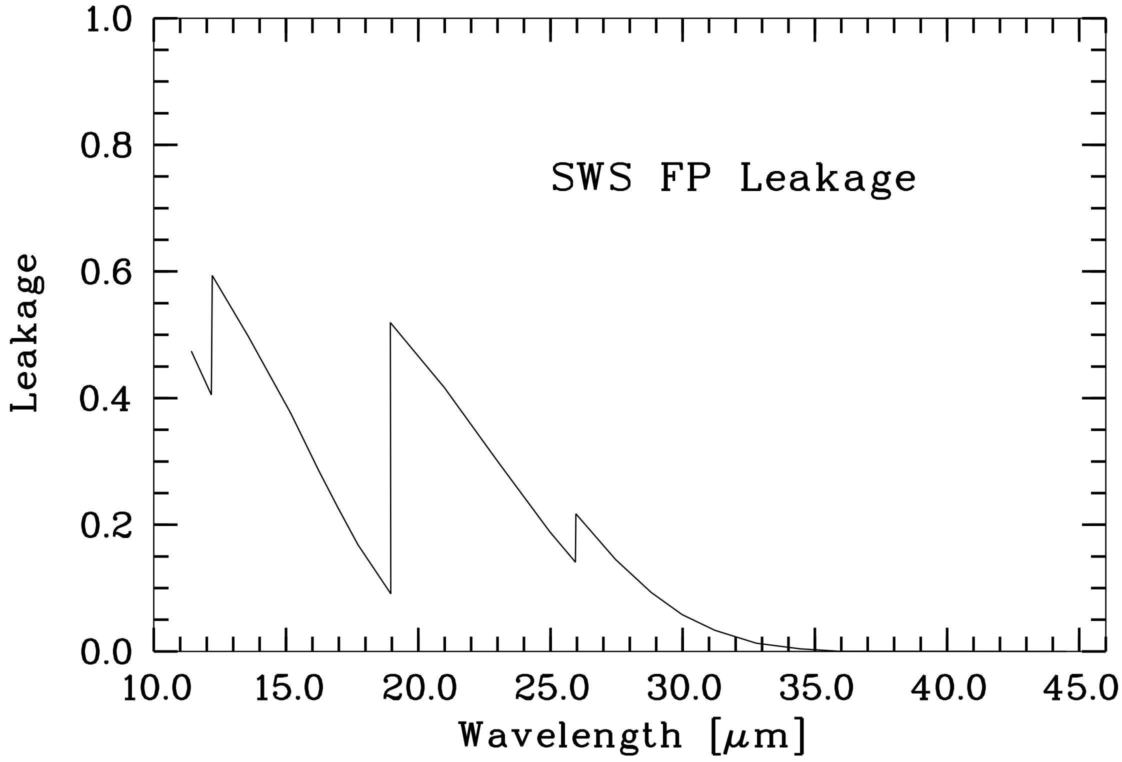

Figure 5.5: SWS Fabry-Pérot leakage. Leakage is defined here as the fraction of the total detected signal that originates in unwanted Fabry-Pérot orders. Preliminary data shown here are based on extrapolation from measurements at a few wavelengths.

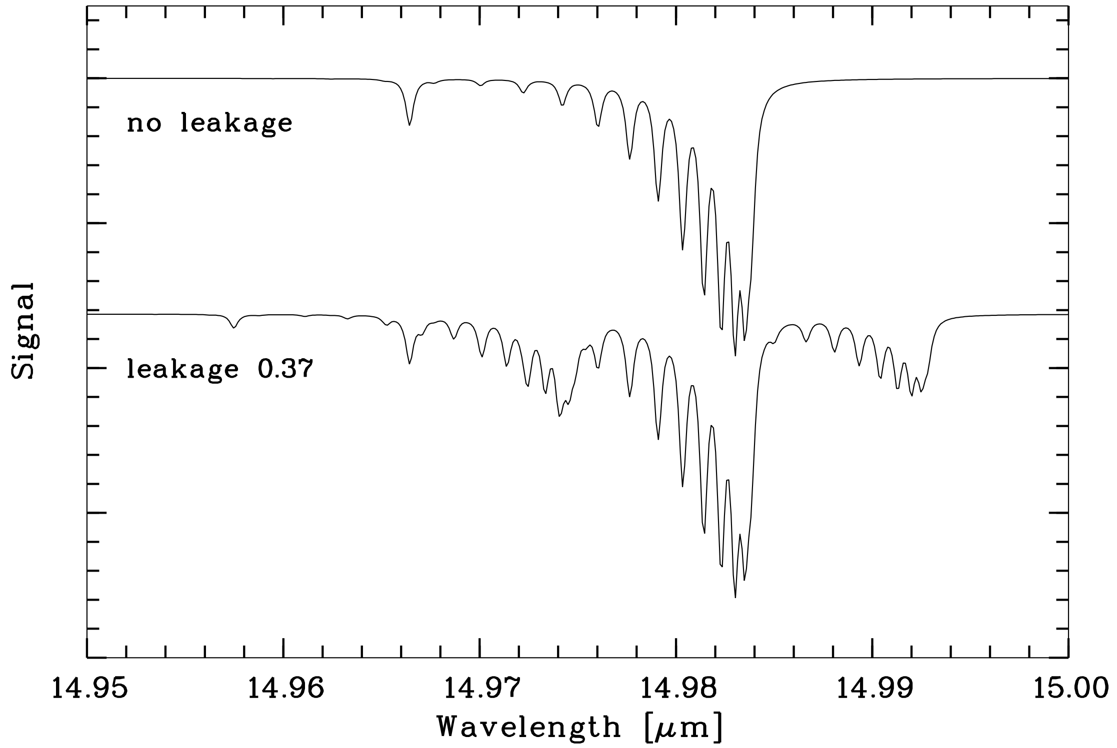

Figure 5.6: Effects of leakage on a crowded spectrum. A wavelength range of high leakage has been selected for demonstration. The upper line shows the assumed true source spectrum at the SWS F-P spectral resolution, the lower line how it will appear in the presence of leakage.

5.4 Detector Noise & Dark Current

Tables 5.2 and 5.3 give average detector dark noise for an entire band for a one second reset interval in column N_D. The detector noise given is that if some processing has been carried out on the data, namely throwing away samples affected by glitches. For comparison, the pre-launch values of detector noise were 0.6 $\mu V/S$ for bands 1, 2, 3 & 5 and 0.9 $\mu V/S$ for bands 4 and 6.

Detector dark noise and dark current values for individual detectors are stored in calibration G files 21_1, 21_2, 21_4 and 21_8, corresponding to the 1, 2, 4 and 8 second reset interval. Units are $\mu V/sec$. Note that 8 second resets were only used early in the mission.

Checks were made at the start of every revolution for the purpose of characterising the dark current and noise throughout the mission. It was found that they were stable for all bands except band 3. Here, the dark currents increased by up to a factor of three, while the dark noise hardly increased for most detectors. In most cases the increase in dark currents was gradual, but occasionally it was from a sudden jump, e.g. detector 36 (band 3 detector 12) on rev 150. Dark currents also decreased - after 250 revolution of high dark currents, those in detector 36 dropped to one-fifth of their high value.

Which detectors in a band are or are not good can change. For example, at the start of the mission band 3 detector 34 was poor. After PV, when its bias voltage was changed, detectors 30, 31 and 36 were the worst in that band. In general a bad detector has either a high dark current or/and a high noise.

The dark currents were higher at the start of a revolution for all bands, decaying with time so that after about four hours they had reached their nominal values. This was especially the case for bands 2, 4 and 6, with increases of between 15% and 100%. This effect was less important for bands 3 and 5, while for band 1 it was only observed in a few detectors.

The dark noise showed no variation throughout a revolution.

Normally all changes in dark current will be automatically corrected during the OLP processing, see section 8.3.4. Cases where the continuum is weak can cause problems for dark current subtraction in the OLP pipeline, especially when memory effects are included. When the amount of flux falling on the detector is small, there may be cases where the output of the detector from (incident flux plus dark current plus noise) is less than the detector from (dark current plus noise), the end result being negative fluxes in the AAR product. The limiting flux for this is of the order of a few Jy for band 2.

5.5 Detector Response

The variation in the detector response throughout the mission, as determined from photometric checks, was below 5%. While for bands 1 and 2 this change was of a random nature, the band 3 responses showed a slight anti-correlation with dark currents, and the band 4 response increased by a small amount.

During a revolution, the band 1 response was stable to within 2%, whereas for band 2 the response was higher by 40% at the start of a revolution, decreasing with time. For bands 3 & 4 this effect was only at the 10% level.

Again, normally all detector response changes will be automatically corrected during the OLP processing, see section 8.3.5

5.6 Behaviour around a reset

As was discussed in section 3.4, “SWS Detectors and operation”, the destructive readouts that occur every 1, 2 or 4 seconds affect the readout electronics, which then take some time to return to normal. An example of this can be seen in figure 5.7 (an example of a glitch). It shows the ERD output of detector against time. A reset interval of 1s is used, therefore there are twenty-four samples per reset.

In this example, the first sample read out from the amplifier after a reset is the one located at a bit value of about 2800. The second is at about 2700 and the third is at 2000 – due to the rate at which the capacitor is charging the third sample appears to be an extrapolation of the previous ramp. When a slope is fit to the 24 Hz readouts the first few readouts are ignored, because they are affected by the destructive readout. The number of detector samples to ignore is given in Cal-G file 3. During PV it was found that the default number of samples to ignore after a reset was different from that thought pre-launch, so the contents of this calibration file was changed.

After the third sample the output of the amplifier seems to have stabilised and the capacitor seems to be charging up linearly, resulting in the increase of the bit value against sample (or time). This is not quite true however. If you look carefully at the figure you can see that each of the ramps has a slight curve in it. This causes errors when trying to fit a slope to the ramps.

During PV it was also found that the entirety of the first second had a slightly different slope to that of subsequent seconds (for reset intervals of 2 or 4 seconds). This was traced to different RC constants for the different seconds, and may be corrected in future versions of the OLP software by having different RC constants for the different seconds. These RC constants are held in Cal-G file 2.

5.7 Glitches

Glitches are caused by such events as fast moving electrons and ions inside the earths magnetic field. Whatever causes a glitch, the effect of one is a sudden large increase of the output voltage which causes a large step (a "glitch") in the affected ramp. Derive-SPD attempts to remove glitches by ignoring the corrupted sample(s) and trying to construct two shorter slopes, one either side of the removed sample(s).

Note that glitches can have an effect that lasts for a long time (they have tails) and that a glitch in one detector can affect other detectors in that detector array.

Figure 5.7 shows an example of a glitch in the 24Hz ERD data. Note that the sets of two points with Bit values of around 2700-2800 are the result of the detector reset every second. The sample immediately after the two high points is also affected but appears okay due to the signal level.

Figure 5.8 shows two examples of a band 4 glitches in the SPD. In both cases the detector requires a long time to stabilise.

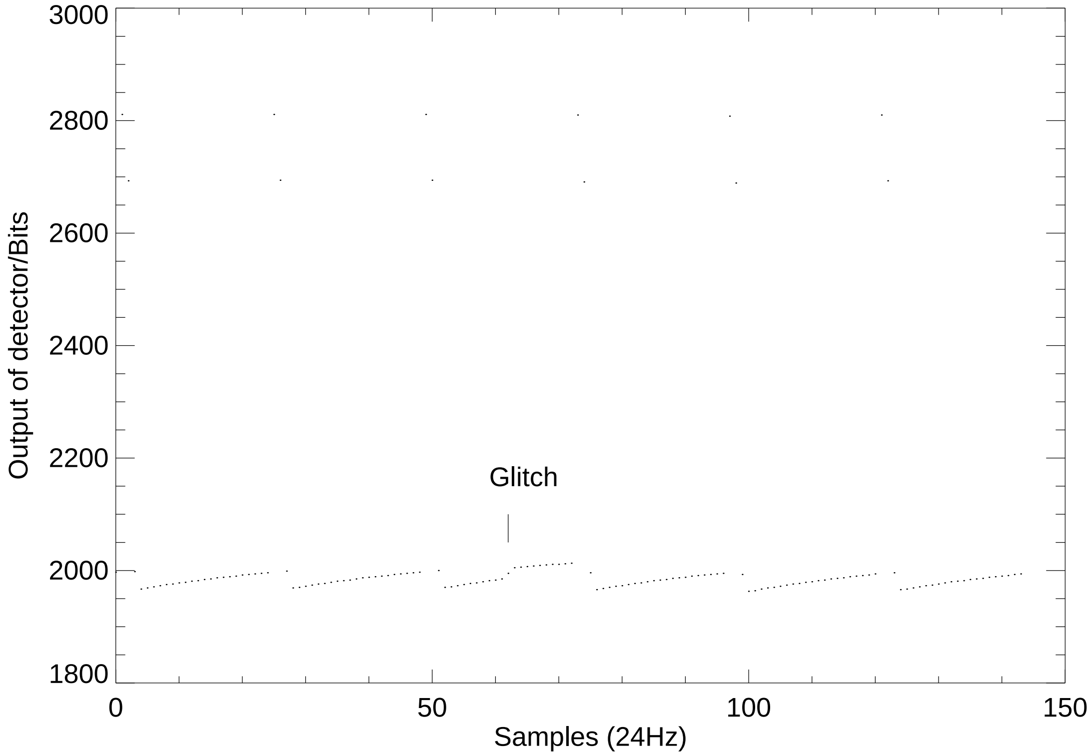

Figure 5.7: An example of a small glitch seen in the ERD

Another type of upset has been observed, called 'scan jumps'. These appear to be similar to glitches, but they affect an entire detector block. The symptoms are that each detector in a block suffers a sudden rise in sensitivity, that slowly decays with time. They usually only affect one of an up-down scan pair, and the only solution is to throw a portion of the affected scan away.

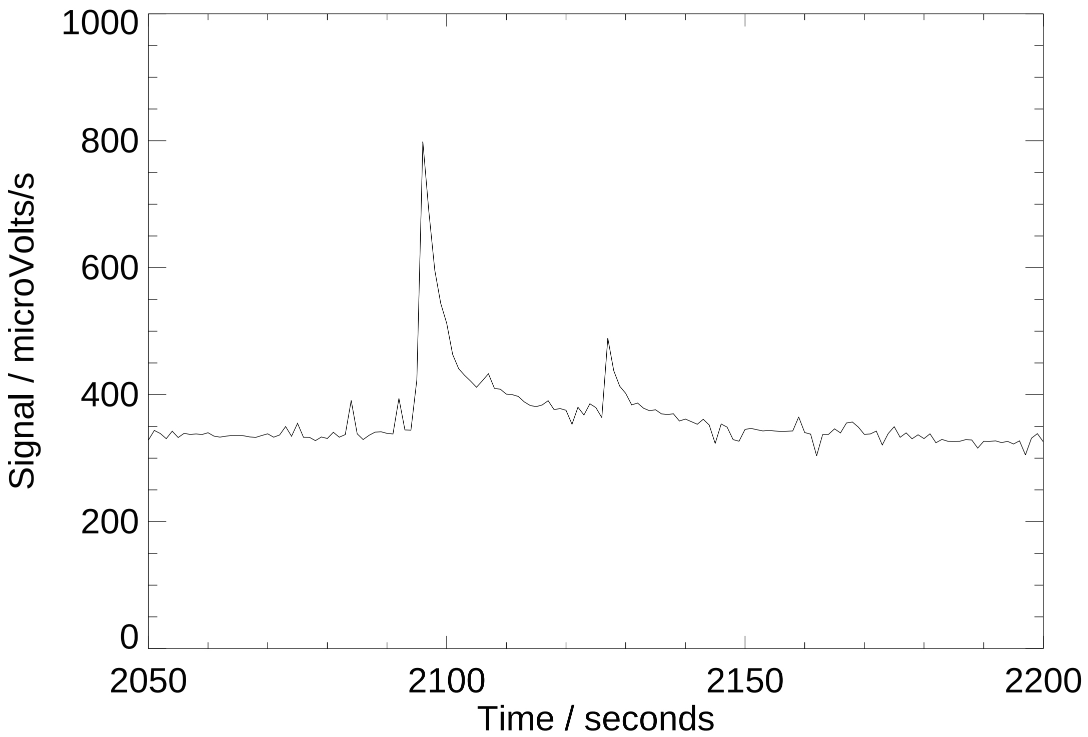

Figure 5.8: Two examples of glitches whose effects last for a long time. The data shown is SPD from a band 4 detector.

5.8 Memory effects

The band 2 and 4 detectors used in SWS "remember" their previous illumination history - bands 1 and 3 are not affected by memory effects. Going from low illumination to high illumination, or vice-versa, results in the detectors asymptotically reaching their new output value. These are referred to as "memory effects". Currently the only memory effects accounted for in the pipeline are those that affect dark currents - the first few dark current readouts are ignored.

An example of memory effects can be seen in Figure 5.9, which shows ERD data from detector 39 (band 4) as the illumination changes during a dark current check. It can be seen that the detector takes a few resets to stabilise both on light-dark or dark-light illumination changes.

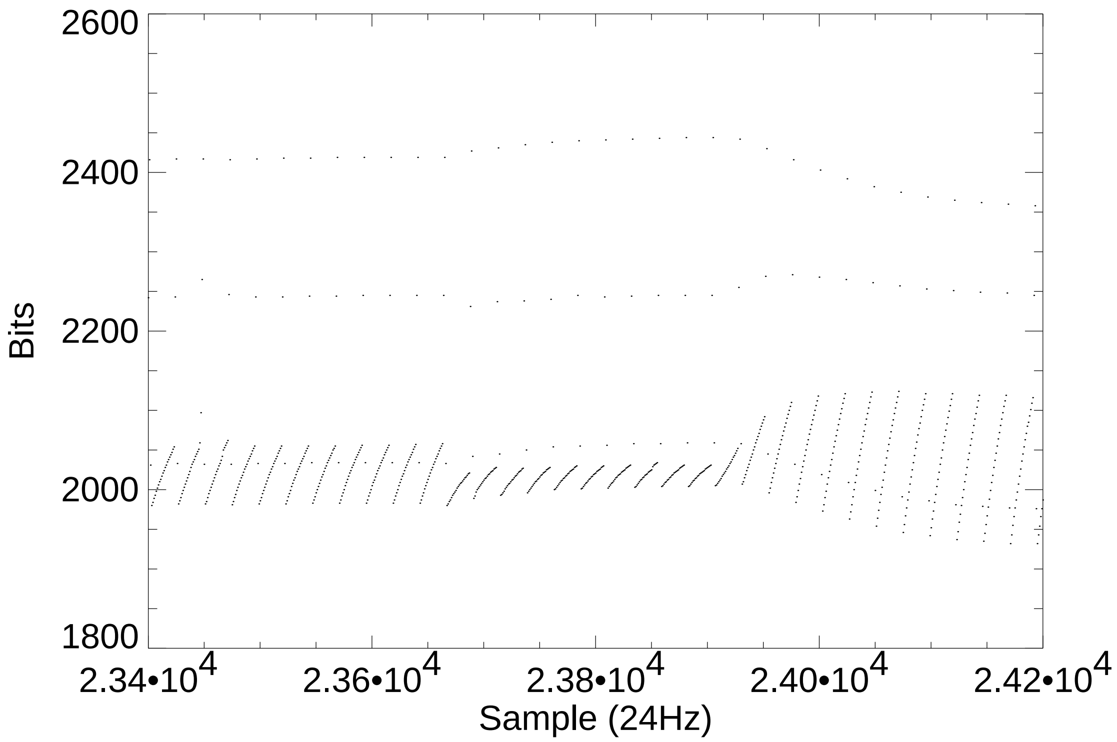

Figure 5.9: Example of memory effects

Another example of memory effects is the effect seen in up-down scans of fairly bright sources. For sources with fluxes greater than about 1000 Jy memory effects cause the up and down scans to differ in response (and hence flux) by up to 20% in bands 2 and 4. This effect can be seen in figures 5.10 and 5.11. Figure 5.10 shows the output of detector 13 against time along with the wavelength of light falling on the detector. It can be seen that the detector output rises from a low state at the start of the observation, and that it does not fall back to its low level at the end. Figure 5.11 shows the result of this in AAR. The top plot is for the up-scan, the lower for the down-scan – the down scan is shifted down by 500 Jy for clarity and remember that the up-scan actually scans down in wavelength (see section 4.6.1). While the short wavelength data for both scans has approximately the same flux level, the long wavelength data (that taken at the start and end of the observation) has quite different flux levels. Realistically, only the down scan should be used.

It is important to stress this - if you see your data is affected you must decide how much data to use and in extreme cases use only one scan.

Memory effects can also change the shape of line profiles. As an example, as the grating scans across a strong gaussian line the sensitivity of the detectors will change. If this change is large enough it will result in one side of the gaussian having a different shape from the other. As lines are scanned in different directions by the up-down scans, the line will have a different shape in both scans. If the scans are averaged the line will be broader than it actually is. Users should check for these effects and if they occur only use the unaffected half of a scan. These effects mainly happen in band 4, due to it's larger memory effects.

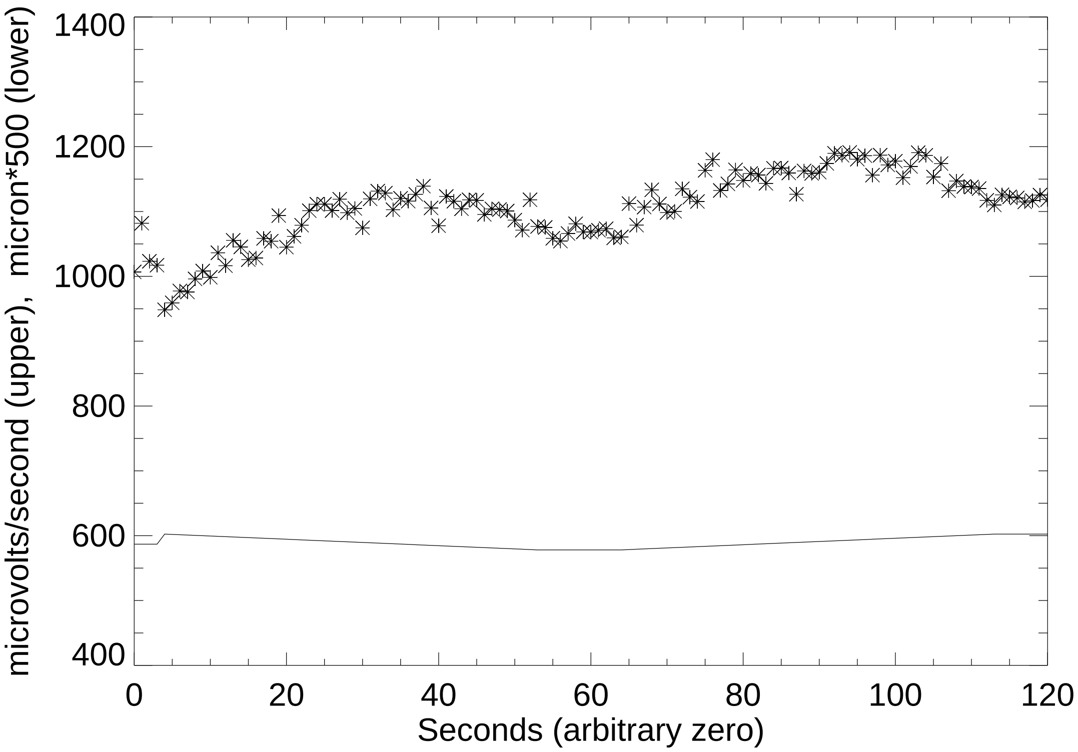

Figure 5.10: Example of memory effects on up-down scans as seen in SPD. Top is the detector output, bottom is the wavelength seen by that detector.

Table 5.8 (based on ground based tests) gives indications of the errors introduced into flux calibration by memory effects.

Table 5.4: Errors introduced by memory effects.

1 InSb	2 Si:Ga	3 Si:As	4 Ge:Be	5 Si:Sb	6 Ge:Be
<< 1%	6 – 15%	<< 1%	8 – 30%	25%	5%

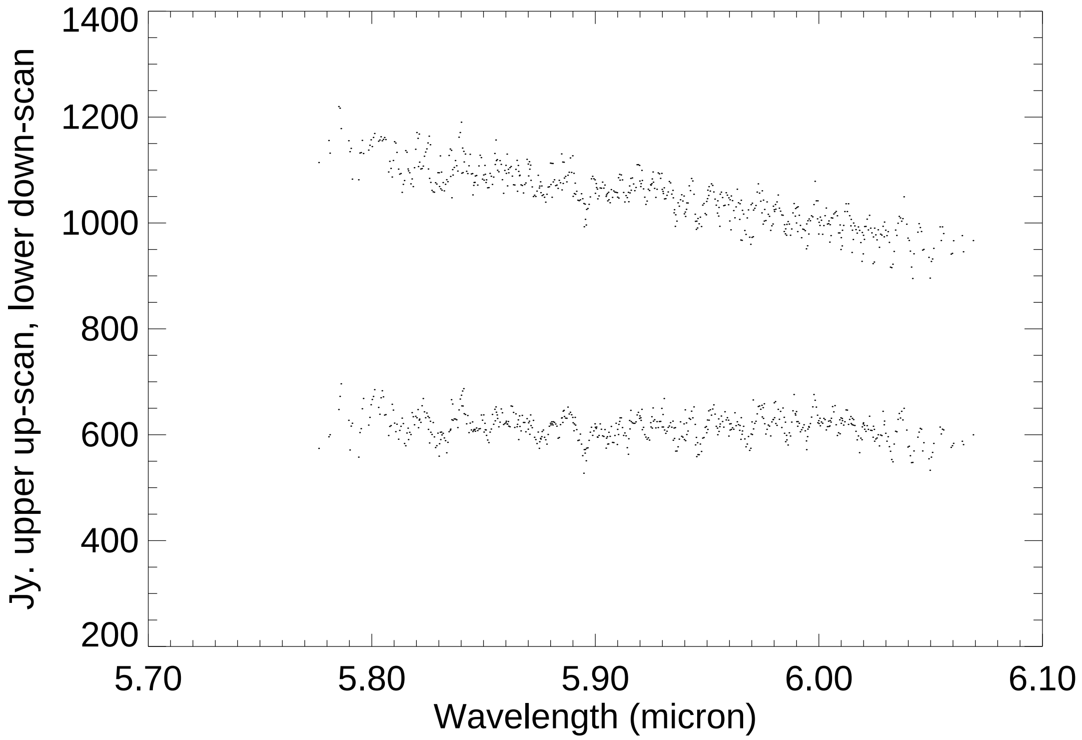

Figure 5.11: Example of memory effects on up-down scans as seen in AAR. The down scan has been shifted down by 500 Jy for clarity.

5.9 Reference Scan Memory Effects

Reference scans, described in section 4.6.2, “Reference scans”, and detector memory effects can combine to affect the data produced from band 2 and band 4 detectors during AOT S06 observations.

This possible problem in the flux calibration of S06 science observations is traceable to memory effects left over from reference scans. The intended science objectives may then be compromised in portions of the spectrum.

The document ‘Possible Detector Memory Effects in SWS Grating range spectra (AOT S06) due to SWS Reference Scans’, by K. Leech & P. Morris, 27 May 1997, gives examples of such effects and indicates what to do if they occur.

5.10 Effects of pointing accuracy

The accuracy of the target input coordinates, and of the pointing, have a large impact on the instrumental throughput, of the point source flux accuracy but only a minor impact on the wavelength accuracy of SWS for point sources. ISO’s random pointing error can also introduce effects in the data if the target coordinates are incorrect or if the target is in a crowded field.

Several documents were written covering the effects of pointing accuracy. ‘Effects seen in data induced by incorrect target coordinates or crowded fields’, by K. Leech & A. Heras, 12 June 1997, gives examples of what can go wrong when incorrect target coordinates are used.

In summary, a star offset from the center of the aperture by $6''$ in the cross-dispersion direction (y-axis) loses approximately 40% in throughput (example taken in the LW, $17\,\mu m$). Incorrect target coordinates can lead to the derived flux being incorrect by large factors. An offset in the dispersion direction (z-axis) affects the wavelength calibration, but the effect is not of the same order of magnitude as the effects on flux. A $4''$ mispointing in the dispersion direction corresponds to about a 1 LVDT (1/8 grating resolution) wavelength offset, so the maximum possible offset is about 2 LVDT, or about 1/4 of a grating spectral resolution element. This error is within the quoted wavelength accuracy.

Also note that problems may occur if there is another object, with a flux similar or greater than the target, $4 - 10$ arcseconds away in the z-direction, as can happen in crowded fields.

This study was extended in ‘The effects of the pointing jitter on SWS observations’, by A. Heras, 6 August 1998. This compares the ratio of on- and off-source observations of a star with the pointing jitter. It finds that sudden flux jumps are associated with pointing fluctuations. It also notes that even for nominally on-source observations (defined to be those where the pointing error is less than about $4''$), there is a correlation between noise in an observation and pointing jitter.

During the ISO mission several stars were observed every few weeks for purposes of wavelength and flux calibration. The flux of one of these targets, Gamma Dra, was seen to have a modulation in it that is suspected to be due to pointing errors. The report ‘Status of study on Gam-Dra fluxes and related pointing errors’ by H. Feuchtgruber, issued on 10 June 1998 can be read for further information on this.

Information on how the spacecraft pointing can affect observations of extended objects can be read in the document ‘Status of study of AOT02 line profiles and fluxes on NGC6543’, by H. Feuchtgruber issued 2 June 1998. In this case the observed line fluxes varied by 10% over the course of several months. This was attributed to the spatial extent of NGC 6543, the SWS slit size projected on the sky, see section 3.3.2, and the change in roll angle between the observations.

5.11 Grating instrumental profile and resolution

The document 'Grating instrumental profile and resolution', by M.E. van den Ancker, R. Voors & K. Leech, 1 July 1997, discusses investigations of the grating instrumental profile and describes possible instrumental effects on emission lines profiles observed with SWS.

Ground-based tests showed the SWS Instrumental Profiles (IPs) to have a Gaussian shape up to accuracies of a few percent. To verify that this would also be the case in-flight, several objects showing strong, narrow, emission lines (mostly Planetary Nebulae) were observed in ISO's performance verification (PV) phase to investigate the influence of parameters such as the position of the source in the aperture, the size of the target and the SWS AOT band.

The conclusions (based on AOT 2 & 6 observations, should be applicable to AOT 7 SW grating observations but are not applicable to AOT 1 observations) are:

- The SWS grating instrumental profile is very close to Gaussian.
- The only systematic differences from a Gaussian profile are a slight "shoulder" on the blue side of the base of the profile and a depression on the red side as compared to a purely Gaussian profile. The only parameter this seems to depend on is the position of the source in the slit.
- The grating resolving power of SWS for all investigated sources is better than expected for extended sources at all wavelengths. This could either mean that none of line-emitting regions in any of the sources fully filled the SWS aperture, or that the SWS resolving power for extended sources is better than expected.
- In AOT bands 2 to 4 the resolving power for point-like sources is slightly better than predicted from the ground.

5.12 Single Detector Signal Jumps

The document 'Single Detector Signal Jumps', by A. Heras, 9 June 1997, summarizes a study made on single detector signal jumps. These effects occur in only one detector at a time and can be generally described as a sudden increase or decrease of the signal, which then remains constant or has a long recovering time ($>> 10$ s) after the jump. These jumps are normally seen at low signal levels. Examples of such jumps in SPD data are shown in figure 5.12

The signal jumps observed for each detector vary significantly between different cases, and may be negative or positive.

Jumps in band 3 are of different nature from jumps in bands 1 and 2.

The frequency of jumps in bands 1 and 2 is of approximately 5 jumps per hour.

The signal jump is more clearly reflected on the first second of the reset interval than in the second one, indicating a relation between the signal jump and a residual after reset pulse effect. This will be further investigated when working on a possible correction for these jumps.

For bands 1 and 2 and for the measurements with a reset interval of 2 seconds, half of the jumps are associated with the detection of glitches. However, no correlation has been found between the characteristics of these jumps and and those of the glitches.

Users are recommended to examine the SPD from their observations to look for such jumps. If they are present the user can either throw the affected portions of the data away or try to adjust the baseline of the affected portion to the pre- and post-jump baseline.

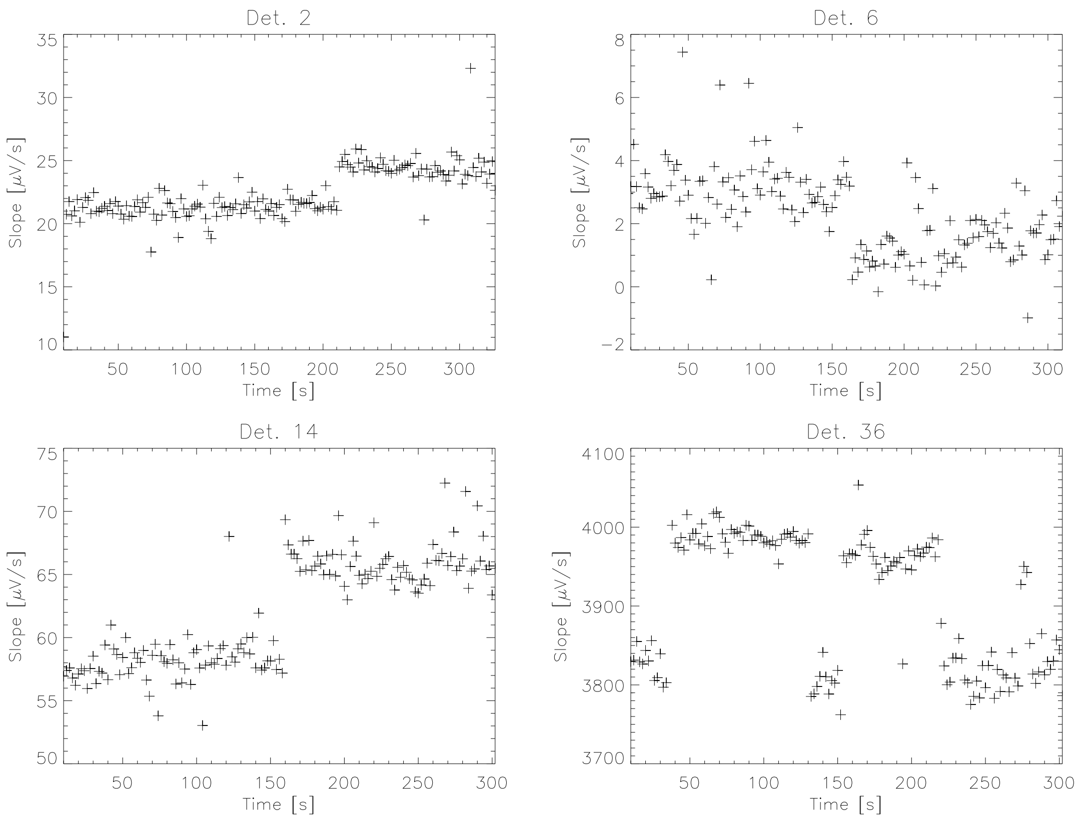

Figure 5.12: Examples of single detector jumps

5.13 Light leakage in band 3D

Band 3D suffers from leakage around $27\mu m$. Figure 5.13 shows band 3 data of an object with flux falling towards longer wavelengths. The slight increase in the flux seen in band 3d from about $27\mu m$ onwards is not real but is due to leakage from approximately $13\mu m$. This leakage is of the order of 10% and will primarily affect objects with flux falling sharply towards long wavelengths.

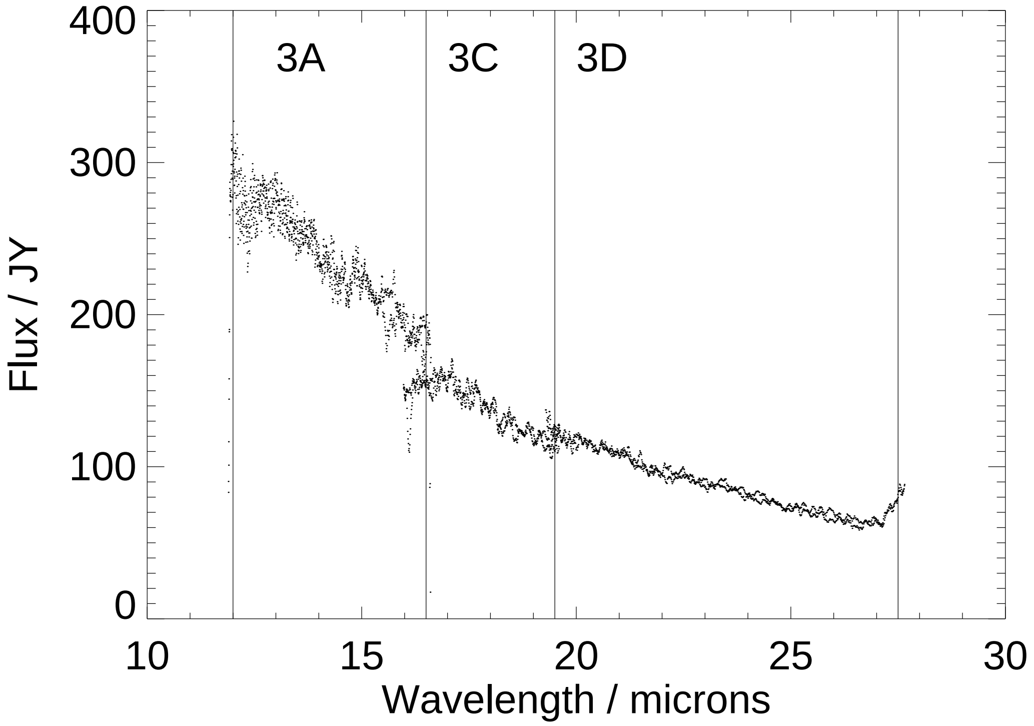

Figure 5.13: Band 3 data showing the leak around 27 microns

5.14 CAM CVF & SWS

In May 1997 cases came to light where the action of a CAM-CVF observation before a SWS observation led to an increased SWS band 3 detector dark current. This increase above the nominal value approached a factor of 100 in some cases. The dark current decreased with time during the SWS observation and reached the nominal dark current less than 30 mins after the CAM-CVF observation. This effect can be seen in affected observations by selecting and plotting all the dark currents from the data (SWSPFLAG bit 27 set) - the dark currents are enhanced and decrease with time. In severe cases this effect can manifest itself in the AAR by band 3 fluxes being negative and in the SPD by the band 3 up and down scans having different shapes.

No correlation between the dark current and the operation of any other instrumental AOT was seen.

All observers who had SWS observations after a CAM-CVF observation were contacted around June 1997. After this date SWS observations were not scheduled until after 30 minutes of a CAM-CVF observation.

5.15 Diffuse Background Emission

SWS does not use spatial chopping, hence all spectra will contain some contribution by zodiacal light and galactic background. In most cases, this will be negligible compared to the source flux. The zodiacal background component is the most important over the largest part of the SWS wavelength range, with a continuous spectrum corresponding to a dust temperature of about 260K, that does not affect searches for line emission. As an order of magnitude estimate, a typical zodiacal light flux density seen within a SWS aperture will be about 0.3Jy.

Chapter 6

The RSRF and Effect of Fringes

6.1 Introduction

The Relative Spectral Response Function (RSRF) is the total throughput of the system. It arises from the convolution of the detector response as a function of wavelength, the filter response as a function of wavelength and takes such effects as geometrical considerations (e.g. slit width, source structure) into account.

Fringes are a modulation with wavelength of the light falling on the detectors. The fringes arise due to constructive/destructive interference in either in the detector material itself (between the front and back of the detector) or similarly in the filter material. To some extent all detector bands suffer from fringes. Bands 1, 2 & 4 are only lightly affected, whereas the fringes are more pronounced in band 3. An example of fringes in the band 3D spectrum of a star can be seen in figure 6.1.

An attempt is made to remove fringes during the OLP processing pipeline. However, because the fringes may shift in wavelength space depending on where the source is in the slit (especially in the dispersion direction) and whether the objects being observed is a point source or extended, fringe removal may not be perfect. This may cause problems for observations of faint sources. Any faint features should always be checked against the relevant Relative Spectral Responsivity File, SWS Cal-G 25_x, to ensure they are not artifacts.

6.2 The RSRF calibration

The RSRF of the SWS Flight Model was intensively measured in the laboratory prior to launch. The calibration source used was a cryogenic black-body source with temperatures between 30 and 300K. After the launch of ISO, the recalibration of the RSRF was performed on standard stars and asteroids using calibration uplink procedures. These scan more than the allowed wavelength range for each AOT band and ensure each scanner position is scanned.

The in-flight RSRFs are derived using the SWS Interactive Analysis package. The measurements are processed as in the standard pipeline up until the flux conversion steps. The RSRF is then obtained by dividing this 'raw' spectrum by a model of the observed source. For stellar sources containing spectral features, small inaccuracies in the model can introduce false features in the RSRF, and thus in every spectrum processed with this RSRF. Therefore, extreme care has to be taken before 'correcting' the RSRF.

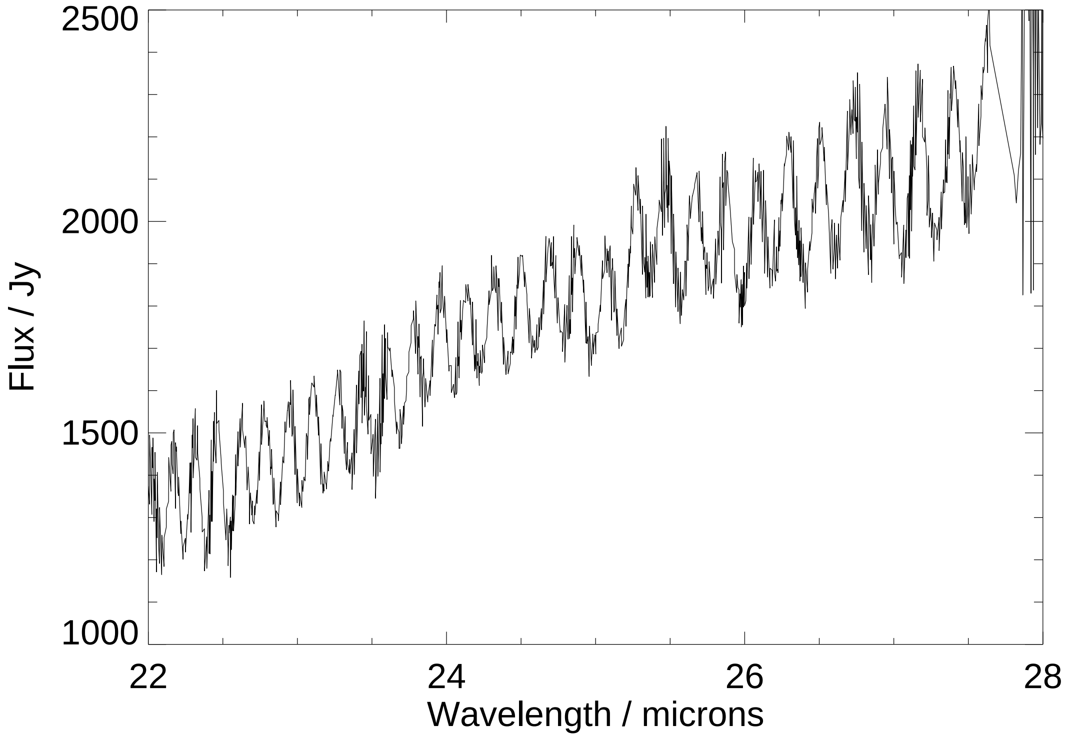

Figure 6.1: Example of fringe effects in band 3

6.3 RSRF Calibration sources and model sources

Black-body measurements made in the laboratory are used to determine the small scale structure of the RSRF's for all bands. If the use of these RSRF's on standard observations result in similar 'features' being seen in many sources, and it is proven these 'features' come from the RSRFs files, they are removed by comparing the RSRF files with AOT 1 or AOT 6 observations of standard astronomical objects for which accurate SEDs are known.

For the shorter wavelengths (2.36-16 microns) α Lyrae (HR7001) is being used as the primary in-orbit calibration source. For the longer wavelengths, the asteroids Ceres and Pallas were initially chosen as the primary calibration sources. Unfortunately, the solar system tracking performance of the ISO satellite disturbs these measurements. Therefore, NML-CYG and Gamma Draconis (HR6705) have been observed in order to uncover possible discrepancies between lab and in-orbit measurements. Other objects used to derive the currents RSRFs are α Boo (HR5340), β Leo (HR4534), Delta Draconis (HR7310) and β Pegasus (HR8775).

Models used for comparison include ones by Cohen, Kurucz and Marcs.

6.4 Differences between lab RSRF and in-orbit RSRF

The differences between the RSRF obtained in the lab and in orbit are twofold:

(1) The overall shape agrees mostly within the current uncertainties of the models and the observations. The only place where the discrepancies are so big that a correction of the calibration makes sense at this stage, is at the short-wavelength edges of bands 1A and 2A. The relative responsivities as measured in the lab appeared up to 60% higher than in orbit. This can be

explained as a leakage problem since the temperature of the calibration source was only 300K.

(2) In the lab only band 3 showed fringes, while in orbit bands 1 and 2 also show fringes. The filters in the detector block have been identified as the cause of these fringes, with the thickness of the filters matching the Fabry-Pérot gap calculated from the observed fringe frequency. The width of the fringes is close to the resolution limit of the instrument. This explains why the effect was not observed in the lab: the external black body source was extended and thus the resolution of the measurements was not high enough to show the fringes.

6.5 What can go wrong when dividing by the RSRF?

6.5.1 Present quality of RSRFs

Derivation of a complete set of in-orbit RSRFs is needed to obtain an optimal flux calibration accuracy. However, this calibration is still ongoing. Until this has been done, the RSRFs measured in the lab have to be used for most bands. For bands 1a and 2a, a correction of the overall shape was applied to compensate for the leakage problem previously mentioned. This correction was done by polynomial fitting of in-orbit and lab data and multiplying the lab data with the ratio of the two fits.

For OLP V6.1 the Cal-G 25_x files containing the RSRF's were updated leading to a significantly improved calibration of the spectra. The few problems found in the new calibration files were, however, almost always present in the previous set of RSRF's.

These problems were:

Band 2C Based on analysis of many sources it was concluded that features seen at 9.35, 10.05, 11.05 μm are most likely due to responsivity correction – see section 6.6.1.

Band 3D There is a leak affecting data taken at 28 μm for some sources – see section 5.13.

Band 3E There is a suspect slope change in the middle of this band in many observations. It was first thought that this reflects a spectral feature in the source that was used to derive band 3E RSRF, NML Cyg. However the fully reduced NML Cyg spectrum also shows this feature, so it was not divided out as one would expect in this case.

Band 4 This file has not been updated, due to a lack of calibration sources for band 4. It bends down on the short and long wavelength edges.

6.5.2 Respcal after wrong dark subtraction

If the dark current subtraction was not correct, and therefore incorrect offset correction applied, the Derive-AAR respcal step (which is a gain correction) can introduce incorrect shapes of the continuum or false features.

A way to check if the dark current subtraction has been done correctly is to overplot the AAR spectrum after respcal with the RSRF and checking to see if any small residual RSRF features remain.

Examples are given in figures 6.2 and 6.3.

6.5.3 Uncertainties of some line flux levels in weak sources

The following section gives an overview of the RSRFs as seen in the lab versus the RSRFs as measured in orbit. These graphs can be used to determine in which regions the RSRF

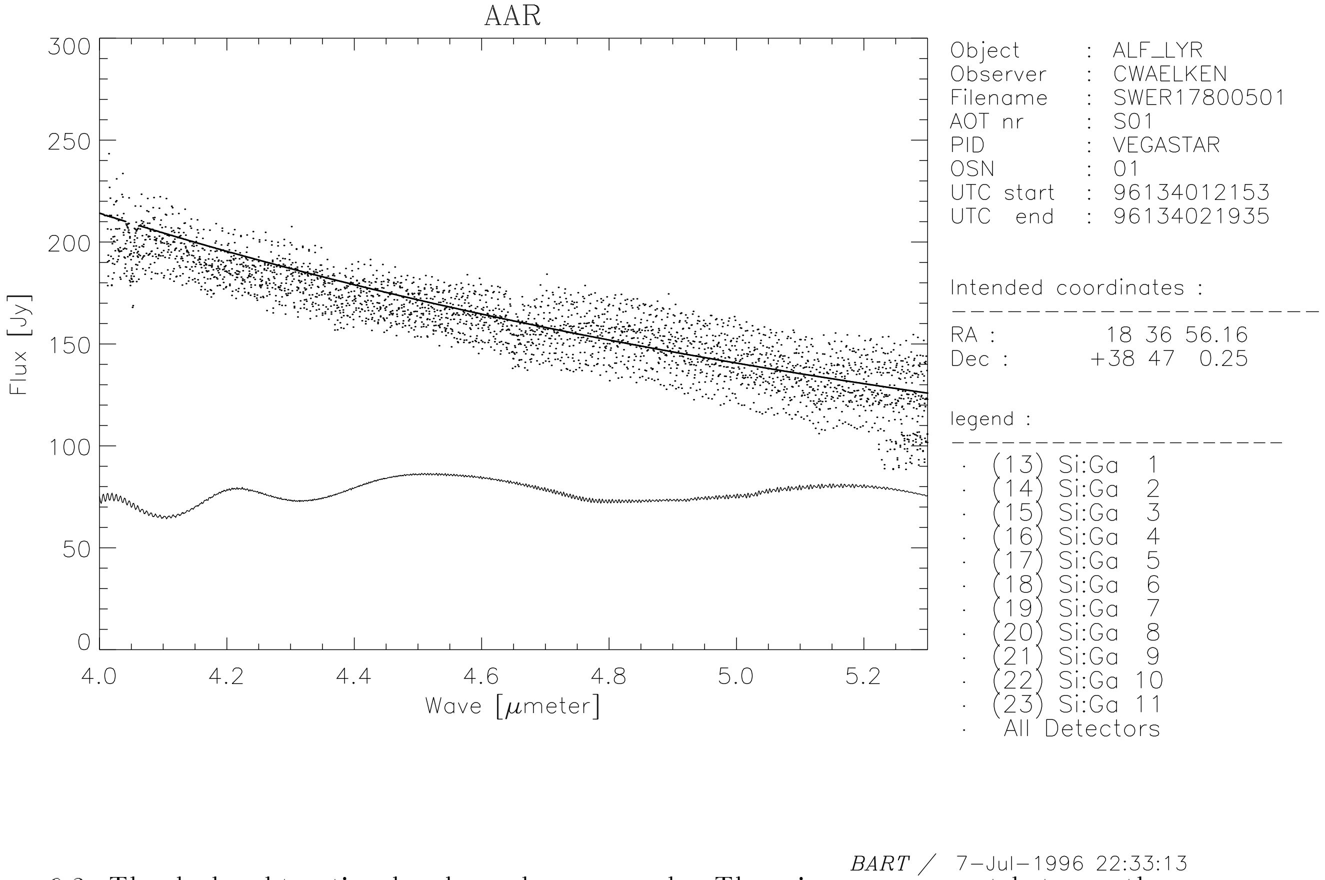

Figure 6.2: The dark subtraction has been done properly. There is no agreement between the features in the RSRF (solid line below the spectrum) and the spectrum. The solid line through the datapoints of the spectrum is a model atmosphere.

calibration is more uncertain. This is mostly at some band edges. They help us to understand inconsistencies as in figure 6.4.

After rebinning the spectrum shown in this figure, the continuum level in band 1e will be in agreement with band 2A. However, the line flux at 4.05 microns will be about 30% lower. One should keep in mind that we're talking about a continuum which is virtually zero – errors in a gain correction (like dividing by RSRF or the absolute flux conversion) will be almost invisible on the continuum, but very clear in the line fluxes.

This means one has to be careful when interpreting line fluxes of spectra with a zero-continuum: if the line is in a region where the lab RSRF is different from the in-orbit RSRF, the flux of the line is less accurate. Thus in the example shown in figure 6.4, the line flux in band 1e has to be believed.

It should be noted that (1) these problems are less likely to occur with spectra with a high continuum because the errors in the gain correction will be applied to the continuum as well (thus the line/cont ratio will be correct) and (2) the differences in line fluxes in the example do not represent the current uncertainties of the RSRF flux calibration in that region: this observation was an early PV observation with the AOT logic not fully optimised.

6.5.4 Uncertainties of line flux levels in band 3

In detector band 3 large fringes are present. These fringes can shift with the position of the source in the slit. A small mispointing (within the specs of ISO) can shift the fringes over 1/4 of

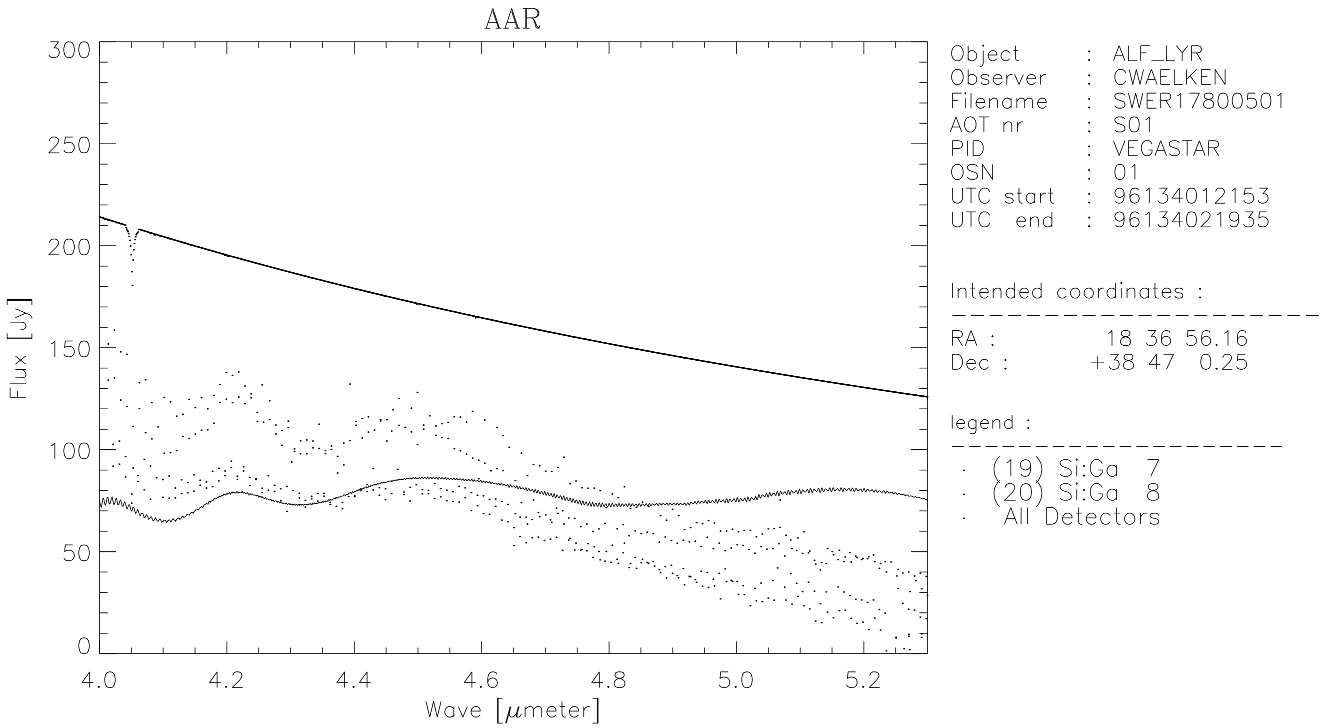

Figure 6.3: The dark subtraction has not been done properly. If we overplot the RSRF (solid line through the spectrum), we see that the features in the spectrum are not real. Also the slope of the spectrum is not real (compare to the model atmosphere printed above the spectrum) Flatfielding the AAR might help to decrease the scatter between the different detectors, but it will never correct for the real problem.

their period. Before measuring line fluxes of unresolved lines in this band, it has to be checked if the fringes in the SPD are in phase with the fringes in the RSRF. If not, the fluxes of unresolved lines in band 3 might be off by 25% since the relative size of the fringes is about 50%.

This also means line fluxes measured with fast AOT 1 observations that cannot resolve the fringes in band 3 are only reliable for less than 25%.

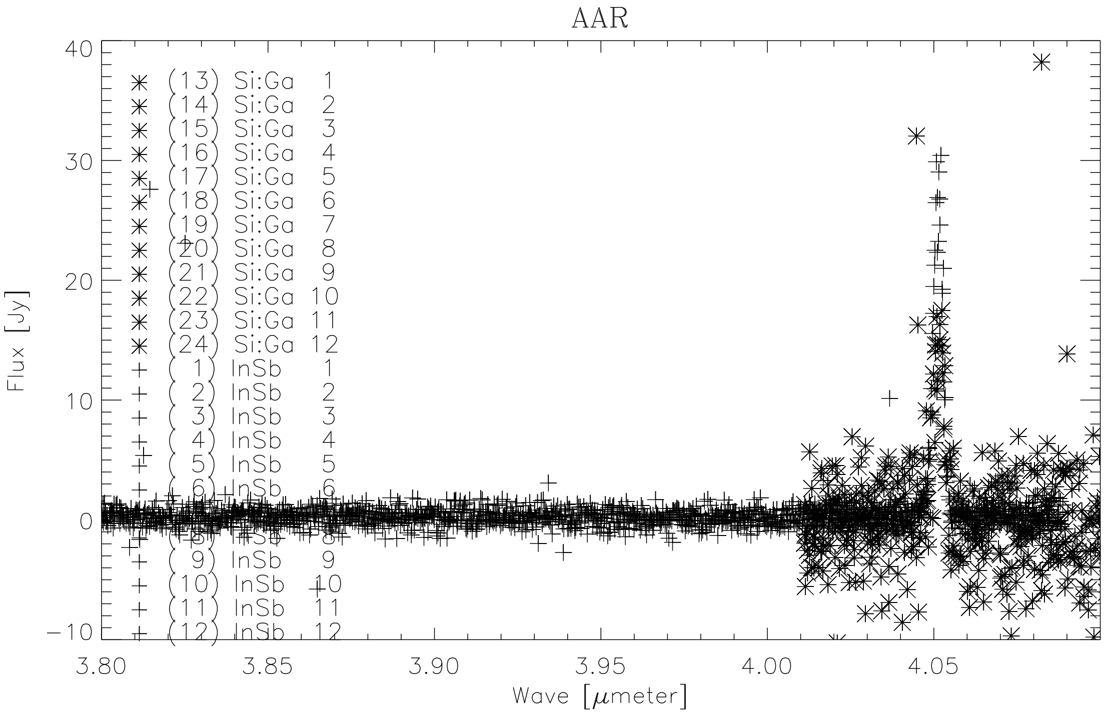

Figure 6.4: The 4.05 micron line as seen in bands 1e (+ symbols) and 2a (* symbols)

6.6 Spurious Narrow Spectral Features

The RSRFs used in OLP 7.0 are based on the pre-launch ILT tests with broad shape corrections derived from in-flight observations of standard stellar sources. The only small scale corrections applied were for four narrow features in the lab RSRF. From careful analysis of data from many sources processed with the lab RSRFs, four narrow spectral features were discovered that were due to the system response. These features were at:

Band 2C 9.35, 10.05 & 11.05 microns

Band 3A 12.3 microns

While the OLP 7.0 RSRF files have been corrected to remove these features, a residual of the emission feature at 11.05 microns can still be seen in very high S/N data.

The first report on the analysis of the band 2C features is printed below for information.

6.6.1 Spurious Spectral Features seen in Band 2C

Introduction

Spurious features may be present in band 2C (7 to 12 microns) that should not be mistaken for actual spectral features from the object of interest. This warning is based on a small sample of observations, and its conclusions should be treated as preliminary at this stage.

Band 2C features are a collection of ubiquitous spectral 'lines' in emission and absorption seen between 7 and 12 microns (SWS Band 2C). An example of these features is shown in Figure 6.5, the normalized flux of an AOT1 speed 1. Also plotted is the Relative Spectral Response Function (RSRF) of Band2c.

The features occur at:

9.35 microns in absorption with a FWHM: 0.3 microns

10.05 microns in emission with a FWHM: 0.1 microns

11.05 microns in emission with a FWHM: 0.1 microns

Data

Forty-three Band 2C spectra were collected from 9 observers in order to find trends in the strength of the features. The spectra are from both carbon and oxygen rich objects which are, in turn, stellar and nebular in origin. Since a rather broad wavelength range is required, only data from AOT SWS01 observations was used. This does not preclude the features being present in the data from other AOTs.

Table 6.1 shows a summary of the 43 sources in the sample with at least one feature. The peak wavelengths, FWHM and Percent of continuum levels ("% Cont", negative meaning absorption, positive emission) are median values in the sample. Also listed are the minimum and maximum values for each parameter that were seen in the dataset. Some of the spread is due to noisy data and the difficulty of measuring the continuum and width of a line.

The summary for the absence of features is shown in Table 6.2. We have listed the number of sources that do NOT show a feature and the continuum level where we expect the feature to be. In general the absence of a feature correlates with the continuum strength. Of the sources that do not show one of of the features, at least 2/3 of these have continua below 100 Jy. Again, this may be an indication of the difficulty in measuring the features.

The remaining sources that have high continua but do not show a feature remain a puzzle. Of the high continuum sources (>100 Jy), 2 do not show the 9.35 micron feature, 3 do not show the 10.05 and 1 does not show the 11.05 feature.

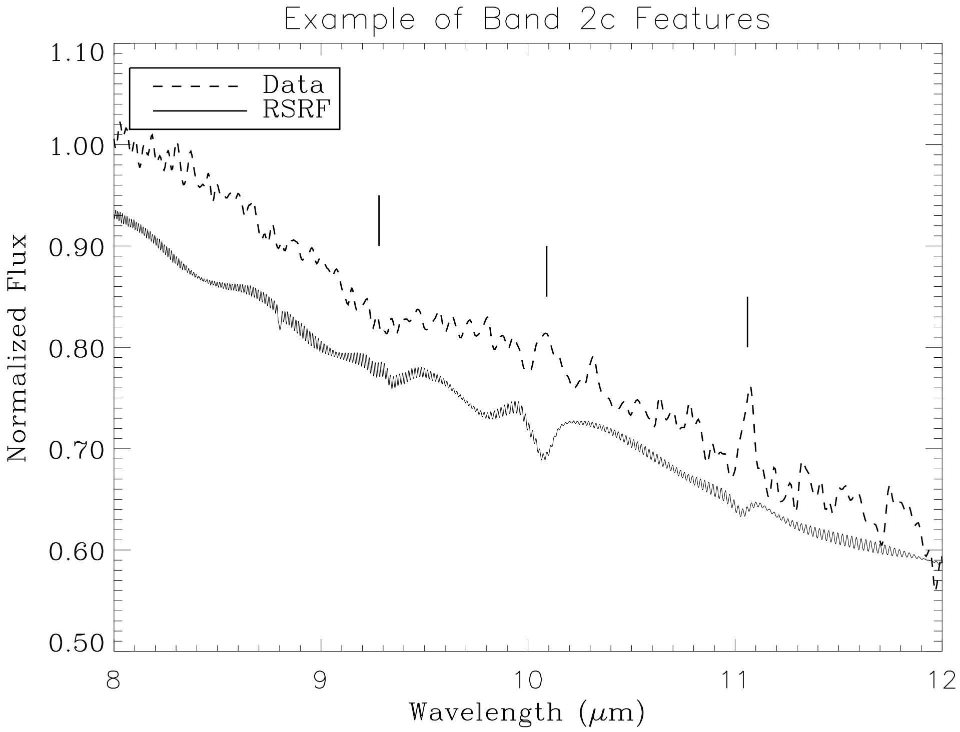

Figure 6.5: SWS spectrum showing spurious features

Since we did not specifically ask for sources that did not show any features, we cannot draw any conclusions about these sources.

Results

From the 43 sources we find the following:

- For the 9.35 micron feature, there is a spread of between 1% to 14% in the strength of the feature peak relative to the continuum.
- For the 10 and 11 micron features, the peak is roughly 5% of the continuum in all but one source greater than 100 Jy.
- There are no apparent trends with Galactic or Ecliptic latitude or longitudes.

Table 6.1: Sources with features

Feature	#	Peak Waveln.	(Min,	Max)	Median FWHM	(Min,	Max)	% Cont	(Min,	Max)
9.35	36	9.26	(9.2 ,	9.4)	0.295	(0.029,	0.482)	-7	(-14,	1)
10.05	30	10.07	(9.96,	10.10)	0.094	(0.017,	0.280)	3	(-5,	11)
11.05	37	11.05	(11.01,	11.11)	0.090	(0.050,	0.180)	6	(4,	15)

Table 6.2: Sources without features

Feature	Number	Median Cont (Jy)	(Min, Max)
9.35	7	63	(20, 4200)
10.05	13	46	(14, 430)
11.05	6	18	(12, 115)

- The equivalent widths of the features show similar trends as the peak fluxes but are more scattered.
- There are 'features' present in the Band 2C Relative Spectral Response Function (RSRF) at or near the positions of the observed features.
- There is one measurement of the 9.35 micron feature in emission (1260 Jy continuum) and one high SN measurement of the 10.05 feature in absorption (316 micron continuum).
- The features are not always present in the spectra.
- We do not have a large database of counter-examples.

Discussion

There are a number of arguments why these features are not astronomical:

- The strength of the features is roughly a constant multiple of the continuum. This strongly suggests that the features are introduced in the Relative Spectral Response Function (RSRF).
- The features appear in all types of sources without any correlation to position on the sky.
- The features appear at wavelengths where the RSRF has significant changes. See Figure 6.5.
- Finally, the RSRF was determined from very strong signals. In the presence of the band 2 memory effects, strong signals can influence the contrast in any measurement including the RSRF measurement itself.

However, the absence of features in some spectra clouds the problem greatly. If these features are introduced in the RSRF, then we must explain what is happening in the sources without the features. Again there are a number of possibilities:

- The spectra are too noisy to measure the features well. This is likely the cause of the variation of the equivalent widths. An example of this problem is seen for the 10 micron feature in Figure 6.5. Due to noise, the continuum beneath the feature is highly uncertain. This would result in a poor determination of the line strength.
- Different data reduction techniques hide the features. SWS_REBIN, an SWS IA tool, can have a significant effect on the features depending on the resolution and method used for computing the rebin.

- In some sources the features may be real. If the features are very strong they could be astronomical. However, until there is a resolution to this issue, they should always be suspect.

Conclusions

From the small number of observations studied the preliminary conclusions on these spectral features are that they appear in all types of objects and are a constant fraction of the source continuum, roughly 5%. At this time, the best explanation is that the features are introduced by the RSRF and are not astronomical in origin.

While only AOT 1's have been checked, these features have been seen in the data from other grating AOT's.

These conclusions should be viewed as preliminary until a more complete investigation is carried out.

6.7 Overview of the RSRF curves

RSRF curves for all bands are plotted in this section. Note that the graphs are not noisy, but are affected by high frequency fringes.

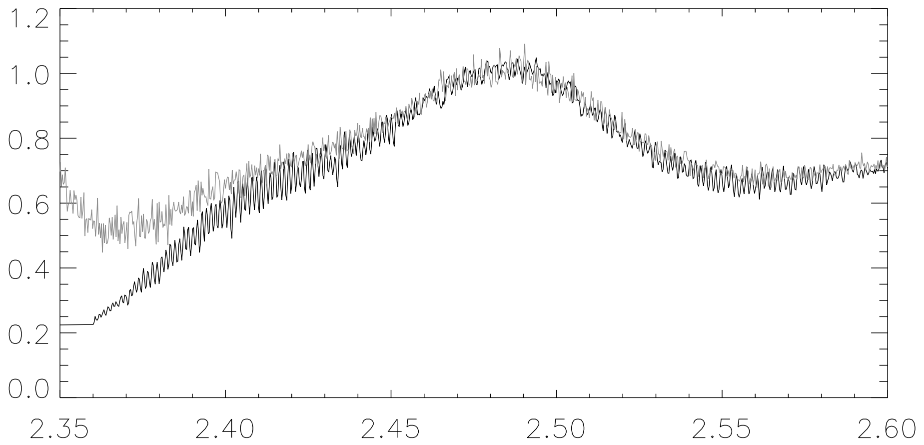

Figure 6.6: The RSRF for band 1A based on a measurement of HR7001 (black) versus the RSRF as measured in the lab (grey). The fringes in the in-orbit-RSRF are real.

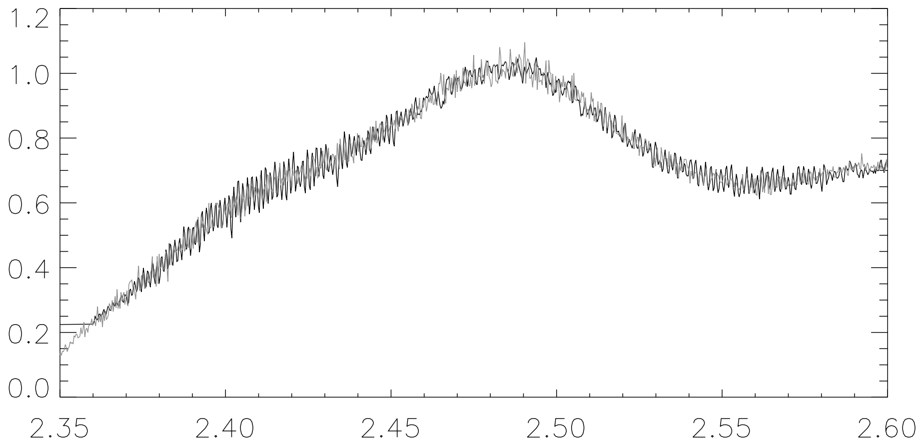

Figure 6.7: The RSRF for band 1A based on a measurement of HR7001 (black) and the lab RSRF corrected to the overall shape of the in-orbit RSRF. Note that not every feature that was seen in the lab has been seen in orbit. Especially the differences in the 2.35 - 2.40 μmregion are relatively large. Similar features seen in SWS spectra might be not real.

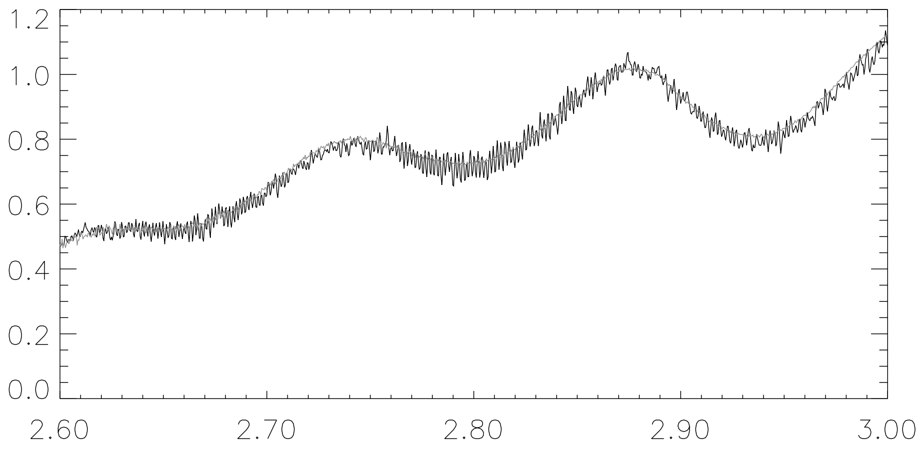

Figure 6.8: The RSRF for band 1b based on a measurement of HR7001 versus the lab RSRF (grey). The fringes in the in-orbit-RSRF are real.

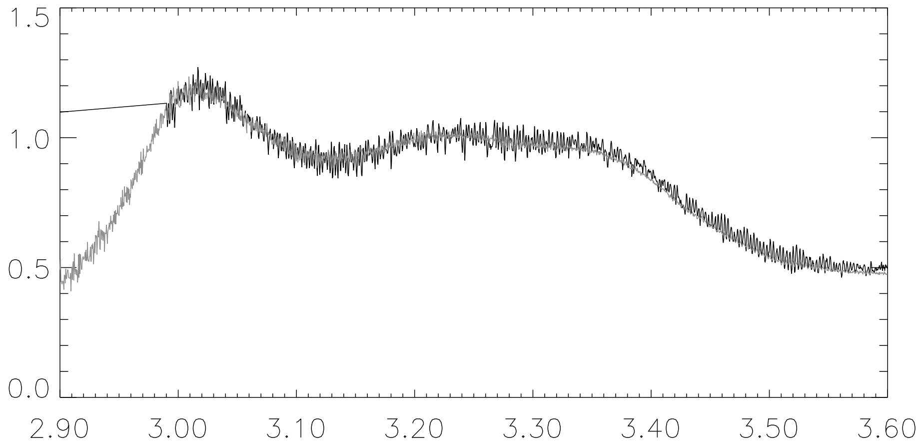

Figure 6.9: The RSRF for band 1d based on a measurement of HR7001 versus the lab RSRF (grey). The fringes in the in-orbit-RSRF are real.

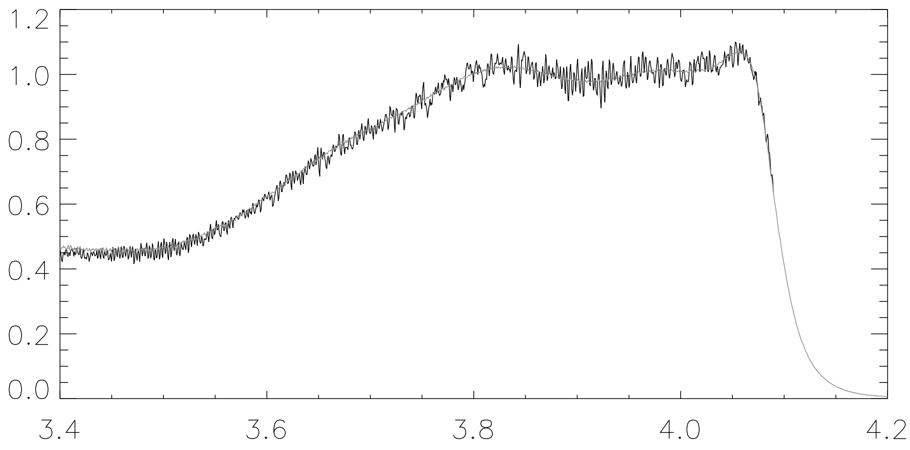

Figure 6.10: The RSRF for band 1e based on a measurement of HR7001 versus the lab RSRF (grey). The fringes in the in-orbit-RSRF are real.

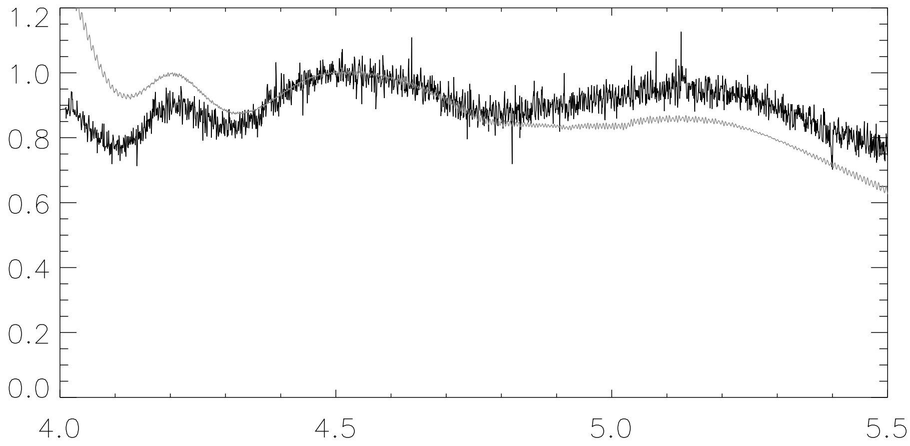

Figure 6.11: The RSRF for band 2a based on a measurement of HR7001 versus the lab RSRF (grey). The fringes in the in-orbit-RSRF are real.

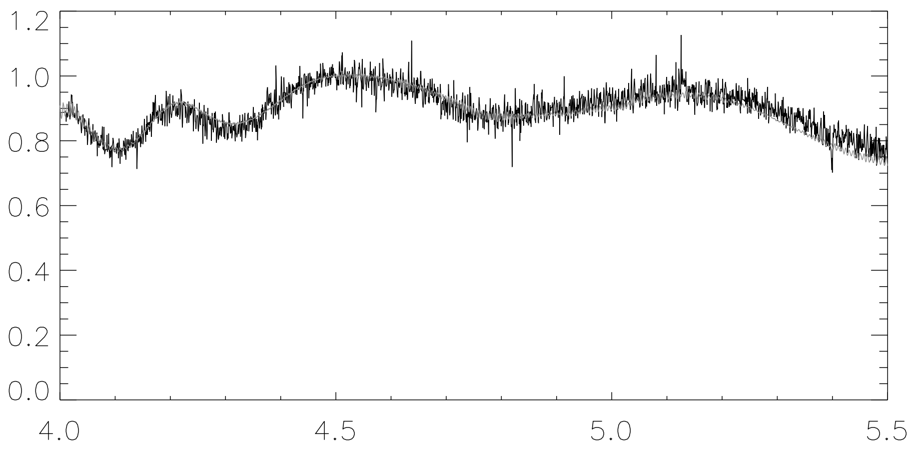

Figure 6.12: The RSRF for band 2A based on a measurement of HR7001 (black) and the lab RSRF corrected to the overall shape of the in-orbit RSRF.

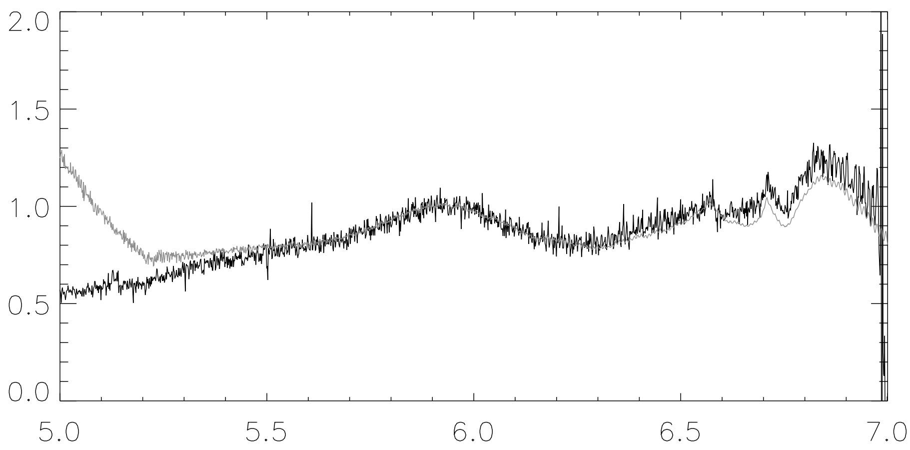

Figure 6.13: The RSRF for band 2b based on a measurement of HR7001 versus the lab RSRF (grey). Also in this band the lab measurements seem to show leakage. Attempts to correct the overall shape did not survive cross-checks with other calibration sources.

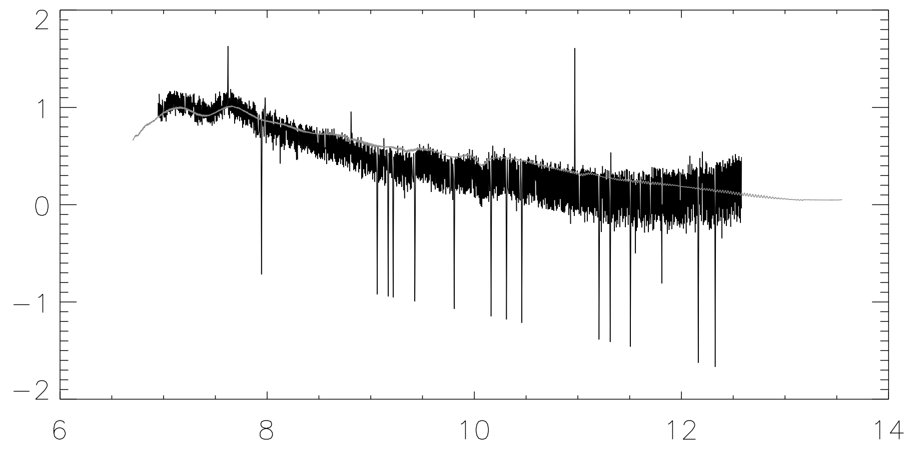

Figure 6.14: The RSRF for band 2c based on an AOT 1 speed 4 measurement of HR5340 (black) versus the lab RSRF (grey). The small features between 7 and 8 microns and around 10 microns can introduce misleading features after incorrect dark. The increase in response beyond 12 microns has been seen in other sources.

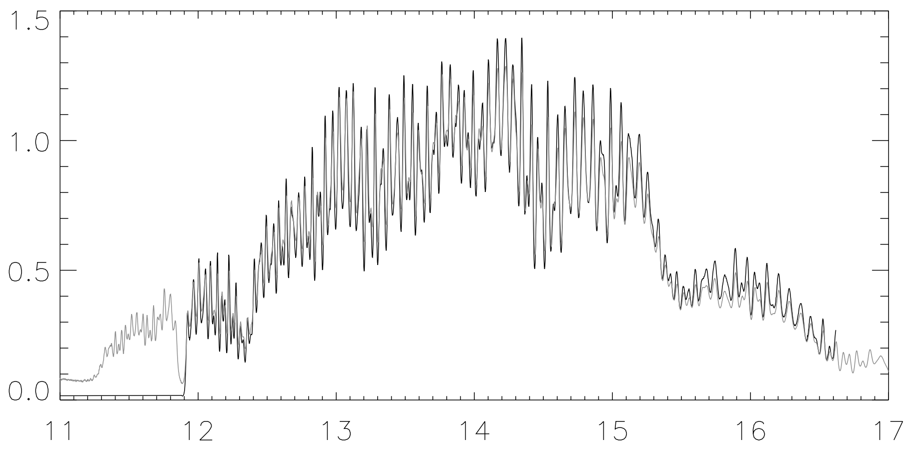

Figure 6.15: The RSRF for band 3a based on a measurement of NML-CYG versus the lab RSRF (grey). There is a good match, even at the fringe level. The fringes are a little "sharper" in the in-orbit RSRF because of the limited resolution of the lab measurements. Wrong dark subtraction will produce many spurious features.

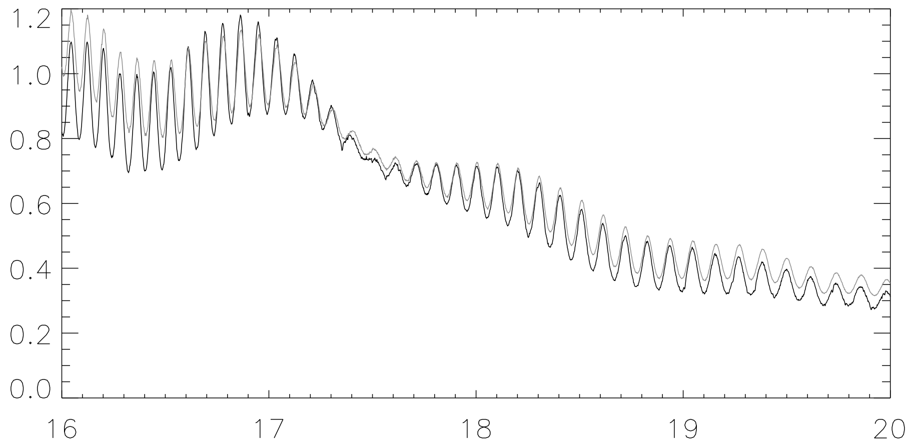

Figure 6.16: The RSRF for band 3c based on a measurement of NML-CYG versus the lab RSRF (grey). There is a good match, even at the fringe level. The fringes are a little 'sharper' in the in-orbit RSRF because of the limited resolution of the lab measurements. Wrong dark subtraction will produce many spurious features.

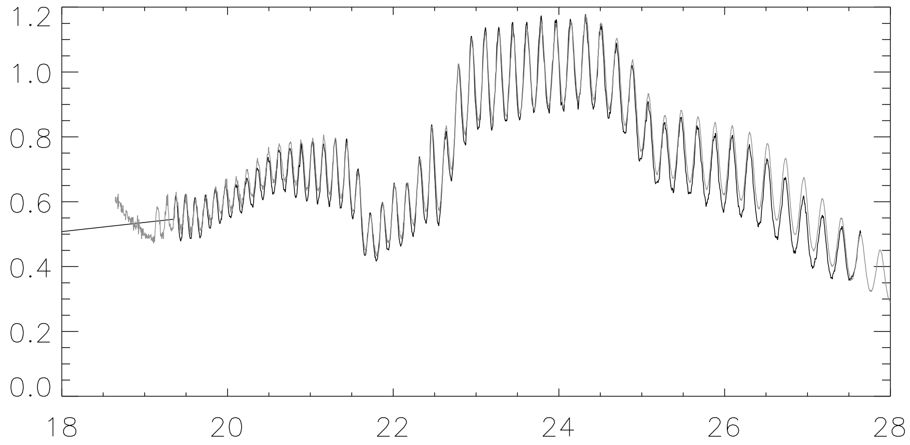

Figure 6.17: The RSRF for band 3d based on a measurement of NML-CYG versus the lab RSRF (grey). There is a good match, even at the fringe level. The fringes are a little 'sharper' in the in-orbit RSRF because of the limited resolution of the lab measurements. Wrong dark subtraction will produce many spurious features.

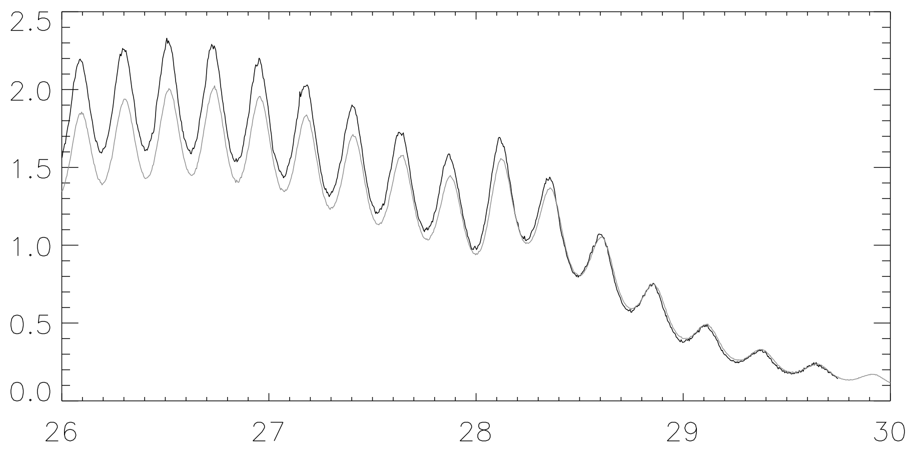

Figure 6.18: The RSRF for band 3e based on a measurement of NML-CYG versus the lab RSRF (grey). There is a good match, even at the fringe level. Wrong dark subtraction will produce many spurious features.

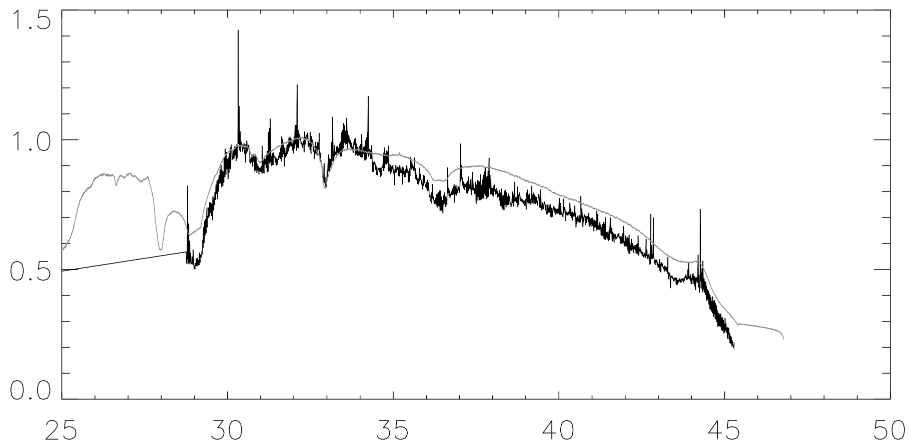

Figure 6.19: The RSRF for band 4 based on a measurement of NML-CYG versus the lab RSRF (grey). Since the model of NML-CYG is only accurate to 30%, it is not clear if the in-orbit RSRF is actually different from the lab RSRF.

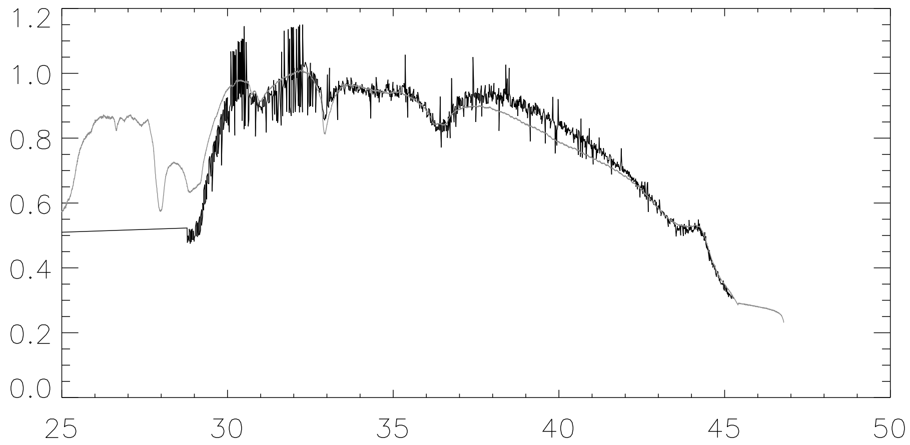

Figure 6.20: The RSRF for band 4 based on an AOT 1 speed 4 measurement of ETA-CAR versus the lab RSRF (grey).

Chapter 7

SWS Calibration

7.1 Introduction

This chapter discusses the expected accuracy of the data obtained by SWS, the products derived from them and indicates where the main sources of error lie. It is based on the SWS Calibration papers "The Photometric Calibration of the ISO Short Wavelength Spectrometer", by S.G. Schaeidt *et al*, "The Wavelength Calibration and Resolution of the Short Wavelength Spectrometer" by E. Valentijn *et al* and the general paper on SWS by de Graauw *et al* in the A&A special issue (November 1996 Vol 315) devoted to ISO.

7.2 Overall Calibration

The overall strategy is discussed in the SWS calibration papers. In summary internal calibration sources were used to tie together extensive ground based calibrations with in-flight observations of astronomical calibration sources. The three types of calibrations that were carried out are:

Determination of focal plane geometry, array geometry and alignment

The relative positions of the various entrance apertures and detectors need to be known to ensure that one grating wavelength calibration can be applied to all combinations of entrance slit and detector. The respective offsets have been calibrated in instrument level tests on the ground. Beam profile measurements and wavelength calibrations on astronomical sources were used for in-orbit checks.

Determination of wavelength scales

In ground-based instrument level tests, the relation between grating position readout and physical grating angle was determined by measurement of wavelength references in the form of vapour absorption lines (H_2O, NH_3, HCl). The spectral features provided by the internal grating wavelength calibrator have been tied to that scale. For the Fabry-Pérot, the position-gap relation has been determined from the spectrum of the internal FP wavelength calibrator, which is known to high accuracy from fourier transform spectroscopy. H_2O and NH_3 vapour absorption lines have been used for additional checks and for determination of the variation of effective FP gap with wavelength.

In orbit, the grating position-angle relation and the FP position-gap relation was re-established during PV, first using the internal calibrators and then astronomical sources. It was then checked regularly during the mission.

Determination of photometric sensitivity

The photometric sensitivity was determined on ground by scanning the spectrum of a calibrated blackbody source within the test cryostat. These tests resulted both in detailed spectral response functions for the various AOT bands and in a first calibration of the signal created by the internal stimulators. The signal from the stimulators was used to monitor variations in the broad band sensitivity of the detectors, e.g. due to memory effects.

In orbit, an extensive program was executed to determine the photometric sensitivity on astronomical sources. It was started during PV and carried on at a lower level during the mission. The dark current measurements needed both on ground and in orbit were done with SWS shutter closed.

7.3 Flux calibration

Flux calibration involves (1) fitting a slope to the 24Hz voltage detector samples and (2) converting this to a flux. This is, of course, complicated by the presence of non-linearities in the system, glitches, and how well the conversion of voltage/sec to fluxes is known. Parts 1 and 2 are handled by Derive-SPD and AA separately.

At constant illumination the output of the SWS detectors can be approximated as a voltage changing linearly with time;

$$V(t) = S \cdot t + O \tag{7.1}$$

The increase of this voltage (i.e. the slope S) is dependent on the radiation falling onto the detector, the physical quantity of interest. In Derive-SPD a slope is derived from the 24 Hz data for each reset interval. See section 8.4 for a discussion of this and the errors on it.

In normal data frames all samples in a reset interval are used. For a 1 second integration this time is 17/24 seconds – the first 7 samples are thrown away as being affected by the reset, leaving 17 samples that can be used. For a two second integration the time is $(17+23)/24$ seconds, as 1 sample is thrown away in the last second due to the reset pulse. For an integration lasting K seconds the effective integration time is $\sim (K-2)+(17+23)/24$ seconds.

The accuracy is directly estimated from the fit residuals which allow the computation of the standard deviation of the derived photo-current. Obviously, the accuracy depends not only on the intensity of the source (I), but also on how well the ramps have been previously linearized and therefore on the measurement error of the RC time constants. A statistical weight is computed which is inversely proportional to the error on I and proportional to the number of measurements between two detector resets. This weight will be used by Auto-Analysis to compute the average photo-current for each ramp. It is expected that this error will dominate all previously described ones.

If within a reset period a glitch (or any other anomaly) is detected, processing of the reset integration is stopped. Processing is subsequently continued after the glitch until a reset pulse (or another glitch) is detected. If glitches have occurred within a reset interval the slopes S of the different parts of the reset interval are averaged together (weighted by the standard deviation σ_S of those slopes).

Currently the SWS flux calibration as performed in AA rests on the assumption that the measured current slope $S(t,\lambda)$ (in μV/sec) is a linear combination of source flux $I(\lambda)$ (in Jy), instrumental gain $G(t,\lambda)$ (μV/sec/Jy) and dark current $D(t)$ (μV/sec);

$$S(t,\lambda) = G(t,\lambda) \cdot I(\lambda) + D(t) \tag{7.2}$$

Note that in this equation it is implicitly assumed that *all* memory effects (see section 5.8) can be neglected or have been removed. A full treatment of these effects would result in some sort of convolution integral for the right hand side of eqn. 7.2.

Following this equation the actual source flux $I(\lambda)$ is reconstructed by first subtracting the dark current from the measured slopes, and subsequently dividing them by the instrumental gain.

The instrumental gain is split into several (hopefully) orthogonal components;

$$G(t,\lambda) = G(t) \cdot G_0 \cdot G(\lambda) \tag{7.3}$$

Here $G(t)$ contains all the gain variations occurring on the timescale of the observation. $G(t)$ is derived from the observation itself, from up-down scan data – see section 4.6.1. In principle $G(t)$ should be unity, in practice it will vary around unity during an observation, and in OLP V6 it is set to 1.

The factor G_0 is used to account for long term (i.e. different SWS observations) variations in the responsivity of the instrument. It is determined by comparing the instrument response when the internal calibrator is switched on to the expected value for that response based on calibration observations.

The conversion from μV/sec to Jy is contained in $G(\lambda)$. It is taken from a calibration table (one for each AOT band) which in turn is derived from special calibration observations (section 8.3.6).

7.4 Flux calibration accuracy

7.4.1 General

Four main effects limit the flux calibration accuracy:

1 The Spectral Energy Distributions (SED's) of the astronomical sources used for flux calibration are only known to between 4 and 10%.

2 Pointing, see section 5.10.

3 Memory effects, see section 5.8, "Memory Effects".

4 Dark current subtraction. See section 5.4, "Detector Noise & Dark Current".

7.4.2 Grating

The errors expected on the flux calibration of the grating are shown in Table 7.4.2. It lists the requirements on ISO, the accuracy achieved in ground tests and the flight objective.

What has been achieved in flight at the time of the OLP V6 delivery (April 97) is shown in table 7.4.2.

Flux reproducibility was checked by observing the standard HR6705 twelve times during various orbits. Fluxes between the various measurements agreed to within 6% for band 1, and 12 to 15 % for bands 2 to 4.

7.4.3 FP

The accuracy expected on the flux calibration of the FP are the same as that on the grating, but add an extra 1 to 20% due to wavelength dependant leakage.

Table 7.1: Grating Flux calibration errors.

	Absolute	Cross-talk[1]	RSRF[2] fast	RSRF[2] slow	Beam diff	Pointing jitter	Non-linearity	Overall w/o memory
Requirements	$(\lambda/2)\%$	$< 2\%$	1%	10%	10%	-	$< 5\%$	$10 - 30\%$
Ground tests	$< 30\%$	$< 2\%$	1%	10%	-	-	$< 10\%$	34%
Flight objective	$(\lambda/2)\%$	$1 - 2\%$	$< 1\%$	$< 5\%$	10%	$< 5\%$	$< 5\%$	-

Notes

1 Crosstalk refers to the amount of electrical crosstalk between detectors in each band. Refer to Section 8.2.6.

2 RSRF is the Relative Spectral Response Function. The errors vary from band to band, and chapter 6 should be read for a complete description of the RSRF.

Table 7.2: Grating Flux calibration Accuracy as of OLP V6 delivery

Band	Key[1] Wavelength μm	Bandpass μm	Key λ 1 σ %	Worst accuracy 1 σ %	Location of worst
1A	2.48	0.05	5	7	edges
1B	2.87	0.07	5	7	edges
1D	3.08	0.07	5	7	edges
1E	3.80	0.10	5	7	edges
2A	4.50	0.10	7	12	4.0 μm
2B	5.90	0.20	7	15	7.0 μm
2C	7.70	0.20	11	25	12.0 μm
3A	14.0	0.30	11	25	12.0 μm
3C	17.0	0.30	11	20	17.0 μm
3D	24.0	0.60	12	20	19.5 μm
3E	28.5	0.60	20	30	29.5 μm
4	32.0	0.60	30	35	edges
5A	11.8	0.01	FP tied to grating LW sections		
5B	14.0	0.01	FP tied to grating LW sections		
5C	17.0	0.01	FP tied to grating LW sections		
5D	24.0	0.01	FP tied to grating LW sections		
6	27.0	0.01	FP tied to grating LW sections		

Notes

1 Key wavelength/bandpass combinations are chosen where the response of the detectors is at it's maximum and where the spectra of astronomical calibration sources are relatively featureless. There is one per band.

7.5 Wavelength calibration

The astronomical quantity of interest is an array of flux as a function of wavelength. Hence, a relationship must be established between each grating scanner position (measured by a Linear Voltage Differential Transducer (LVDT) and colloquially given the units 'LVDT') as contained in the ERD and its corresponding wavelength. The relation is calculated in two steps: first the scanner position is converted to a scanner angle using a calibration file. Then the following equation can be applied to calculate the wavelength of light falling on the detectors:

$$\frac{\lambda \times N}{D} = \sin(\theta + \beta) + \sin(\theta + \delta) \tag{7.4}$$

where,

β is the angle from the optical axis to the entrance or light source used, as seen from the collimator,

δ is the angle from the optical axis to the detector pixel,

θ is the angle of incidence on the grating for a beam entering along the optical axis for the current scanner position,

D is the grating constant,

N is the spectral order.

β, δ and D are constants, taken from calibration file 16. The spectral order N is determined by calculating all the orders that give wavelengths consistent with the transmission limits of the band/order/aperture/filter combination. For valid observations only one order should give a wavelength that satisfies this criterion.

The wavelength range – band/order/aperture/filter combination relationship is shown in Table 3.1.

For the Fabry-Pérot, first the grating wavelength is calculated. Calibration file 12 then transforms the nominal FP-position (an engineering parameter of no interest to the observer) into a FP-gap. This mechanical gap width must be corrected to get the optical gap width. The wavelength which passes through the FP is the one of which a whole multiple fits exactly in two times the optical gap width.

7.6 Wavelength calibration accuracy

The goal was to achieve an accuracy of between 10 and 20% of a resolution element for the two gratings. An accuracy of 10% was hoped for the LW grating as this is used by the FP wavelength calibration.

The errors expected on the wavelength calibration of the grating are shown in Table 7.6. It lists the requirements on ISO, what has been achieved in ground tests and during operations.

The limitation on the grating wavelength calibration accuracy appear to come from pointing, see section 5.10.

The wavelength calibration stabilisation was very good. A slight shift was seen in the wavelength calibration between PV and rev 450 of about 1 LVDT which was corrected by an update of the calibration files. Overall, the wavelength calibration of the SWS was kept accurate to within 1 LVDT. Further information on the wavelength calibration of the grating during the in-orbit

Table 7.3: Grating Wavelength calibration errors.

	SW	LW	
		$< 40\mu$	$> 40\mu$
Requirements	$< \lambda/10000$	$< \lambda/10000$	$< \lambda/10000$
Obtained on	< 1 LVDT	$< 0.5 - 1.0$ LVDT	2.0 LVDT
ground	$\lambda/10000$	$\lambda/12000 - \lambda/20000$	$\lambda/6000$
Flight Achieved	1 LVDT	0.5 - 1 LVDT	
	$\lambda/5000 - \lambda/12000$	$\lambda/8000 - \lambda/16000$	

lifetime or ISO can be found in the document 'Wavelength Calibration' by Do Kester, Douwe Beintema & Edwin Valentijn, 2 July 1998.

For the two FPs relevant information concerning wavelength calibration accuracies is shown is shown in Table 7.6. Throughout the mission no wavelength shifts of more than 1 FP scan step were found, within the requirements listed in the table. More information on this can be found in the document 'Status of SWS Fabry-Pérot wavelength calibration and instrumental profile' by H. Feuchtgruber, 5 May 1998.

Table 7.4: FP Wavelength calibration errors.

	SW-FP1	LW-FP1
Requirements	$< \lambda/100000$	$< \lambda/100000$
Obtained on ground	$\lambda/125000$	$< \lambda/125000 - \lambda/200000$
Flight Achieved	$\lambda/10^5$	$\lambda/10^5$

Chapter 8

The Pipeline and its effects

8.1 Introduction

The Standard Product Generation (SPG) Pipeline (otherwise known as Off-Line Processing, OLP) processes the raw data telemetered down from ISO (in terms of microvolts, scanner positions etc) into more conventional astronomical units of flux against wavelength. This chapter describes the Standard Product Generation Pipeline, the error propagation through it and any side-effects noted on the processed data.

The SPG pipeline is composed of three parts:

• Extracting from the raw data stream the instrument data and placing it into Edited Raw Data (ERD) files. This process is a reformatting only and will not be discussed further.

• ERD to Standard Processed Data (SPD) stage, known as Derive-SPD. This involves removing all instrumental effects on timescales of less than 1 reset interval, converting detector readouts (voltages against time) into slopes and assigning, where possible, wavelengths with detectors.

• SPD to Auto-Analysis Results (AAR) stage, known as Auto-Analysis. This further process the SPD removing instrumental effects on timescales of greater than 1 reset interval and converts slopes to fluxes.

In the course of Derive-SPD and Auto-Analysis several files are used that describe the behaviour of the instrument and its performance. These files are known, for historical reasons, as Cal-G files. They contain such things as the conversion between scanner position and wavelength, the relationship between voltages per second and fluxes, etc.

Examples of the data produced by these steps are given throughout this manual. Sections 4.2 to 4.5 show ERD, SPD and AAR examples for each AOT. Sections 4.6.2, 4.6.1 and 5.8 give examples of short stretches of observations to highlight certain features.

8.2 ERD to SPD (Derive-SPD)

Derive-SPDs main input is Edited Raw Data (ERD), 24 Hz data containing detector readout voltages of the target's flux, of internal flux standards, of wavelength calibration exposures, of dark currents and of housekeeping data. Derive-SPD also reads in pointing and instrument status files.

For each detector, all data for one full reset interval are combined to a single current estimate at single wavelength and are then saved in the Standard Processed Data (SPD) file for that AOT. No attempt is made within Derive-SPD to average measurements of the same type (e.g. dark current measurements) or to do processing on any time scale longer than one reset interval.

A basic overview of the Derive-SPD processing is given in figure 8.1 and the ERD and SPD files are described in sections 9.2.1 and 9.3.1.

Each measurement for one reset interval of a given AOT is saved separately inside the same SPD product in chronological order of acquisition. The motivation for this is to offer to the observer the possibility of judging the stability and repeatability of SWS measurements. There is an one-to-one correspondence between AOT's and SPD files. That is, one AOT produces one SPD file.

The individual processing steps are described as follows:

8.2.1 Read data of one reset interval

Data is read in for one reset interval (SW and/or LW reset interval). As discussed above, each AOT generates different types of data: astronomical measurements from the source, measurements from the spectral reference sources (grating and FP), measurements with the calibrators and dark currents. Each of these different types of data has a different physical meaning and serves a different purpose. Hence, the data must be flagged according to their type.

Each ERD data record is tagged with a Instrument Time Key (ITK) which points toward a unique record in the SSTA Compact Status History (CSH) file (see section 9.2.2). Cross-correlating the ERD ITK with the CSH, Executed Observation History per ICS (EOHI) and General Housekeeping (GEHK) files (both described in the ISO Satellite & Data Manual) allows an unambiguous determination of the status of the SWS instrument at the time of the measurement and therefore of the type of the data recorded and the actual wavelength range covered (to be verified during the wavelength check stages).

8.2.2 Determine Data Range

This marks data affected by capacitor being short circuited at the end of the reset interval or data out of limits. To do this it uses Cal-G files 3 and 4.

8.2.3 Subtract MIDBIT Values

The detector readouts voltages of between -10 and +10 V are converted into a bit number ranging from 0 to 4095. The midbit is the bit value that corresponds to 0 Volts, approximately 2048, and is different for each detector. This data is stored in Cal-G file 2A.

This module was only active for OLP Version 4.3. During testing, unusual results were obtained that have not been explained yet. Therefore from OLP V5.0 onwards Cal-G file 2A has been filled with neutral values exactly half of 4095, i.e. 2047.50.

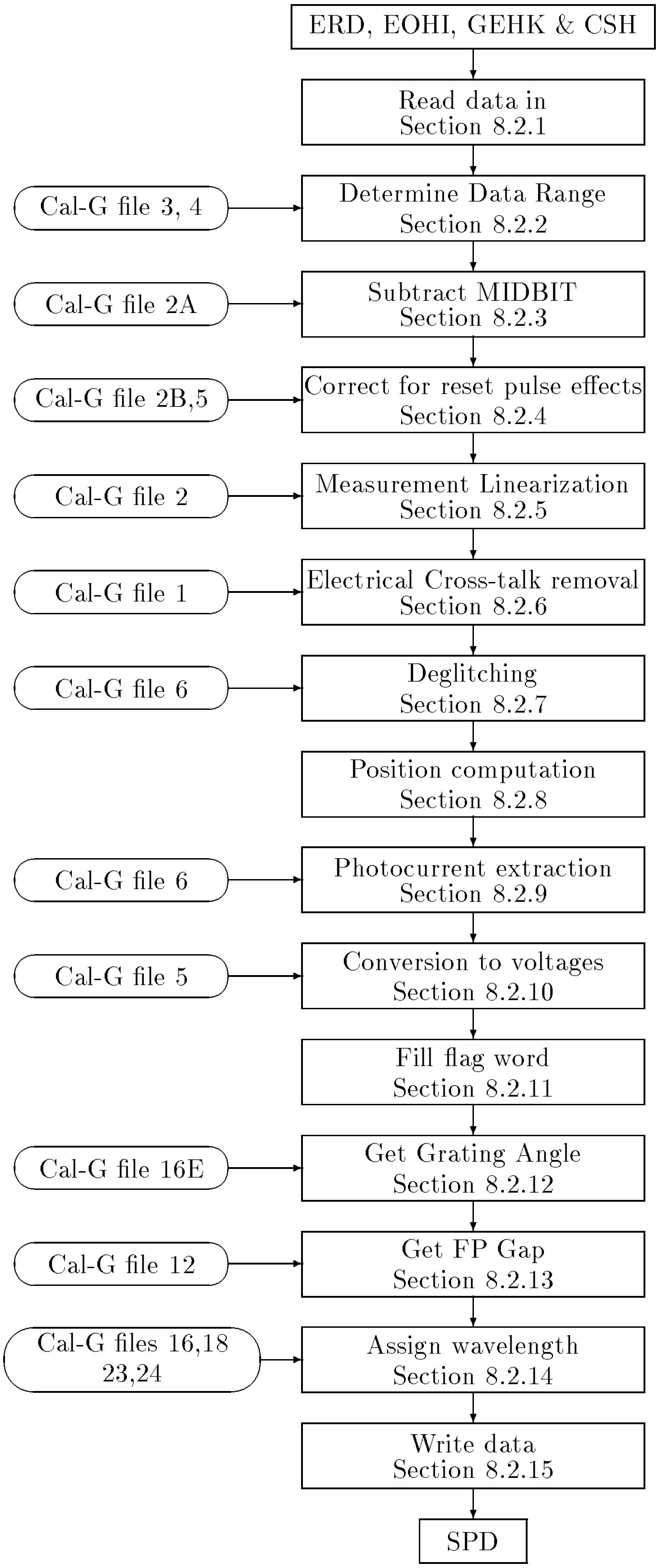

Figure 8.1: SWS Derive-SPD process.

8.2.4 Correct for reset pulse effects

Cal-G 2B contains information describing the shape of the pulse at the end of the reset interval. This calfile is used to subtract the effect of the reset pulse from the data. Cal-G file 5 is also used in this.

This module was only active for OLP Version 4.3. During testing, unusual results were obtained that have not been explained yet. Therefore from OLP V5.0 onwards Cal-G file 2B has been filled with zeros that result in this module doing nothing.

8.2.5 Correction of the integration ramp for the RC time constant

The amplifier chain contains a high pass filter. For a constant voltage gradient input the response of the amplifier is to asymptotically approach a constant value, i.e.

$$\frac{dV(t)}{dt} + \frac{V(t)}{t_0} = \frac{dV_o(t)}{dt} \tag{8.1}$$

where $V(t)$ is the output voltage at time t, V_o the input voltage applied on the capacitance due to the accumulation of charges on the detector, and t_o the detector time constant. In order to later reconstruct the true photo-current, it is first necessary to linearize the ramps, i.e. determine the actual input voltages $V_o(t)$ applied on the detector.

Knowing the RC time constant t_o, it is straightforward to invert the above formula and derive the input voltage. Each detector i has its own time constant $t_o(i)$, stored in Cal-G 2.

8.2.6 Removal of Electrical Cross-talk

Due to parasitic capacitance between neighbouring detectors any signal in one grating detector will 'leak' to other detectors (primarily the adjacent ones) in the same array. This 'leak' to the adjacent detector is of the order of 10%.

Assuming the detector response is a linear function of the intensity of the signal, a set of cross-talk matrices can be determined with constant correction factors. The read-outs D of each individual detector j in the detector array may then be corrected by applying the following formula:

$$D_j^{corr} = D_j - \sum_{i \neq j} F_{i,j} * D_i \tag{8.2}$$

The sum is over all detectors of index i different from j, where i goes from 1 to M. M being the number of detectors in the array (12 for the gratings and 2 for the FP). This cross-talk correction matrix is held in Cal-G file 1.

Assuming an error matrix $E_{i,j}$ on the individual values of $F_{i,j}$ can be derived at the same time as the cross-talk matrix, it is then straightforward to propagate these uncertainties.

$$E(D_j^{corr}) = \sqrt{\sum_{i \neq j} (E_{i,j} * D_i)^2} \tag{8.3}$$

where the summation has the same meaning as in the previous formula.

These errors are not calculated in the generation of the array $F_{i,j}$ and hence their effects on D are not calculated. Also, if the dependance of $F_{i,j}$ on signal intensity is not linear equation 8.2 will not correctly describe the necessary correction and so any errors will be larger than given by equation 8.3.

8.2.7 Deglitching

Glitches (ref section 5.7) are recognized in the differentiated voltages. The median of the 24 Hz bit values is computed and used, in conjunction with a value α held in Cal-G 6, to define how high a glitch might be. If any differentiated 24 Hz bit values are higher than this value they, and N-samples (currently one, also defined in Cal-G file 6) before and after the glitch, are marked as being affected by a glitch. If the glitch is so strong that the detector gets saturated all measurements up to the end of the ramp are discarded.

If the glitch is not too strong the following measurements do not have to be discarded. In the case of one or two glitches in a slope the software tries to average the partial slopes between the glitches to one slope. One has to be aware, however, that the slope after a glitch is generally higher than the slope before a glitch (especially for a large glitch).

It is not possible to compute reasonable slopes for reset intervals affected by more than three glitches. The current pipeline does not flag this data as invalid, although the calculation of the slopes is imperfect.

The accuracy of deglitching depends not only on how well a glitch can be identified, but also on the effects of the glitch with time (the so called glitch-tails). Studies of slope variations after glitches are ongoing

The SWS Glitch History (SWGH) file contains a list of all glitches detected during processing along with a short characterisation, such as glitch height, skipped samples, etc. For a description of this file see section 9.3.2

8.2.8 Position computation

This computes the grating and FP positions.

8.2.9 Extraction of the photo-currents and their uncertainties

A least-square fit is applied to the data taken over one reset interval in order to estimate its slope S.

$$V = S \times t + O \tag{8.4}$$

$$S = I \times k \tag{8.5}$$

where,

k is a constant which depends on the internal capacitance, put explicitly to be a constant 1. This implies that I has units of Amp per Farad. It does not need to be explicitly measured as it cancels out when the relative flux calibration is applied.

O is the charge offset at the zero-point of each ramp.

The time t is counted in seconds since the start of the ramp.

This module uses the glitch information generated by the deglitching algorithm above to raise a flag when the slopes are affected by 1, 2 or more glitches, are saturated or when there is no data (see SWSPFLAG in Table 9.8 for details). Because of this the routine uses Cal-G file 6.

Refer to section 7.3 for more details on flux calibration.

8.2.10 Conversion of digitized read-out's to output voltages

The electronics amplify the detector read-out voltages with a commandable gain factor before the analog to digital (AD) conversion. Each detector can be operated at three different gains of the amplifier chain. The output voltage must be reconstructed from the digitized read-out's and corrected for the gain factor.

The input to the AD converter is related to the voltage across the detector by

$$V_{In} = V_{Det} \times G \tag{8.6}$$

where G is the gain which can be set to one of three values. The slope in V/s is related to the output of the AD converter, in $Bits/sample$, by

$$Slope = Digital\_value * conversion\_factor \tag{8.7}$$

The conversion factor is given by

$$conversion\_factor = \frac{V_{range}}{bits_{max}} * \frac{sample}{s} = \frac{-20}{4095} * \frac{24}{1} \tag{8.8}$$

The numerical values originate from the fact the A/D converter has a maximum input range of 20 V which are converted into 4095 steps, with the input voltage inverted, and that there are 24 samples per second.

Once we have calculated the slope from the digital output we can divide by the gain factor to get the detector voltage.

Values for this are held in Cal-G file 5.

8.2.11 Fill flag word

This generates and fills the flag word with all relevant data.

8.2.12 Get Grating angle

This module converts the grating position to a grating angle, which is then used to calculate the wavelength of the light falling on the detectors. See section 7.5.

It uses Cal-G file 16E.

8.2.13 Get Fabry-Pérot gap

This module determines the Fabry-Pérot gap from the telemetered currents. See section 7.5.

It uses Cal-G file 12.

8.2.14 Assign wavelength for grating and FP

This module calculates the wavelength of light falling on the detectors. Refer to sections 7.5 and 7.6 for a discussion of the philosophy behind this and the likely accuracy.

For the grating, this involves applying equation 7.4. The grating angle, calculated in section 8.2.12 is used along with various calibration files to determine the wavelength of light falling on each detector. Only bands with an unique order falling on their detectors are assigned a wavelength, all others are flagged as confused. It should be noted that all bands with an unique order falling on their detectors are assigned a wavelength, even if the band was not requested or contains useless data (although for non-FP observations the FP data is not transferred to the AAR).

For an AOT 01 measurement, where the grating moves during a reset interval, the grating position in the SPD is set to the grating position at the start of the reset interval. The wavelength in the SPD, however, is taken from the middle valid sample. e.g., for a one second reset interval, the grating position is that of the first sample. As samples are thrown away due to the reset pulse (see section 5.6, operation described in section 8.2.2), the wavelength is that from sample (24 - Cal-G file 3) / 2.

For the Fabry-Pérot, once the grating wavelength is calculated the mechanical gap width (calculated in section 8.2.13 is corrected to get the optical gap width (calibration file 18). The wavelength which passes through the FP is the one of which a whole multiple fits exactly in two times the optical gap width.

8.2.15 Writing data out

The data produced by the processing chain above is written out to the SPD and glitch list SWGH files. Each AOT results in one SPD file. For a definition of the SPD file see section 9.3.1. Note that the SPD file, like an ERD file, contains science data interleaved with calibration data.

A SPD record is produced for every reset interval. Complexities arise when the reset intervals for the SW and LW gratings are different. In this case there will be one SPD record (containing data for all detectors) for each of the shorter reset interval, with the SPD for the longer reset interval having its flag word set to 'No data' for the records when it did not contain a reset (see table 9.8). As an example, if the SW grating had a reset interval of 1 second and the LW one of 2 seconds, a SPD record would be produced every second. Every SPD record for the SW detectors (1–24) would contain valid data, while only every other record for the LW detectors would contain valid data, the others being marked as 'No data'.

8.3 SPD to AAR (Auto-Analysis)

Auto-Analysis (AA) is the processing stage that starts from SPD, corrects for all instrumental effects lasting longer than one reset interval and generates sets of fluxes against wavelength (spectra). These spectra are generated irrespective of the observation specifications. Figure 8.2 gives an overview of AA processing. Most of the SWS AA processing steps are independent of AOT number as most of the special options (e.g. reference scans, see table 4.1) are used in several different AOT's and thus are implemented as part of the main processing flow.

These steps are described in more detail in the following pages.

8.3.1 Read all data from SPD

The data and header information are read from the input SPD. Errors occur when e.g. SPD does not exist or cannot be read etc.

8.3.2 Determine AOT and Velocity correction

The AOT number, needed for the further processing of the data, is determined from the `EOHAAOTN` keyword in the SPD FITS header. The velocity of the spacecraft with respect to heliocentric is similarly obtained, and for AOT SWS01 the speed is also obtained.

8.3.3 Correction for time dependent detector behaviour

The detector data may need to be corrected for time dependant effects such as detector hysteresis.

Currently, only a number of readouts at the beginning and end of dark currents are rejected.

8.3.4 Subtraction of dark currents

For every block of dark current data, the median of valid dark current data is calculated for each detector. The reset interval is computed from the reset pulses (extracted from the status code) and the gain is extracted from the detector flag.

Whenever possible a (linearly) interpolated dark current is subtracted from each non-dark current scan. The interpolation is done over the dark current directly preceding the scan and the nearest dark current following the scan. This means the dark currents must have the same reset time and gain as the scan. The interpolation is performed in time and the beginning and end of the interpolation are taken as the last frame of the first dark current and the first frame of the second dark current.

If there is no dark current preceding a scan, the dark current after the scan is subtracted or the mean of all dark current in the spd with the same reset and gain as the scan.

For the PHOTOMETRIC CHECKS only the dark current preceding the measurement is subtracted. No interpolation is done.

The calculated dark current values are also subtracted from the dark current frames themselves.

If there is no valid dark current point in a block, either the next useful dark current is used or the mean value of all dark dark current in the AOT with the same gain and reset.

Each calculated dark current is compared against the value in the calibration file (CAL21_*) and the limits for the dark current therein. If the calculated dark current is outside the defined limits a warning is issued. The calculated dark current is however subtracted.

If no dark current can be found for a specific detector, the data are flagged invalid.

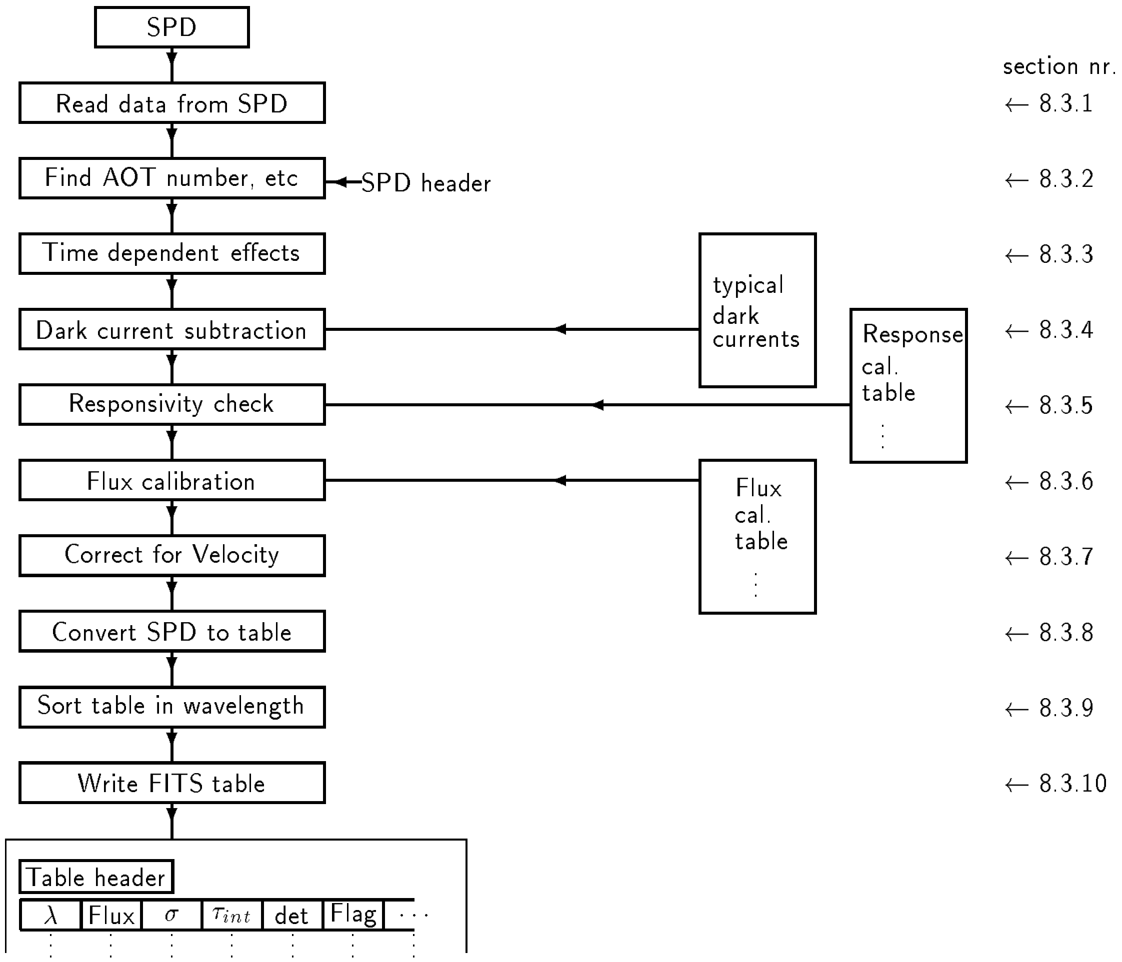

Figure 8.2: Auto-Analysis flow-diagram

It is (most likely incorrectly) implicitly assumed that the dark current data have not been affected by (or are completely corrected for) detector memory effects.

8.3.5 Responsivity check

For each AOT band the wavelength dependent responsivities are normalized with respect to the key wavelength. This is done per detector and stored in the Cal-G files 25_x. The signals that belong to a certain AOT band are then divided by the normalized responsivities for that AOT band.

Additionally, for an AOT 1 the responsivities are smooth by doing a flux conserving interpolation using wavelength dependent factors which determine the range of wavelengths over which the smoothing has to be done. These factors depend both on AOT speed and on the AOT band as well as on wavelength. This factors are stored in Cal-G file 19.

8.3.6 Flux calibration

The conversion from signal to flux is carried out by normalizing the signal of the photometric check, where data obtained with the internal stimulator are collected and averaged, by that in the Cal-G file 13 from pre-flight measurements. This value is multiplied by the ratio of flux over signal of an external calibration source. Finally the obtained conversion factors are applied to the data.

In case the data does not contain a valid photometric check (such as e.g. in detector band 1, for which photometric checks were taken out of the AOT logic) the values are taken straight from Cal-G file 13. I.e. the normalized signal of the photometric check is assumed to be one.

8.3.7 Velocity Correction

The velocity component (V) in the line of sight towards the target, due to the combined motions of the spacecraft and of the earth is corrected for in this module. This then ensures that the AAR wavelength is heliocentric.

8.3.8 Extracting data from the SPD

All good data (wavelength, fluxes etc.) are transferred to internal arrays. Data for which no wavelength was assigned in Derive-SPD are skipped.

Prior to OLP V6 dark current and photometric check data were transferred into the internal arrays and a therefore present in the AAR. From OLP V6 this is not the case.

8.3.9 Sort the internal table in wavelength

The internal table of wavelengths, fluxes etc. is sorted by wavelength using an appropriate sort algorithm.

8.3.10 Output table files

The table containing wavelength and flux calibrated data is written to a FITS AAR file. For a definition of this file see section 9.4.1.

8.4 The Error Propagation of the SWS Pipeline

8.4.1 Introduction

This paper summarizes the error propagation of the SWS pipeline, based on pipeline version 6.0. During this study it turned out that it is possible to improve the error handling of this pipeline version. Thus a few modifications were done within the IA3 environment (SPR_S0166). Especially the DERIVE AAR s/w changed drastically in some cases of the error computation.

The computed errors in the Auto Analysis product do not reflect all known uncertainties to the 'flux' value in the AAR. An attempt has been made to correctly propagate the detector noise through all steps of flux calibration, and to include other effects like the statistical error of dark current measurements. There are, however, effects like slow detector drifts which may significantly affect the measured flux but cannot be precisely quantified. The 'stdev' is hence more a number which might be suitable for comparison purposes, e.g. assessing which part of the spectrum are 'more noisy', than for quantifying the absolute uncertainty in (continuum) flux.

Due to technical reasons it is not meaningful to compare errors of different detectors. It is more intended to give an impression about the relative errors for one detector.

8.4.2 DERIVE SPD

At constant illumination the output of the SWS detectors can be approximated as a voltage changing linearly with time;

$$V(t) = S \cdot t + O \tag{8.9}$$

An equation of the form:

$$y = a + bt \tag{8.10}$$

The increase of this voltage (i.e. the slope S) is dependent on the radiation falling onto the detector, the physical quantity of interest. In Derive-SPD a slope and offset (O) are derived from the 24 Hz data for each reset interval. See sections 7.3, "Flux calibration" and 8.2.9, "Extraction of the photo-currents and their uncertainties".

To calculate the slope in the ISO detector data, we take the AC-corrected detector outputs for every reset interval versus time. Be aware that due to uncertainties in the AC-constants of every detector the slope might be slightly curved. This method to compute the error could give a sigma value even if the input before AC-correction is perfect. So the computed error is not suited to compare between detectors, moreover it represents the relative error of one detector.

As usual we write the χ^2-equation as

$$\chi^2 = \sum (a + bt - y)^2 \tag{8.11}$$

In the first instance the summation is over one second of data. Later, the equation can be re-summed over the complete reset interval. We want to find a minimum in χ^2. To this end we differentiate the equation to a and b and put both equations to 0: the normal equations.

$$\frac{\partial\chi^2}{\partial a} = aN + b\sum t - \sum y = 0 \tag{8.12}$$
$$\frac{\partial\chi^2}{\partial b} = a\sum t + b\sum t^2 - \sum ty = 0 \tag{8.13}$$

N : number of samples in 1 reset period

The solutions to this set of equations is

$$\Delta \equiv N\sum t^2 - \sum t \sum t \tag{8.14}$$
$$a = \frac{\sum t^2 \sum y - \sum t \sum ty}{\Delta} \tag{8.15}$$
$$b = \frac{N\sum ty - \sum t \sum y}{\Delta} \tag{8.16}$$

And:

$$\chi^2 = \sum y^2 - a\sum y - b\sum ty. \tag{8.17}$$

The variance of the solution is $\chi^2/(N-2)$ and hence the standard deviation is:

$$\sigma = \sqrt{\chi^2/(N-2)} \tag{8.18}$$

N : number of samples

We can now calculate the formal errors in the offset and the slope.

$$\sigma_a = \sigma\sqrt{\sum t^2/\Delta} \tag{8.19}$$
$$\sigma_b = \sigma\sqrt{N/\Delta} \tag{8.20}$$

The 'standard deviation of the slope', σ_b was passed into the SPD product in field SWSPSTDV for OLP version 5.x.

Pipeline version 6.0 computes a slightly different 'standard deviation of the slope', σ_b:

$$\Delta = \sum y - a - bt \tag{8.21}$$
$$\sigma = \sqrt{\chi^2/(N - \sum\Delta * \sum\Delta)} \tag{8.22}$$
$$\sigma_b = \sigma\sqrt{N/\Delta} \tag{8.23}$$

8.4.3 DERIVE AAR

To understand the error handling of this part of the s/w it is unavoidable to mention some basics how the DERIVE AAR s/w is working. The DERIVE AAR part of the pipeline is noted step by step. Every section heading is starting with the related IA3 module call, a short explanations what this module should do is appended. In some cases the pipeline FORTRAN modules are mentioned to support pipeline module maintenance.

ANTIMEM : Remove memory effects

No error calculation done.

DARK : Dark Current subtraction

In the standard case a dark current measurement is precedes and follows a scan with the same gain and reset settings. The medians of this dark current measurements are used and applied to the scan data by linear interpolation.

Also, the actual dark is subtracted from the dark current itself. In some cases (old AOTs or to many bad data during dark current measurement) only one valid dark current measurement is taken for subtraction.

The square data of the 'standard deviation of the slope', σ_b as given in the SPD are collected for the valid data of a dark current block:

$$err\_dark\_block = \sum \sigma_b^2/N \tag{8.24}$$

Where N is the number of slopes in the dark current block.

After computing the median from the dark current block data a number suited for error propagation (delta_med) is returned:

$$\begin{aligned} lo &= index((total\_number + 1) * 1/4) && (8.25)\\ hi &= index((total\_number + 1) * 3/4) && (8.26)\\ err\_med &= (dark(hi) - dark(lo))/2.0 && (8.27) \end{aligned}$$

total_number	: total number of valid data points during dark block
index	: ordered indices of dark current data block
dark	: ordered array of slopes during dark current measurement
err_med	: a width value which is used for error propagation (error of the MEDIAN)

This calculation is done for every dark current block.

The error returned from the MEDIAN calculation and the error of the dark current block itself are combined to:

$$err\_block = \sqrt{err\_med^2 + err\_dark\_block^2} \tag{8.28}$$

For the dark current block data itself the error is computed for each slope as:

$$err\_out\_dark = \sqrt{\sigma_b^2 + err\_block^2} \tag{8.29}$$

For the scan data the flux and error for a reset interval is computed:

$$flux\_out = flux\_in - err\_block_1 - \frac{err\_block_2 - err\_block_1}{(time_2 - time_1)} \tag{8.30}$$

$$err\_out\_data = \sqrt{\sigma_b^2 + err\_block_1^2 + (ac\_time - time_1)^2 * \sqrt{\frac{err\_block_2^2 + err\_block_1^2}{(time_2 - time_1)}}} \quad (8.31)$$

err_out_data	: new computed error
err_block$_1$	: median of dark current data block before scan (equation 8.28)
err_block$_2$	: median of dark current data block after scan (equation 8.28)
σ_b	: error given with the input data (pipeline σ_b)
ac_time	: ITK of slope
time$_1$	: ITK of dark current measurement before scan
time$_2$	: ITK of dark current measurement after scan

RESPCAL : Responsivity Calibration

To aid understanding and to help maintain the pipeline code pipeline modules are named where calculations happen.

aas_read_conv_factors:

First the AOT band related calibration file 25 is read in. Calfile 25 contains the data of the RSRF (resfac) for several wavelength of an AOT band. Every calfile 25 entry is associated with a related error (reserr). How this error is computed is subject of the related CAP.
For a given key wavelength the related calfile 25 RSRF-factor (resfac_kw) is determined by searching in the array of data. Then a linear interpolation conserving the flux is applied to the calfile 25 data.

aas_fc_intpol:

The flux at key wavelength (resfac_kw) is the total integral of fluxes (obtained using the trapezoid rule) between flux at key wavelength minus FWHM and flux at key wavelength plus FWHM divided by FWHM. For AOT1 the FWHM is obtained from Cal-G file 19, for all other AOTs it is set to 0 and no division takes place

It is assumed that the error follows the same integration formulae as the fluxes (reserr_kw), except that the error is divided by the square root of a dilution factor being the ratio between the FWHM and the local stepsize in wavelength. Integrating over more wavelength's yields a smaller error while interpolating over a small part one wavelength interval a larger error.

aas_read_conv_factors:

Every array entry (resfac) is normalized to the computed factor at key wavelength (resfac_kw):

$$resfac\_n = \frac{resfac}{resfac\_kw} \quad (8.32)$$

The errors of the normalized calfile 25 data are calculated in OLP V5 as:

$$errres\_n = resfac * (ABS(reserr/resfac) + ABS(reserr\_kw/resfac\_kw)) \quad (8.33)$$

The current IA3 system (and future OLP V6) computes the error differently:

$$errres\_n = resfac * \sqrt{(reserr/resfac)^2 + (reserr\_kw/resfac\_kw)^2} \tag{8.34}$$

aas_det_conv_factor:

For every wavelength the related table of resfac_n (equation 8.32) is searched and the actual value at the wavelength of interest is determined by linear interpolation, to produce resfac_ni. For AOT1 data Cal-G 19 is accessed and a special FWHM value is extracted. This value goes into the interpolation conserving the flux algorithm as above (err_ni). Errors are treated as before (aas_fc_intpol). For the simple linear interpolation (non AOT1 data), the error is also computed by linear interpolation (err_ni). Now the Cal-G 25 data are prepared to be applied.

aas_resp_cal:

Finally the new flux is computed:

$$flux\_out = \frac{flux\_in}{resfac\_ni} \tag{8.35}$$

$$err\_out = flux\_out * (ABS(err\_in/flux\_in) + ABS(err\_ni/resfac\_ni)) \tag{8.36}$$

flux_out : new computed flux
flux_in : flux input from equation 8.30
err_out : new error computed
err_in : error input from equation 8.31

The current IA3 implementation (and OLP V6) computes the error as:

$$flux\_out = \frac{flux\_in}{resfac\_ni} \tag{8.37}$$

And the new error:

$$err\_out = flux\_out * \sqrt{(err\_in/flux\_in)^2 + (err\_ni/resfac\_ni)^2} \tag{8.38}$$

FLUXCON : Flux Conversion

aas_det_lt_resp_factor:

The first photometric check is used to compute the reference value for flux conversion (flux_pm). For this purpose first a three value-box-car filter is applied on the photometric check data, the data are ordered (flux_p) and the median is taken.

$$flux\_pm = flux\_p(N/2) \tag{8.39}$$

N : number of data (reset intervals) of the photometric check

To calculate the error on the median a one point offset against the median is computed:

$$err\_p\_p1 = ABS(flux\_p(\frac{N}{2}) - flux\_p(\frac{N}{2} + 1)) \tag{8.40}$$

$$err\_p\_m1 = ABS(flux\_p(\frac{N}{2}) - flux\_p(\frac{N}{2} - 1)) \tag{8.41}$$

$$err\_p = \frac{err\_p\_p1 + err\_p\_m1}{2.} \tag{8.42}$$

err_p_p1 : plus one sample deviation against MEDIAN
err_p_m1: minus one sample deviation against MEDIAN
N : number of data of the photometric check
flux_p : ordered array of photometric check data

aas_read_cal_factor:

The relative flux data (rel_flux) and the error of the relative flux (err_13) are taken from calibration file 13, one per band. How to compute this error in the relative flux is described in the related CAP and is not part of this paper.

aas_flux_con:

The new flux and associated error are calculated for each reset interval by:

$$flux\_out = \frac{flux\_in * rel\_flux}{flux\_pm} \tag{8.43}$$

$$err\_out = flux\_out * (ABS(\frac{err\_in}{flux\_in}) + ABS(\frac{err\_13}{rel\_flux}) + ABS(\frac{err\_pm}{flux\_pm})) \tag{8.44}$$

flux_out : new computed flux which is part of the AAR
flux_in : flux input from equation 8.35
err_out : new computed error which is part of the AAR
err_in : error input from equation 8.36

Also here the current IA3 system (and OLP V6) calculates the error differently:

$$err\_out = flux\_out * \sqrt{(err\_in/flux\_in)^2 + (err\_13/rel\_flux)^2 + (err\_p/flux\_p)^2} \tag{8.45}$$

VELCOR : Velocity Correction

This works on wavelengths alone, and no error calculation is done.

EXTRACT_AAR : AAR Extraction

No error calculation necessary, as this is just data extraction.

8.5 Glitch removal effects in fast speed AOT 1 observations

8.5.1 Introduction

The purpose of the study reported here was to check if the glitch removal process included in Derive-SPD has an impact on spectral lines detected in fast speed AOT 1 observations. The spectra of three Planetary Nebulae with strong emission lines were selected for this test.

8.5.2 Processing

The following steps were followed:

1. Check the AAR derived with the OLP version 5.2 to see if there are points belonging to the spectral line which are flagged as glitched.
2. Derive a new SPD and AAR in which glitch detection is disabled by setting the parameter alpha in CAL06 to a very high value.
3. Compare those lines in which some points are identified as glitched in the standard AAR, to the corresponding ones in the non-deglitched AAR.
4. Flatfield/Rebin both AARs and fit a Gaussian to the lines of interest to calculate the line fluxes.

8.5.3 Results

The attached figures show several examples of the comparison between the standard AAR product (crosses) and the non-deglitched AAR (asterisks).

Table 8.1 displays the results of the line flux calculation after a Gaussian fit, for all those lines in the three observations in which points flagged as glitched were found.

Table 8.1: Comparison between different processing methods

Source	Line (μm)	Line flux standard AAR (W cm^{-2})	Line flux non-deglitched AAR (W cm^{-2})	% discrepancy
1	24.31	4.70×10^{-17}	5.31×10^{-17}	11.5
	25.88	7.79×10^{-17}	8.78×10^{-17}	11.3
2	15.55	4.81×10^{-17}	6.11×10^{-17}	21.3
3	10.51	3.01×10^{-18}	5.48×10^{-18}	45.1
	15.55	3.88×10^{-18}	1.10×10^{-17}	64.7
	25.88	3.38×10^{-18}	4.77×10^{-18}	29.1

The results of the analysis are:

1. Most spectral lines are not affected by glitch removal.

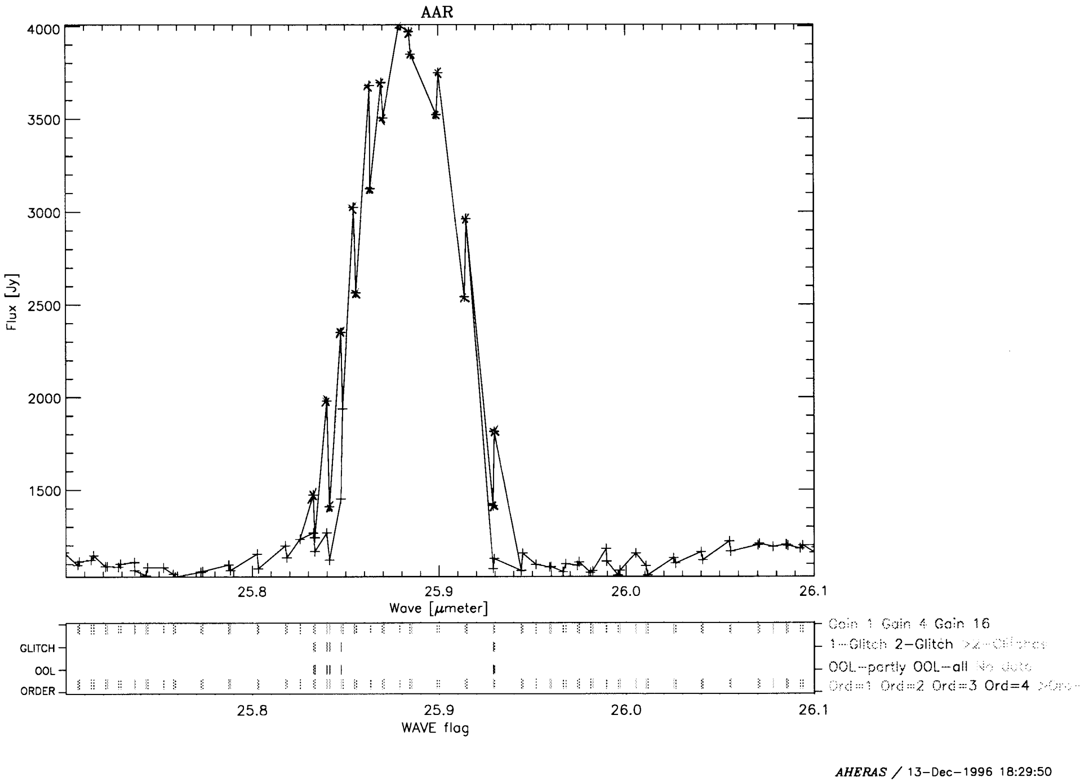

Figure 8.3: Good AOT 1 line fitting

2. In few lines, some points at the wings of the line are flagged as glitched, causing the line profile in this region to deviate from the non-deglitched one.

3. In few lines, many points belonging to the line are flagged as glitched. Glitch removal applied to these points introduces a substantial error in the line profile and in the line flux.

4. For those cases described above, the non-deglitched line profiles can be fitted by a Gaussian function much better than the deglitched ones.

8.5.4 Conclusions

Generally the spectrum resulting from a fast speed AOT 1 observation is improved after glitch removal. However, when points belonging to spectral lines are flagged as glitched, one must be cautious about the line profiles and fluxes (except for band 4) because the line profile may be significantly distorted by glitch removal.

If a user wants to derive line fluxes from fast AOT 1's it will be necessary to check the datapoints around a line to see if they are flagged glitched. If they are it may be necessary to visit one of the data centers so that additional data processing can occur.

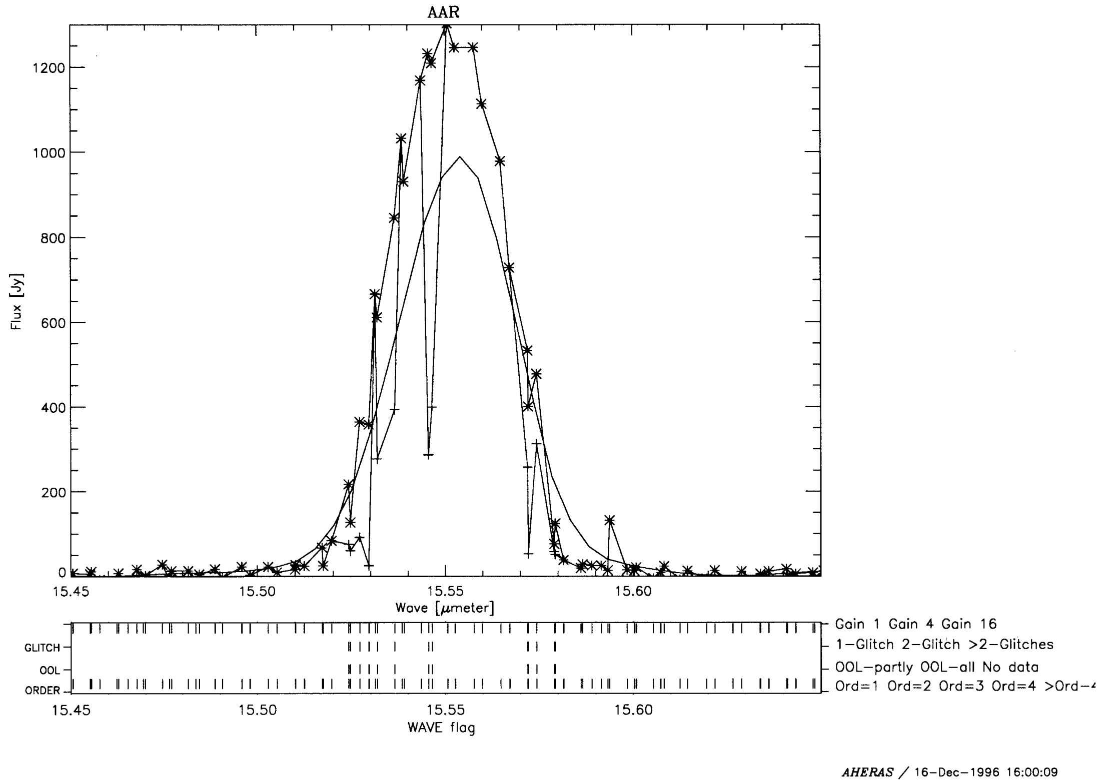

Figure 8.4: Bad AOT 1 line fitting

8.6 Version history of the SPG pipeline

The SPG pipeline went through several revisions during the ISO mission. From OLP version 5.0 all SWS products were declared scientifically valid. Prior to that version only the ERD had been declared valid.

To find out which version of the OLP software produced a FITS product look at the header field OLPVERS.

The history of the OLP pipeline is as follows:

V2.3 - released from 27 Oct 95

V2.3.1 - released from 13 Nov 95

V2.3.2 - released from 21 Nov 95

V2.3.3 - released from 8 Dec 95

V2.3.4 - released from 18 Dec 95

V2.3.5 - released from 26 Dec 95

V2.3.6 - released from 8 Jan 96

V2.3.7 - released from 10 Jan 96

V2.4 - released from 24 Jan 96

V2.4.1 - released from 5 Feb 96

V2.4.2 - released from 12 Feb 96

V2.4.3 - released from 19 Feb 96

V3.0 - released from 11 Mar 96

V3.1 - released from 18 Mar 96

V3.2 - released from 25 Mar 96

V3.3 - released from 2 Apr 96

No changes relevant to SWS.

V4.0 - active from 13 May 1996.

Often does not produce (proper) LW output and the wavelengths are incorrect for fast AOT 1 (speed 1,2,3).

V4.1 - active as of about 21 May 1996.

LW output (in terms of flux level) is corrected again, wavelengths for fast AOT 1's still bad.

V4.2.1 - active as of 11 June 1996.

SWS AC correction improved and standard deviation in SWS SPD now calculated correctly.

V4.3 - active 19 June 1996.

Column SWAALINE in SWS AA now filled properly.

V5.0 - active as of 19 August 1996

Scientifically validated pipeline.

V5.1 - active as of 1 October 1996

The system was changed so that when reprocessing data from a revolution the Cal-G files pertaining to that revolution would be used, instead of the latest ones. This is in case, e.g. the wavelength calibration changed during the mission leading to several wavelength calibration files each relevant for a portion of the entire mission. This was a transparent modification as far as users are concerned.

V5.2 - released as of 19 November 1996

No changes relevant to SWS.

V5.3 - released as of 13 December 1996

No changes relevant to SWS.

V6.0 - released as of 5 May 1997

Many changes. They can be found by looking through this document for the words 'OLP V6'. The most important are a better flux and wavelength calibration, the filling of the standard deviation field in the output (SWSPSTDV) with valid information, the extracting into the AAR only the science data rather than all data for which a valid wavelength could be assigned and the removal of several bugs.

V6.1 - released as of 1 Aug 1997

Cal-G files 13 and 25_x used by OLP 6.0 were derived with calibration analysis software inconsistent with the OLP V6.0 software (this was noted only after the deadline for OLP V6.0). Cal-G files 13 and 25_x were therefore re-derived to be consistent. The opportunity was also taken to re-derive some of the Cal-G 25_x files using observations of standard stars.

V7.0 - released as of 1 May 1998

This was the first post-mission pipeline.

Chapter 9

Product Description

9.1 Introduction

This chapter is split into four sections describing the Raw data (ERD and CSH) files; the standard processed (SPD) files; the Auto-Analysis Results (AAR) files and the Calibration-G files. Note that the format for all these files is binary FITS format and is described in the IDPD.

9.2 Raw data files (ERD and Compact Status)

There are two files in this section: SWER SWS Edited Raw Data and SSTA SWS Compact Status.

9.2.1 SWS Edited Raw Data

These files are normally named SWER*.FITS, where '*' is a number generated from the revolution the observation was made, the order the observations were performed in that day and the order it appeared in the proposal.

Headers

The ERD files contain primary headers described in Table 9.2.1. In this table example information is used to fill the header.

Most keywords are self explanatory. Those that are not include:

TMRATE The Telemetry Rate can only be 32, indicating 32 kbps.

EOHAAOTN This can take the values S01, S02, S06 or S07, for the appropriate AOT. This is copied from the field of the same name in the EOHA file for the observation, see the ISO Satellite & Data Manual for an explanation of this file.

EOHAPCAT indicates the proposal category as entered by the user in PGA. The categories were European GT, NASA GT, ISAS GT, OT or Calibration, and these are coded in EOHAPCAT as the ASCII numbers 1 to 5 respectively. This is copied from the field of the same name in the EOHA file for the observation.

EOHATTYP indicates the scientific category as entered by the user in PGA. The categories were Solar System, Interstellar Matter, Stellar Physics, Extragalactic Systems or Cosmology, and these are coded in EOHATTYP as the ASCII numbers 001 to 005 respectively. This is copied from the EOHASCAT field in the EOHA file for the observation.

ATTUTCS should be close in value to EOHAUTCS. If the observation contains micro-slews (e.g. SWS aperture changes) this value will refer to the first pointing.

ATTOTFTH AOT on target flag. When the pointing is within this accuracy of the target the on target flag is set.

ATTTYPE Can be set to “T” for solar system tracking, “P” for fine pointing (single target) or “R” for a raster operation.

Time keys The various time keys, referred to by TREFUTK, TREKITK and TREFITKU, are described in the ISO Satellite & Data Manual.

VERSn indicates the version numbers of the various files used to generate this product.

Table 9.1: ERD primary headers

Header keyword	Contents	Comment
SIMPLE =	T	
BITPIX =	8	
NAXIS =	0	
EXTEND =	T	
ORIGIN =	'ESA '	European Space Agency
TELESCOP=	'ISO '	Infrared Space Observatory
INSTRUME=	'SWS '	Instrument used
COMMENT		SWS Edited Raw Data
FILENAME=	'SWER23300209'	File name in ISO archive
DATE =	'26/09/95'	Creation date 95/269
FILEVERS=	'0377 '	Version ID in ISO archive
OLPVERS =	'LATEST '	SOC OLP system version
CALGVERS=	'CALG_40 '	/ SOC OLP CAL-G files version
USERNAME=	'PIPELINE'	/
VERS1 =	'1411/EOHA282'	/ Version ID of each input file
VERS2 =	'1411/EOHI282'	/ Version ID of each input file
VERS3 =	'0804/APPH282'	/ Version ID of each input file
OBJECT =	'NGC6543 '	Target ID as given by proposer
OBSERVER=	'SWS '	Proposer ID in ISO Mission DB
EQUINOX =	2000.0	Equinox
TMRATE =	32	Telemetry rate in Kbps (Kbits/sec)
EOHAUTCS=	'96130004435'	Approx. UTC of start of observation
EOHAUTCE=	'96130013951'	Approx. UTC of end of observation
EOHAAOTN=	'S06 '	AOT name

EOHAPLID=	'SWS_EE2 '	Proposal ID
EOHAOSN =	'09 '	Observation sequence number
EOHAPSN =	'00 '	Pointing sequence number
EOHAPCAT=	'4 '	Proposal category
EOHACIND=	' '	Calibration indicator
EOHATTYP=	'003 '	Target type
AOTVERS =	'95118180436'	AOT-to-OCT logic version
TREFCOR1=	241288656	/UTC of 1st reference time
TREFPHA1=	282.19191	/Orbital phase at TREFCOR1
TREFCOR2 =	241289612	/UTC of 2nd reference time
TREFPHA2 =	282.20301	/Orbital phase at TREFCOR2
TREFCOR3 =	241290568	/UTC of 3rd reference time
TREFPHA3 =	282.21411	/Orbital phase at TREFCOR3
ATTUTCSL=	'96130004411'	UTC of start time of slew to intended target
ATTUTCS =	'96130004421'	UTC of time of first arrival at intended target
ATTOTFTH=	10.0	On-target flag threshold (arc secs)
ATTRA =	303.56	Intended Right Ascension of instrument viewing, in degrees
ATTDEC =	28.0	Intended DEClination (with ATTRA), in degrees
ATTTYPE =	'R '	Type of attitude operation (P/R/T)
ATTGUIDE=	150002	Guide star reference number
ATTSAANG=	92.6	Solar aspect angle (degrees)
ATTERROR=	0	CONTINGEncy flag(0=success; 1=target not acq'd)
TREFUTC1=	231986675	UTC (whole seconds since 01-01-1989)
TREFUTC2=	4101430	UTC (remaining fraction of second)
TREFUTK =	1781286624	ISO Uniform Time Key (UTK)
TREFITK =	1781286624	ISO INSTRUMENT Time Key (ITK)
TREFITKU=	0.04166666666667	ITK unit length in seconds

Records

The ERD file contains records with the fields described in Table 9.2.

Table 9.2: Records in the ERD file

Field name	Number	Format	Comment
GPSCTKEY	1	I*4	Instrument time key
GPSCRPID	2	I*1	Raster point ID
GPSCFILL	1	I*2	Filler
SWERDR5	12	I*2	5-micron array readouts
SWERDR10	12	I*2	10-micron array readouts
SWERDR20	12	I*2	20-micron array readouts
SWERDR35	12	I*2	35-micron array readouts
SWERDRFP	4	I*2	FP detector readouts
SWERHK1	1	I*2	SW scanner - actual position (if mode = 0,1)
SWERHK2	1	I*2	SW scanner - LVDT output (if mode = 0,1)
SWERHK3	1	I*2	SW scanner motor current (if mode=1)
SWERHK4	1	I*2	SW scanner DAC output (if mode=1)
SWERHK5	1	I*2	LW scanner - actual position (if mode = 0,2,3)
SWERHK6	1	I*2	LW scanner - LVDT output (if mode = 0,2,3)
SWERHK7	1	I*2	LW scanner motor current (if mode=2)
SWERHK8	1	I*2	LW scanner DAC output (if mode=2)
SWERHK9	1	I*2	Last received internal command (if mode=3)
SWERHK10	1	I*2	Temp. sensor FP cal. source (if mode=3)
SWERHK11	1	I*2	Fabry-Pérot main current
SWERHK12	1	I*2	Fabry-Pérot correction current 1
SWERHK13	1	I*2	Fabry-Pérot correction current 2
SWERSLHK	1	I*2	Slowly commutated Housekeeping (HK)
SWERIRC	1	I*2	Internal readout counter
SWEREXEC	1	I*2	"Execute" flags

Notes:

1. Twenty-four records are generated each second.
2. The five SWERDR fields contain the detector readouts, whereas the thirteen SWERHK fields allow the wavelength falling on each detector to be calculated.
3. The two GPSCRPID fields should always contain '1's for SWS, unless a SSO is being tracked.
4. The selection of which of fields SWERHK1 to SWERHK10 contain valid information is mode-dependent. The "mode" can be 0 (default), 1, 2 or 3. A change in mode implies the start of a new measurement period, and the value of the mode is contained in the corresponding Compact Status field SSTAHKMD.
5. Whereas all other fields repeat at the rate of 24 Hz, SWERSLHK repeats at 0.5 Hz. The meaning of any individual readout depends on the accompanying value of SWERIRC.
6. SWERIRC begins at 1 (for the first readout cycle of a new format), then increments up to 48. It is derived from the "SWS internal frame counter" and indicates the sequence of information in SWERSLHK.
7. SWEREXEC is extracted from the more significant byte of the SWS internal frame counter. Because the flags are telemetered at a rate of 12 Hz, they appear only in ERD records for which SWERIRC is a multiple of 2; the flags are set to zero for the intervening records. The more significant byte of SWEREXEC is always set to zero, i.e. the sign bit for the flags is not extended.

9.2.2 SWS Compact Status

These files are normally named SSTA*.FITS.

Headers

The CSH files primary header, filled with example information, is described in Table 9.2.2. Most keywords are self explanatory, or have been described above.

Table 9.3: CSH primary headers

Header keyword	Contents	Comment
SIMPLE =	T	/
BITPIX =	8	/
NAXIS =	0	/
EXTEND =	T	/
ORIGIN =	'ESA '	/ European Space Agency
TELESCOP=	'ISO '	/ Infrared Space Observatory
INSTRUME=	'SWS '	/ Instrument used
COMMENT		/ SWS Compact Status
FILENAME=	'SSTA26400248'	/ File name in ISO archive
DATE =	'09/07/95'	/ Creation date 95/190
FILEVERS=	'0298 '	/ Version ID in ISO archive
OLPVERS =	'OLP_21 '	/ SOC OLP system version
CALGVERS=	'CALG_40 '	/ SOC OLP CAL-G files version
USERNAME=	'PIPELINE'	/
VERS1 =	'0298/SCSH264'	/ Version ID of each input file
VERS2 =	'1411/EOHA282'	/ Version ID of each input file
VERS3 =	'1411/EOHI282'	/ Version ID of each input file
EQUINOX =	2000.0	/ Equinox
TMRATE =	32	/ Telemetry rate in Kbps (Kbits/sec)
EOHAUTCS=	'96166223020'	/ Approx. UTC of start of observation
EOHAUTCE=	'96166223818'	/ Approx. UTC of end of observation
EOHAAOTN=	'S07 '	/ AOT name
EOHAPLID=	'MPEWARM1'	/ Proposal ID
EOHAOSN =	'48 '	/ Observation sequence number
EOHAPSN =	'0 '	/ Pointing sequence number
EOHAPCAT=	'1 '	/ Proposal category
EOHACIND=	' '	/ Calibration indicator
EOHATTYP=	'2 '	/ Target type
AOTVERS =	'94350161513'	/ AOT-to-OCT logic version

TREFCOR1=	241288656	/UTC of 1st reference time
TREFPHA1=	282.19191	/Orbital phase at TREFCOR1
TREFCOR2 =	241289612	/UTC of 2nd reference time
TREFPHA2 =	282.20301	/Orbital phase at TREFCOR2
TREFCOR3 =	241290568	/UTC of 3rd reference time
TREFPHA3 =	282.21411	/Orbital phase at TREFCOR3
ATTUTCSL=	'96166222532'	/ UTC of start time of slew to intended target
ATTUTCS =	'96166222627'	/ UTC of time of first arrival at intended target
ATTOTFTH=	10.0	/ On-target flag threshold (arc secs)
ATTRA =	302.66	/ Intended Right Ascension of instrument viewing, in degrees
ATTDEC =	27.8	/ Intended DEClination (with ATTRA), in degrees
ATTTYPE =	'P '	/ Type of attitude operation (P/R/T)
ATTGUIDE=	150002	/ Guide star reference number
ATTSAANG=	115.9	/ Solar aspect angle (degrees)
ATTERROR=	0	/ CONTINGEncy flag(0=success; 1=target not acq'd)
TREFUTC1=	241288656	/ UTC (whole seconds since 01-01-1989)
TREFUTC2=	1428250	/ UTC (remaining fraction of second)
TREFUTK =	617295744	/ ISO Uniform Time Key (UTK)
TREFITK =	617295744	/ ISO INSTRUMENT Time Key (ITK)
TREFITKU=	0.04166666666667	/ ITK unit length in seconds

Records

The Compact Status file contains records with the fields described in Table 9.4. The records are defined in the binary header of the FITS file.

Table 9.4: CSH file

Field name	Number	Format	Comment
CSGPUKST	1	I*4	UTK start time
CSGPUKEN	1	I*4	UTK end time
CSGPIKST	1	I*4	ITK start time
CSGPIKEN	1	I*4	ITK end time
CSGPUTST	2	I*4	UTC start time
CSGPUTEN	2	I*4	UTC end time
CSGPOSN	1	I*1	Observation Sequence Number
CSGPFILL	15	I*1	Spare
SSTASHUT	1	I*2	Shutter position (0=closed, or 1/2/3)
SSTAGAIN	6	I*2	Nominal gain in each of the bands (1/4/16)
SSTACALS	4	I*2	Calibration source status
SSTARESP	2	I*2	Reset interval in frames (SW/LW)
SSTAHKMD	1	I*2	House keeping mode
SSTAFPS	1	I*2	FP selection (1=FP1, 2=FP2)
SSTASPAR	9	I*2	Spare

The four elements of SSTACALS are:

1. Grating calibrator
2. Flusher
3. FP calibrator
4. Diffuse calibrator

A zero in a SSTACALS field indicates that the respective calibrator is off. 1 indicates it is on low, 2 that it is on high.

9.3 Standard processed (SPD) files

There are two files in this section:

SWSP SWS Standard Processed Data

SWGH SWS Glitch History Data

9.3.1 SWS Standard Processed Data

These files are normally named SWSP*.FITS.

Headers

The SPD files contain primary headers described in Table 9.3.1. In this table example information is used to fill the header.
Most keywords are self explanatory, or have been described above.

Table 9.5: SPD primary headers

Header keyword	Contents	Comment
SIMPLE =	T	/
BITPIX =	8	/
NAXIS =	0	/
EXTEND =	T	/
ORIGIN =	'ESA '	/ European Space Agency
TELESCOP=	'ISO '	/ Infrared Space Observatory
INSTRUME=	'SWS '	/ Instrument used
COMMENT		SWS Standard Processed Data
FILENAME=	'SWSP26400248'	/ File name in ISO archive
DATE =	'17/10/95'	/ Creation date 95/290
FILEVERS=	'0399 '	/ Version ID in ISO archive
OLPVERS =	'LATEST '	/ SOC OLP system version
CALGVERS=	'CALG_40 '	/ SOC OLP CAL-G files version
USERNAME=	'JSTERNBE'	/ Unofficial data product
INSTRA =	102.66474	/Reference instrument J2000 right ascension (deg
INSTDEC =	+21.81240	/Reference instrument J2000 declination (deg)
INSTROLL=	318.89	/Reference instrument J2000 roll angle (deg)
CINSTRA =	188.96338	/Corrected reference instrument J2000 right ascension (deg)
CINSTDEC=	-40.78920	/Corrected reference instrument J2000 declination (deg)
CINSTROL=	319.71	/Corrected reference instrument J2000 roll angle (deg)
OBJECT =	'TEST_OBJ'	/ Target ID as given by proposer
OBSERVER=	'KLEECH'	/ Proposer ID in ISO Mission DB
EQUINOX =	2000.0	/ Equinox
TMRATE =	32	/ Telemetry rate in Kbps (Kbits/sec)
EOHAUTCS=	'96166223020'	/ Approx. UTC of start of observation
EOHAUTCE=	'96166223818'	/ Approx. UTC of end of observation

```
EOHAAOTN=                'S07 '  / AOT name
EOHAPLID=             'KLTEST '  / Proposal ID
EOHAOSN =                 '48 '  / Observation sequence number
EOHAPSN =                  '0 '  / Pointing sequence number
EOHAPCAT=                  '1 '  / Proposal category
EOHACIND=                   ' '  / Calibration indicator
EOHATTYP=                  '2 '  / Target type
ATTUTCSL=         '96166222532'  / UTC of start time of slew to intended target
ATTUTCS =         '96166222627'  / UTC of time of first arrival at intended target
ATTOTFTH=                  10.0  / On-target flag threshold (arc secs)
ATTRA   =                102.66  / Intended Right Ascension of instrument viewing
ATTDEC  =                  21.8  / Intended DEClination (with ATTRA)
ATTTYPE =                  'P '  / Type of attitude operation (P/R/T)
ATTGUIDE=                150002  / Guide star reference number
ATTSAANG=                 115.9  / Solar aspect angle (degrees)
ATTERROR=                     2  / CONTINGEncy flag(0=success; 1=target not acq'd)
TREFUTC1=             235175420  / UTC (whole seconds since 01-01-1989)
TREFUTC2=               8505250  / UTC (remaining fraction of second)
TREFUTK =            1857816480  / ISO Uniform Time Key (UTK)
TREFITK =            1857816480  / ISO INSTRUMENT Time Key (ITK)
TREFITKU=      0.04166666666667  / ITK unit length in seconds
TREFCOR1=             235175420  / UTC of 1st reference time
TREFPHA1=             282.09099  /Orbital phase at TREFCOR1
TREFHEL1=               -253.41  / Heliocentric correction +(s) at TREFCOR1
TREFDOP1=                -13.92  / ISO velocity towards target (km/s) at TREFCOR1
TREFCOR2 =            235175659  / UTC of 2nd reference time
TREFPHA2 =            282.09430  /Orbital phase at TREFCOR2
TREFHEL2 =              -253.40  / Heliocentric correction +(s) at TREFCOR2
TREFDOP2 =               -13.93  / ISO velocity towards target (km/s) at TREFCOR2
TREFCOR3 =            235175898  / UTC of 3rd reference time
TREFCOR3 =            241280569  /Orbital phase at TREFCOR3
TREFHEL3 =              -253.39  / Heliocentric correction +(s) at TREFCOR3
TREFDOP3 =               -13.94  / ISO velocity towards target (km/s) at TREFCOR3
ISRRSEV =                     0  / RTA maximum severity level = OK
ISRQSEV =                     1  / QLA maximum severity level = WA
ISRRWARN=                   ' '  / RA-warning flag from IS user
ISRNOOSL=                     0  / No. of out-of-soft-limit errors
ISRNOOHL=                     0  / No. of out-of-hard-limit errors
ISRNMW  =                     0  / No. of monitor warnings
ISRNCVW =                     0  / No. of command verification errors
ISRNBTW =                     0  / No. of bad telemetry errors
ISRNMVW =                     0  / No. of memory verification errors
ISRNSQLA=                     9  / No. of severe QLA errors
```

VERS1 =	'0298/SSTA26400248'	/ Version ID of each input file
VERS2 =	'0298/GEHK26400248'	/ Version ID of each input file
VERS3 =	'0298/EOHI264'	/ Version ID of each input file
VERS4 =	'0298/SWER26400248'	/ Version ID of each input file
VERS5 =	'0976/SC03_010'	/ Version ID of each input file
VERS6 =	'0976/SC04_010'	/ Version ID of each input file
VERS7 =	'0976/SC02A_010'	/ Version ID of each input file
VERS8 =	'0976/SC02B_010'	/ Version ID of each input file
VERS9 =	'0976/SC05_010'	/ Version ID of each input file
VERS10 =	'0976/SC02_010'	/ Version ID of each input file
VERS11 =	'0976/SC01_010'	/ Version ID of each input file
VERS12 =	'0976/SC06_010'	/ Version ID of each input file
VERS13 =	'0976/SC16E_013'	/ Version ID of each input file
VERS14 =	'0976/SC12_010'	/ Version ID of each input file
VERS15 =	'0976/SC23_010'	/ Version ID of each input file
VERS16 =	'0976/SC24_010'	/ Version ID of each input file
VERS17 =	'0976/SC18_010'	/ Version ID of each input file
VERS18 =	'1490/IRPH28299000'	/ Version ID of each input file
VERS19 =	'1350/ORBIT'	/ Version ID of each input file
VERS20 =	'0718/SISR28299000'	/ Version ID of each input file

Records

The SPD file contains records with the fields described in Table 9.6. In the FITS file they are defined in the binary header.

Table 9.6: Records in SPD file

Field name	Number	Format	Unit	Comment
GPSCTKEY	1	I*4		Instrument time key
GPSCRPID	2	I*1		Raster point ID
GPSCFILL	1	I*2		Filler
SWSPSTAT	1	I*4		Status of this record
SWSPGPOS	2	R*4		Average positions for gratings 1/2
SWSPGANG	2	R*4	degrees	Angles for SW & LW gratings
SWSPFPOS	1	I*4		Position of FP
SWSPFCUR	3	R*4		Average main current for FP coils
SWSPFGAP	2	R*4	μm	Gaps for FP
SWSPWAVE	52	R*4	μm	Detector wavelength
SWSPFLUX	52	R*4	$\mu V/sec$	Detector slopes
SWSPOFFS	52	R*4		Number of 24 Hz samples used to calculate the slope
SWSPSTDV	52	R*4	$\mu V/sec$	Standard deviation of the detector slope
SWSPFLAG	52	I*4		Flags per detector

Notes:

1. One record is generated every reset interval (1, 2 or 4 seconds).
2. Because SWS has no raster AOTs, the raster point IDs will always be set to 1 EXCEPT when tracking a Solar System Object.
3. The I*4 status number SWSPSTAT, one per measurement, can be decoded by referring to Table 9.7.
4. The I*4 status number SWSPFLAG, one per detector, can be decoded by referring to Table 9.8.

Table 9.7: Decoding of Status word SWSPSTAT

Meaning	Bits set	
dark	00000000000000000000000000000000	0
aperture 1	00000000000000000000000000000001	1
aperture 2	00000000000000000000000000000010	2
aperture 3	00000000000000000000000000000011	3
reset band 1 & 2	00000000000000000000000000000100	4
reset other bands	00000000000000000000000000001000	8
reset all bands	00000000000000000000000000001100	12
diffuse cal normal	00000000000000000000000000010000	16
diffuse cal high	00000000000000000000000000110000	48
fp check normal	00000000000000000000000001000000	64
fp check high	00000000000000000000000011000000	192
flusher normal	00000000000000000000000100000000	256
flusher high	00000000000000000000001100000000	768
grating check normal	00000000000000000000010000000000	1024
grating check high	00000000000000000000110000000000	3072
fp nr 2 active	00000000000000000001000000000000	4096
BAND1 requested	00000000000000000010000000000000	8192
BAND2 requested	00000000000000000100000000000000	16384
BAND3 requested	00000000000000001000000000000000	32768
BAND4 requested	00000000000000010000000000000000	65536
BAND5 requested	00000000000000100000000000000000	131072
BAND6 requested	00000000000001000000000000000000	262144
fp execute flag	00000000000010000000000000000000	524288
FP run flag	00000000000100000000000000000000	1048576
low resolution scan	00000000001000000000000000000000	2097152
reference scan	00000000010000000000000000000000	4194304
photometric check	00000000100000000000000000000000	8388608
defined dark measurement	00000001000000000000000000000000	16777216
SW grating run flag	00000010000000000000000000000000	33554432
LW grating run flag	00000100000000000000000000000000	67108864
SW scan direction	00001000000000000000000000000000	134217728
LW scan direction	00010000000000000000000000000000	268435456

Note that the value of SWSPSTAT may represent the sum of two or more bits.

Table 9.8: Decoding of Flag word SWSPFLAG

Meaning	Bits set	
No order	00000000000	0
1 glitch	00000000001	1
2 glitches	00000000010	2
3 glitches	00000000011	3
Partly Out of limit	00000000100	4
Totally Out of limit	00000001000	8
No data	00000010000	16
Order 1	00000100000	32
Order 2	00001000000	64
Order 3	00001100000	96
Order 4	00010000000	128
Multiple orders (confused)	00011100000	224
Gain bit 1 = gain 1	01000000000	512
Gain bit 2 = gain 4	10000000000	1024
Gain bit 3 = gain 16	11000000000	1536

Notes:

1. Bits 11 to 22 of SWSPFLAG are used internally by Derive-SPD and therefore contain no information useful to the observer.
2. The value of SWSPFLAG may represent the sum of two or more bits.

9.3.2 SWS Glitch History Data

This file has only been produced from OLP version 5 onwards. The files are normally named SWGH*.FITS.

Headers

The SWGH files contain primary headers described in Table 9.3.2, filled with example information.

Most keywords are self explanatory, or have been described before.

Table 9.9: SWGH primary headers

Header keyword	Contents	Comment
SIMPLE =	T	/
BITPIX =	8	/
NAXIS =	0	/
EXTEND =	T	/
ORIGIN =	'ESA '	/ European Space Agency
TELESCOP=	'ISO '	/ Infrared Space Observatory
INSTRUME=	'SWS '	/ Instrument used
COMMENT		SWS Glitch History Data
FILENAME=	'SWGH28600101'	/ File name
DATE =	'17/10/95'	/ Creation date 95/290
FILEVERS=	'0399 '	/ Version ID in ISO archive
OLPVERS =	'LATEST '	/ SOC OLP system version
CALGVERS=	'CALG_40 '	/ SOC OLP CAL-G files version
USERNAME=	'JSTERNBE'	/ Unofficial data product
VERS1 =	'0298/SSTA26400248'	/ Version ID of each input file
VERS2 =	'0298/GEHK26400248'	/ Version ID of each input file
VERS3 =	'0298/EOHI264'	/ Version ID of each input file
VERS4 =	'0298/SWER26400248'	/ Version ID of each input file
VERS5 =	'0976/SC03_010'	/ Version ID of each input file
VERS6 =	'0976/SC04_010'	/ Version ID of each input file
VERS7 =	'0976/SC02A_010'	/ Version ID of each input file
VERS8 =	'0976/SC02B_010'	/ Version ID of each input file
VERS9 =	'0976/SC05_010'	/ Version ID of each input file

VERS10 =	'0976/SC02_010'	/ Version ID of each input file
VERS11 =	'0976/SC01_010'	/ Version ID of each input file
VERS12 =	'0976/SC06_010'	/ Version ID of each input file
VERS13 =	'0976/SC16E_013'	/ Version ID of each input file
VERS14 =	'0976/SC12_010'	/ Version ID of each input file
VERS15 =	'0976/SC23_010'	/ Version ID of each input file
VERS16 =	'0976/SC24_010'	/ Version ID of each input file
VERS17 =	'0976/SC18_010'	/ Version ID of each input file
VERS18 =	'1261/SC16A_011'	/ Version ID of each input file
VERS19 =	'0976/SC16B_010'	/ Version ID of each input file
VERS20 =	'0976/SC16C_010'	/ Version ID of each input file
VERS21 =	'1490/IRPH28200427'	/ Version ID of each input file
VERS22 =	'1350/ORBIT'	/ Version ID of each input file
VERS23 =	'0718/SISR28200427'	/ Version ID of each input file

Records

The SWGH file contains records with the fields described in Table 9.10.

Table 9.10: Records in the SWGH file

Field name	Number	Format	Unit	Comment
GPSCTKEY	1	I*4		Instrument time key
SWGHS_S1	52	I*2		Start sample of first glitch
SWGHS_E1	52	I*2		End sample of first glitch
SWGHHGT1	52	R*4	μV	Glitch height of first glitch
SWGHS_S2	52	I*2		Start sample of second glitch
SWGHS_E2	52	I*2		End sample of second glitch
SWGHHGT2	52	R*4	μV	Glitch height of second glitch
SWGHN_GL	52	I*2		Number of glitches

9.4 Auto-Analysis Results (AAR) files

There is one file in this section:
SWAA SWS Auto-Analysis Results

9.4.1 SWS Auto-Analysis Results

Headers

The AAR files contain primary headers described in Table 9.4.1. In this table example information is used to fill the header.

Most keywords are self explanatory, or have been described above. Those that are not include:

INSTRA This, along with INSTDEC and INSTROLL, are described in the IS0 Satellite & Data Manual.

Table 9.11: AAR primary headers

Header keyword	Contents	Comment
SIMPLE =	T	/
BITPIX =	8	/
NAXIS =	0	/
EXTEND =	T	/
ORIGIN =	'ESA '	/ European Space Agency
DATE =	'17/10/95'	/ Creation date 95/290
TELESCOP=	'ISO '	/ Infrared Space Observatory
INSTRUME=	'SWS '	/ Instrument used
COMMENT		SWS Auto Analysis Results
FILENAME=	'SWAA26400248'	/ File name in ISO archive
FILEVERS=	'0399 '	/ Version ID in ISO archive
OLPVERS =	'LATEST '	/ SOC OLP system version
USERNAME=	'JSTERNBE'	/ Unofficial data product
OBJECT =	'TEST_OBJ'	/ Target ID as given by proposer
OBSERVER=	'KLEECH'	/ Proposer ID in ISO Mission DB
EQUINOX =	2000.0	/ Equinox
TMRATE =	32	/ Telemetry rate in Kbps (Kbits/sec)
EOHAUTCS=	'96166223020'	/ Approx. UTC of start of observation
EOHAUTCE=	'96166223818'	/ Approx. UTC of end of observation
EOHAAOTN=	'S07 '	/ AOT name
EOHAPLID=	'KL_TEST'	/ Proposal ID
EOHAOSN =	'48 '	/ Observation sequence number
EOHAPSN =	'0 '	/ Pointing sequence number
EOHAPCAT=	'1 '	/ Proposal category
EOHACIND=	' '	/ Calibration indicator
EOHATTYP=	'2 '	/ Target type
ATTUTCSL=	'96166222532'	/ UTC of start time of slew to intended target

ATTUTCS =	'96166222627'	/ UTC of time of first arrival at intended target
ATTOTFTH=	10.0	/ On-target flag threshold (arc secs)
ATTRA =	102.66	/ Intended Right Ascension of instrument viewing
ATTDEC =	27.8	/ Intended DEClination (with ATTRA)
ATTTYPE =	'P '	/ Type of attitude operation (P/R/T)
ATTGUIDE=	150002	/ Guide star reference number
ATTSAANG=	115.9	/ Solar aspect angle (degrees)
ATTERROR=	2	/ CONTINGEncy flag(0=success; 1=target not acq'd)
TREFUTC1=	235175420	/ UTC (whole seconds since 01-01-1989)
TREFUTC2=	8505250	/ UTC (remaining fraction of second)
TREFUTK =	1857816480	/ ISO Uniform Time Key (UTK)
TREFITK =	1857816480	/ ISO INSTRUMENT Time Key (ITK)
TREFITKU=	0.04166666666667	/ ITK unit length in seconds
TREFCOR1=	235175420	/UTC of 1st reference time
TREFHEL1=	-253.41	/Heliocentric correction +(s) at TREFCOR1
TREFDOP1=	-13.92	/ISO velocity towards target (km/s) at TREFCOR1
TREFCOR2 =	235175659	/UTC of 2nd reference time
TREFHEL2 =	-253.40	/Heliocentric correction +(s) at TREFCOR2
TREFDOP2 =	-13.93	/ISO velocity towards target (km/s) at TREFCOR2
TREFCOR3 =	235175898	/UTC of 3rd reference time
TREFHEL3 =	-253.39	/Heliocentric correction +(s) at TREFCOR3
TREFDOP3 =	-13.94	/ISO velocity towards target (km/s) at TREFCOR3
INSTRA =	102.66474	/Reference instrument J2000 right ascension (deg)
INSTDEC =	+27.81240	/Reference instrument J2000 declination (deg)
INSTROLL=	318.89	/Reference instrument J2000 roll angle (deg)
CALGVERS=	'CALG_40 '	/ SOC OLP CAL-G files version
AOTVERS =	'03.30 '	/ AOT-to-OCT logic version
TREFPHA1=	282.19191	/ Orbital phase at TREFCOR1
TREFPHA2 =	282.20301	/ Orbital phase at TREFCOR2
TREFPHA3 =	282.21411	/ Orbital phase at TREFCOR3
CINSTRA =	309.77666	/ Corrected reference instrument J2000 right ascension (deg)
CINSTDEC=	68.037530	/ Corrected reference instrument J2000 declination (deg)
CINSTROL=	336.08000	/ Corrected reference instrument J2000 roll angle (deg)
ISRRSEV =	1	/ RTA maximum severity level = WA
ISRQSEV =	1	/ QLA maximum severity level = WA
ISRRWARN=	'OK '	/ RA-warning flag from IS user
ISRNOOSL=	0	/ No. of out-of-soft-limit errors
ISRNOOHL=	0	/ No. of out-of-hard-limit errors
ISRNMW =	0	/ No. of monitor warnings
ISRNCVW =	2	/ No. of command verification errors
ISRNBTW =	0	/ No. of bad telemetry errors
ISRNMVW =	0	/ No. of memory verification errors
ISRNSQLA=	122	/ No. of severe QLA errors

VERS31	= 'cal21_1_011.fits'	/ calfile 21_1 for dark subtraction
VERS32	= 'cal21_2_011.fits'	/ calfile 21_2 for dark subtraction
VERS33	= 'cal21_4_011.fits'	/ calfile 21_4 for dark subtraction
VERS34	= 'cal21_8_010.fits'	/ calfile 21_8 for dark subtraction
VERS37	= 'cal25_1a_030.fits'	/ calfile 25 used for flux conversion
VERS38	= 'cal25_1b_030.fits'	/ calfile 25 used for flux conversion
VERS39	= 'cal25_1d_030.fits'	/ calfile 25 used for flux conversion
VERS40	= 'cal25_1e_030.fits'	/ calfile 25 used for flux conversion
VERS41	= 'cal25_2a_030.fits'	/ calfile 25 used for flux conversion
VERS42	= 'cal25_2b_030.fits'	/ calfile 25 used for flux conversion
VERS43	= 'cal25_2c_030.fits'	/ calfile 25 used for flux conversion
VERS44	= 'cal25_3a_030.fits'	/ calfile 25 used for flux conversion
VERS45	= 'cal25_3c_030.fits'	/ calfile 25 used for flux conversion
VERS46	= 'cal25_3d_030.fits'	/ calfile 25 used for flux conversion
VERS47	= 'cal25_3e_031.fits'	/ calfile 25 used for flux conversion
VERS50	= 'cal25_5b_010.fits'	/ calfile 25 used for flux conversion
VERS51	= 'cal25_5c_010.fits'	/ calfile 25 used for flux conversion
VERS52	= 'cal25_5d_010.fits'	/ calfile 25 used for flux conversion
VERS53	= 'cal25_6_010.fits'	/ calfile 25 used for flux conversion
VERS54	= 'cal13_116.fits'	/ calfile 13 for flux conversion

Records

The AAR file contains records with the fields described in Table 9.12. In the FITS file they are defined in the binary header.

Table 9.12: Records in the AAR file

Field name	Number	Format	Unit	Comment
SWAAWAVE	1	R*4	μm	Wavelength of data point
SWAAFLUX	1	R*4	Jy	Flux
SWAASTDV	1	R*4	Jy	Standard deviation of the flux
SWAATINT[1]	1	I*4	samples	Number of samples used
SWAADETN[2]	1	I*4		detector number
SWAAITK	1	I*4		SWS instrument time key
SWAAUTK	1	I*4		ISO uniform time key
SWAARPID[3]	2	I*1		raster point id
SWAASPAR	2	I*1		spare
SWAALINE[4]	1	I*4		line number
SWAASDIR[5]	1	I*4		scan direction
SWAASCNT[4]	1	I*4		scan number
SWAASTAT[6]	1	I*4		status word
SWAAFLAG[7]	1	I*4		flag word

Notes:

1. SWAATINT is the total number of 1/24 second samples used to calculate the flux of this data point. See section 7.3 for a definition of this. The units for this for pre-OLP V7 files were given as seconds, rather than the correct (1/24 seconds) samples.
2. SWAADETN can be used to determine which detector observed each data point by referring to table 3.2.
3. SWAARPID, the raster point id, is copied over from the GPSCRPID in the SPD. As SWS has no raster AOTs it is always (1,1) (unless a Solar System Object is being tracked), but is included so that the format of SWS AA is compatible with LWS AA.
4. Section 9.4.2 discusses SWAALINE and SWAASCNT.
5. SWAASDIR is used to identify if the datapoint is from an up-scan (1) or a down scan (-1). 0 is undefined (and don't use the data). See section 4.6.1 for a definition of up-down scans.
6. SWAASTAT is copied over from SWSPSTAT. For a description of this see Table 9.7.
7. SWAAFLAG is copied over from SWSPFLAG. For a description of this see Table 9.8.

9.4.2 SWAALINE and SWAASCNT

SWAALINE and SWAASCNT are both counts of the valid data present in an AAR.

SWAALINE is a count of the valid ranges in a dataset. For AOT 1, it is filled with the AOT band number (see table 3.2). For an AOT 2 observing X lines it will count from 1 to X, with 0 reserved for any datapoints not associated with a line. Note that the datapoints associated with SWAALINE set to, e.g. 1, may not correspond to the first entered line number in your AOT as the logic may re-arrange them to increase efficiency. For AOT 6 it counts the number of scans, for an example see table 9.13. Users should note that there is a difference in the behaviour of SWAALINE for AOT 2's and 6's – for AOT 2 there is one value per each up-down pair, whereas for an AOT 6 there is one value per individual up- or down-scan.

Table 9.13: Line number against detector band

Operation	line number for detector band			
	1	2	3	4
REF	1	2	3	4
SCAN UP	5	6	7	8
REF	9	10	11	12
SCAN DOWN	13	14	15	16
REF	17	18	19	20
.	.	.	.	.

Note that this is an example of an 'old' (pre mid-1997) AOT 6 and that the scans may be different for a different AOT 6 operation.

SWAASCNT has nothing to do with the number of scans required for an AOT. It is a count of the number of lines/bands containing requested (i.e. what was requested in the AOT) data, starting with 1. Any data outside the requested ranges will have SWAASCNT set to 0. Note that even if SWAASCNT is greater than 0, the flag and status word should be checked to ensure the data is okay. For AOT 1 SWAASCNT is filled with 1.

The decision whether to increment SWAALINE or SWAASCNT depends on whether a scan starts and ends at the same grating position as the preceeding scan. Initially both are set to one. If a scan starts and ends at the same grating position as the preceeding scan the line counter is not incremented but the scan counter is. If the wavelength range is different the line counter is incremented and the scan counter is (re-)set to one.

A slight problem exists in the counting of SWAALINE in that the counter can count up too much, resulting in a higher count than the number of lines. This will be fixed in a later release of OLP.

9.5 Calibration-G files

There are forty-nine files in this section:

SC01	SWS Cal-G 1	Electrical crosstalk matrices
SC02	SWS Cal-G 2	RC correction timescales
SC02A	SWS Cal-G 2A	Midbit values
SC02B	SWS Cal-G 2B	Shape correction values
SC03	SWS Cal-G 3	Reset cutout lengths
SC04	SWS Cal-G 4	Amplifier limits
SC05	SWS Cal-G 5	Switchable gains
SC06	SWS Cal-G 6	Glitch reject levels
SC07	SWS Cal-G 7	Grating detector noise characteristics
SC08	SWS Cal-G 8	Grating calibration specifications
SC09	SWS Cal-G 9	LVDT-Angle relation
SC10	SWS Cal-G 10	Key wavelengths
SC11	SWS Cal-G 11	FP calibration spectrum
SC12	SWS Cal-G 12	Gap-position relation
SC13	SWS Cal-G 13	Relative flux
SC14	SWS Cal-G 14	Intensity of internal calibration sources
SC15	SWS Cal-G 15	Intensity of calibration sources
SC16A	SWS Cal-G 16A	Aperture offsets
SC16B	SWS Cal-G 16B	Element offsets
SC16C	SWS Cal-G 16C	Grating constants
SC16D	SWS Cal-G 16D	Telescope area
SC16E	SWS Cal-G 16E	Scanner curve coefficients
SC18	SWS Cal-G 18	Effective gap correction
SC19	SWS Cal-G 19	AOT 1 resolution factors
SC20	SWS Cal-G 20	Relative detector responsivity
SC21_1	SWS Cal-G 21_1	Detector dark current/noise for 1 sec reset
SC21_2	SWS Cal-G 21_2	Detector dark current/noise for 2 sec reset
SC21_4	SWS Cal-G 21_4	Detector dark current/noise for 4 sec reset
SC21_8	SWS Cal-G 21_8	Detector dark current/noise for 8 sec reset
SC22	SWS Cal-G 22	Detector response to internal diffuse source and flusher
SC23	SWS Cal-G 23	Wave limits for bands
SC24	SWS Cal-G 24	Wave limits for apertures
SC25_1A	SWS Cal-G 25_1A	Spectral responsivity for band 1A - RSRF file
SC25_1B	SWS Cal-G 25_1B	Spectral responsivity for band 1B
SC25_1D	SWS Cal-G 25_1D	Spectral responsivity for band 1D
SC25_1E	SWS Cal-G 25_1E	Spectral responsivity for band 1E
SC25_2A	SWS Cal-G 25_2A	Spectral responsivity for band 2A

SC25_2B	SWS Cal-G 25_2B	Spectral responsivity for band 2B
SC25_2C	SWS Cal-G 25_2C	Spectral responsivity for band 2C
SC25_3A	SWS Cal-G 25_3A	Spectral responsivity for band 3A
SC25_3C	SWS Cal-G 25_3C	Spectral responsivity for band 3C
SC25_3D	SWS Cal-G 25_3D	Spectral responsivity for band 3D
SC25_3E	SWS Cal-G 25_3E	Spectral responsivity for band 3E
SC25_4	SWS Cal-G 25_4	Spectral responsivity for band 4
SC25_5A	SWS Cal-G 25_5A	Spectral responsivity for band 5A
SC25_5B	SWS Cal-G 25_5B	Spectral responsivity for band 5B
SC25_5C	SWS Cal-G 25_5C	Spectral responsivity for band 5C
SC25_5D	SWS Cal-G 25_5D	Spectral responsivity for band 5D
SC25_6	SWS Cal-G 25_6	Spectral responsivity for band 6

Some of these files have identical formats and so are discussed together.

In all cases the ISO Data Product Document should be referred to for the exact file layout.

9.5.1 SWS Cal-G 1 Electrical crosstalk matrices

This file is used in Derive-SPD to correct for the effects of electrical crosstalk (see section 8.2.6).

The file contains 12 records, each 52 integers in length. The first 12 numbers in each record contain the crosstalk for band 1, the next 12 for band 2 etc. Record 1 contains the crosstalk between detector 1 in each band and the other detectors in that band, record 2 contains the crosstalk between detector 2 in each band and the other detectors in that band, etc. Only records 1 and 2 contain information for bands 5 and 6 (the FP bands with only 2 detectors in each).

9.5.2 SWS Cal-G 2 RC correction timescales

This file, used in Derive-SPD, contains the time constants for the high pass filter in the amplifier chain (see section 8.2.5). It contains 52 numbers, the timescales per detectors in seconds.

9.5.3 SWS Cal-G 2A Midbit values

This file, used in Derive-SPD, contains the midbit value for each detector (see section 8.2.3). The detector readouts are between 0 and 4095 (bits) corresponding to -10 to 10 Volts. The midbit is the bit value that corresponds to 0 Volts, approximately 2048, and is different for each detector.

Currently this calfile is filled with 2047.50.

9.5.4 SWS Cal-G 2B Shape correction values

This is used in Derive-SPD. After the slope has been corrected for the reset pulse it is not straight. This files contains values to correct it, see section 8.2.4.

Currently this calfile is filled with zeros which results in the OLP chain not correcting for reset pulse shape.

9.5.5 SWS Cal-G 3 Reset cutout lengths

This file, used in Derive-SPD and Auto-Analysis, contains the number of 24Hz readouts to ignore after a reset (short circuit of the capacitor) (see section 8.2.2). It contains 52 numbers, the number of readouts to ignore per detector.

9.5.6 SWS Cal-G 4 Amplifier limits

This file, used in Derive-SPD, contains the SWS amplifier limits, the minimum and maximum allowable voltages from the amplifiers (see section 8.2.2). There are 52 records, each of which contains the minimum and maximum voltages for the three gains (gain 1, 4 and 16), in telemetry units.

9.5.7 SWS Cal-G 5 Switchable gains

This file, used in Derive-SPD, contains the gains used to convert between the slopes generated from the 24Hz information and the voltages on the detectors (see section 8.2.10). There are 52 records, one per detector. Each record contains three numbers, one for each gain.

9.5.8 SWS Cal-G 6 Glitch reject levels

This file, used in Derive-SPD, contains information used to recognise glitches and reject them (see section 8.2.7). It contains 52 records, one per detector. Each record contains four numbers: α; the number of readouts to ignore before and after a glitch; and the minimum width of a glitch. The last three are in units of 24 Hz samples.

9.5.9 SWS Cal-G 7 Grating detector noise characteristics

Currently not used.

9.5.10 SWS Cal-G 8 Grating calibration specifications

Currently not used.

9.5.11 SWS Cal-G 9 LVDT-Angle relation

Currently not used.

9.5.12 SWS Cal-G 10 Key wavelengths

Currently not used.

9.5.13 SWS Cal-G 11 FP calibration spectrum

Currently not used.

9.5.14 SWS Cal-G 12 Gap-position relation

This file, used in Derive-SPD, contains information on the gap, current and position relationship of the two FPs (see sections 8.2.13 and 7.5). Each record contains the FP position (a telemetered number) applicable to both FPs, and then for each FP the main current and two correction currents necessary to achieve this position, and then the corresponding gap for those currents, in μm.

9.5.15 SWS Cal-G 13 Relative flux

This file, used in Auto-Analysis, contains information used in the flux calibration. There is one row per key wavelength. Each row has the name of the AOT band, the key wavelength, two numbers defining the passband used. Then come conversion numbers for each detector in that band (by default 12, with 10 blank for FP bands) in $\mu V/sec/Jy$, then 12 internal calibration signals (in $\mu V/sec$), then 12 relative flux calibrations (in Jy), then errors on the conversion numbers (in $\mu V/sec/Jy$), errors on the internal calibrations (in $\mu V/sec$), errors on the relative flux calibrations (Jy) and finally the grating start and end position.

9.5.16 SWS Cal-G 14 Intensity of internal calibration sources

Currently not used.

9.5.17 SWS Cal-G 15 Intensity of calibration sources

Currently not used.

9.5.18 SWS Cal-G 16A Aperture offsets

This file, used in Derive-SPD, contains the angles, in degrees, from the optical axis to the entrance or light source used, as seen from the SW and LW collimators (see section 7.5).

9.5.19 SWS Cal-G 16B Element offsets

This file, used in Derive-SPD, contains the angles, in degrees, from the optical axis to the detectors for each of the detectors (see section 7.5).

9.5.20 SWS Cal-G 16C Grating constants

This file, used in Derive-SPD, contains two grating constants, in μm, for the SW and LW gratings (see section 7.5).

9.5.21 SWS Cal-G 16D Telescope area

Currently not used.

9.5.22 SWS Cal-G 16E Scanner curve coefficients

This file, used in Derive-SPD, contains the scanner curve coefficients (see section 7.5).

9.5.23 SWS Cal-G 18 Effective gap correction

This file, used in Derive-SPD, contains information of the effective gap correction. For each possible FP wavelength there is a gap correction for each of the two FPs. All units are μm.

9.5.24 SWS Cal-G 19 AOT 1 resolution factors

Cal-G 19 is used in the processing of all speed AOT 1's. It contains the factors needed to smooth the RSRF's of each AOT band down to the spectral resolution of the AOT 1 being processed and hence match the resolutions.

This was added in OLP V5.0 but the file was described incorrectly in the SWS IDUM V3.0.

9.5.25 SWS Cal-G 20 Relative detector responsivity

Currently not used.

9.5.26 SWS Cal-G 21_x Detector dark current/noise for x sec reset

These 4 files, Cal-G 21_1, Cal-G 21_2, Cal-G 21_4 and Cal-G 21_8 contain information on the dark current. There is one file per reset interval. Each file contains 52 records, each containing the detector number, the average measured dark current (from ground and PV phase tests). the noise in the dark current and finally the minimum and maximum valid dark currents. Dark currents are measured in $\mu V/sec$.

9.5.27 SWS Cal-G 22 Detector response to internal diffuse source

Currently not used.

9.5.28 SWS Cal-G 23 Wave limits for bands

This file, used in Derive-SPD, contains information on the wavelength limits for the AOT bands. There is one row for each band, and each row contains the lower and upper wavelength limits in μm.

9.5.29 SWS Cal-G 24 Wave limits for apertures

This file, used in Derive-SPD, contains information on the wavelength limits for the three apertures. There are three rows, one row for each aperture, and each row contains the lower and upper limit wavelength limit for the two subsystems, in μm.

9.5.30 SWS Cal-G 25_x Spectral responsivity for band x

These files, Cal-G 25_1A, Cal-G 25_1B, Cal-G 25_1D, Cal-G 25_1E, Cal-G 25_2A, Cal-G 25_2B, Cal-G 25_2C, Cal-G 25_3A, Cal-G 25_3C, Cal-G 25_3D, Cal-G 25_3E, Cal-G 25_4, Cal-G 25_5A, Cal-G 25_5B, Cal-G 25_5C, Cal-G 25_5D and Cal-G 25_6, contain the spectral responsivity information (RSRF) for each band.

Each is composed of the number of detectors in that band (twelve for grating, two for the FP files Cal-G 25_x and 25_6) times three numbers. These are the wavelength at which the responsivity is measured (in μm), the responsivity and the error on it, both in $\mu V/sec/Jy$.

Chapter 10

Products sorted by AOT

10.1 AOT 1, Low Resolution Full Grating Scan

From the files listed in chapter 9, all are useful except calibration files 11, 12, 25_5A, 25_5B, 25_5C, 25_5D, 25_6. These files are only used in reducing FP observations.

10.2 AOT 2, Grating Line Profile Scan

From the files listed in chapter 9, all are useful except calibration files 11, 12, 25_5A, 25_5B, 25_5C, 25_5D, 25_6. These files are only used in reducing FP observations.

10.3 AOT 6, Grating Scan

From the files listed in chapter 9, all are useful except calibration files 11, 12, 25_5A, 25_5B, 25_5C, 25_5D, 25_6. These files are only used in reducing FP observations.

10.4 AOT 7, Combined Fabry-Pérot Line Scan and SW Grating Scan

All of the files listed in chapter 9 are useful except calibration files 25_3x and 25_4, used to calibrate the LW grating.

Appendix A

List of Acronyms and Symbols

This appendix lists acronyms and symbols specific to SWS. For a more general list refer to the ISO Satellite & Data Manual.

AA	Auto Analysis – software used to process data, see section 8.3
AAR	Auto Analysis Result file - output of AA, defined in section 9.4.1
AOT	Astronomical Observation Template – see chapter 4
CAM	ISO Camera – one of the four instruments onboard the satellite
d	Fabry-Pérot gap width
Derive-AAR/DAAR	The OLP stage that processes SPD data to the AAR level. See section 8.3
Derive-SPD/DSPD	The OLP stage that processes ERD data to the SPD level. See section 8.2
ERD	Edited Raw Data – raw data from the satellite, defined in section 9.2.1
FITS	Flexible Image Transport System
FM	Flight Model (of SWS)
FS	Flight Spare model (of SWS)
FWHM	Full Width at Half Maximum
F-P	Fabry-Pérot Spectrometer
IA	Interactive Analysis
ILT	Instrument Level Test (SWS laboratory test)
ISDM	Acronym for the ISO Satellite & Data Manual
ITK	Instrument Time Key - see the ISO Satellite & Data Manual for a description of this key
JFET	Junction Field Effect Transistor
LW	Long Wavelength section of SWS
LWS	ISO Long Wavelength Spectrometer – one of the four instruments onboard the satellite
L_{AOT}	Number of scan steps per AOT band
L_F	Number of scan steps per FWHM of spectral resolution
L_s	Step size in scanner steps
λ	Wavelength

n	Fabry-Pérot order
n_i	Number of integrations
n_{int}	Number of samples taken from a single spectral resolution element
n_{scan}	Number of scans
n_{step}	Number of steps
N_D	Dark current noise
N_R	Read noise
N_S	Shot noise
OLP	Off-Line Processing – the pipeline, also known as SPG
PHT	ISO Photopolarimeter – one of the four instruments onboard the satellite
QLA	Quick Look Analysis - a quick assessment carried out on the data
RTA	Real Time Assessment - a quick assessment carried out on the data
R	Spectral Resolution
SNR	Signal-to-Noise Ratio
SOC	Science Operations Center (Villafranca)
SPD	Standard Processed Data - output of DSPD, defined in section 9.3.1
SPG	Standard Product Generation – the pipeline, also known as OLP
SW	Short Wavelength section of SWS
SWS	ISO Short Wavelength Spectrometer – one of the four instruments onboard the satellite
S	Signal Strength (μV/s)
S_ν	Flux density (Jy)
TDATA	Transparent Data
TDF	Telemetry Distribution Format
TDT	Target Dedicated Time
t_r	Detector reset time (sec)
UTK	Uniform Time Key - see the ISO Satellite & Data Manual for a description of this key

Index